CLIMATE CHANGE IMPACT ON THE SPATIAL DISTRIBUTION OF DROUGHTS IN KIRINDI OYA AND MADURU OYA DRY ZONE RIVER BASINS IN SRI LANKA

W.M.R.T.Y. Wijekoon

(228077B)

Degree of Master of Science

Department of Civil Engineering

University of Moratuwa

Sri Lanka

January 2024

CLIMATE CHANGE IMPACT ON THE SPATIAL DISTRIBUTION OF DROUGHTS IN KIRINDI OYA AND MADURU OYA DRY ZONE RIVER BASINS IN SRI LANKA

W.M.R.T.Y. Wijekoon

228077B

Thesis submitted in partial fulfillment of the requirements for the degree

Master of Science in Civil Engineering

Department of Civil Engineering

Faculty of Engineering

University of Moratuwa

Sri Lanka

January 2024

DECLARATION

I declare that this is my own work and this thesis/dissertation does not incorporate without acknowledgement any material previously submitted for a degree or diploma in any other University or Institute of higher learning and to the best of my knowledge and belief it does not contain any material previously published or written by another person except where the acknowledgement is made in the text. I retain the right to use this content in whole or part in future works (such as articles or books).

Signature: Date: 18/12/2023

The above candidate has carried out research for the PhD/MPhil/Masters thesis/dissertation under my supervision. I confirm that the declaration made above by the student is true and correct.

Name of Supervisor: Prof. R. L. H. L. Rajapakse

Signature of the Supervisor: Date: 18/12/2023

Abstract

Climate Change Impact on the Spatial Distribution of Droughts in Kirindi Oya and Maduru Oya Dry Zone River Basins in Sri Lanka

Drought, a consequence of prolonged precipitation deficiencies, is a significant hazard exacerbated by climate change. Sri Lanka, highly susceptible to extreme climatic events, faces drought as its most prominent hazard, necessitating a comprehensive assessment of its impact. This study focuses on the escalating impact of drought intensified by climate change on the Maduru Oya and Kirindi Oya dry zone basins, crucial due to their vulnerability to altered hydroclimatic dynamics. With the substantial contribution of the dry zone to the paddy cultivation of the country, early detection of agricultural droughts is crucial for effective water allocation planning. Recognizing the importance of meteorological droughts as precursors to physical droughts, proactive monitoring and forecasting are essential for planning against subsequent agricultural droughts, while monitoring hydrological droughts is imperative for ensuring a reliable water supply for irrigation and other purposes. Thus, this research primarily focuses on evaluating meteorological and hydrological droughts.

The research employs the Standardized Precipitation Index (SPI) and the Streamflow Drought Index (SDI) for the monitoring of meteorological and hydrological droughts, respectively. It considers six CMIP6 (sixth Phase of the Coupled Model Inter Comparison Project) Global Climate Models (GCMs), and the CNRM-HR-1 model was selected as the preferred model. The two future projection scenarios, SSP1-2.6 and SSP5-8.5, were selected for the analysis. In the meteorological drought assessment, maps illustrating the spatial distribution of meteorological droughts were generated for both current and future climate scenarios. In order to generate maps, a future gridded rainfall dataset was developed by developing statistical relationships with the Climate Hazards Group InfraRed Precipitation with Station data (CHIRPS) set and observed precipitation data. For the hydrological drought assessment, machine learning methods, including Recurrent Neural Network and Random Forest Algorithm, were used to predict future streamflow at specific gauging stations, with the Random Forest model selected for its superior performance. Additionally, the climatic indices formulated by the Expert Team on Climate Change Detection and Indices (ETCCDI) were used in this study to monitor the occurrence of climate extremes of precipitation in the past.

The meteorological and hydrological drought assessments reveal significant insights into the anticipated impacts of climate change. In the Maduru Oya basin, meteorological droughts exhibit varying percentage increases under SSP1-2.6 and SSP5-8.5 scenarios. Extreme and severe droughts experience increases of 18%, and 16%, respectively, under SSP1-2.6, and 31%, and 2%, under SSP5-8.5. Conversely, the Kirindi Oya basin displays significant susceptibility to extreme meteorological droughts, with increases of 49% under SSP1-2.6 and 37% under SSP5-8.5, particularly with extreme droughts surging by over 35% under both scenarios. Furthermore, the hydrological drought assessment highlights the heightened vulnerability of the Padiyathalawa sub-basin in the Maduru Oya basin, indicating a significant increase in the occurrence of moderate hydrological droughts at the 12-month timescale under both future scenarios. Conversely, the Wellawaya sub-basin in the Kirindi Oya basin also shows susceptibility to frequent moderate hydrological droughts along with an 80% increase in the occurrence of severe hydrological droughts under the SSP5-8.5 scenario at the 12-month scale. Therefore, both basins are expected to face water scarcity in the future, emphasizing the importance of implementing measures to ensure a reliable water supply for irrigation and domestic purposes, given the substantial impact of climate change on watershed hydrology.

Keywords: Climate-driven water stress, CMIP6 GCM projections, Drought resilience in water resources, Drought vulnerability

ACKNOWLEDGEMENT

Foremost, I would like to express my deepest gratitude to my research supervisor, Prof. R.L.H.L. Rajapakse, professor at the Department of Civil Engineering, University of Moratuwa, for his tremendous support, motivation, and enthusiasm. His guidance and extensive knowledge were instrumental throughout the research and writing of this thesis.

I also extend my sincere thanks to my co-supervisor, Dr. Karthikeyan Matheswaran, a Regional Researcher focusing on Water Productivity at the International Water Management Institute (IWMI-CGIAR), for the substantial support that contributed to the successful completion of my research. I appreciate the opportunity to collaborate with IWMI and express my sincere gratitude to all the experts and researchers at IWMI who supported me in conducting this research.

I express my sincere gratitude to the SAF-Madanjeet Singh Research Scholar scheme and the Department of Civil Engineering, University of Moratuwa for the financial assistance provided for me to complete this research successfully.

My gratitude extends to the Department of Civil Engineering for the guidance, and I sincerely thank the UNESCO Madanjeet Singh Centre for South Asia Water Management (UMCSAWM) staff for their assistance throughout the study. Simultaneously, I would like to thank my colleagues at the Department of Civil Engineering, University of Moratuwa, and the International Water Management Institute (IWMI), Colombo Headquarters, for their support and stimulating discussions throughout this research.

In addition, I express my gratitude to the Department of Irrigation and the Department of Meteorology for providing the data necessary to carry out this research.

W. M. R. T. Y. Wijekoon,
Graduate Research Assistant,
UNESCO Madanjeet Singh Center for South Aisa Water Management (UMCSAWM),
Department of Civil Engineering,
University of Moratuwa.

TABLE OF CONTENTS

LIST OF FIGURES

LIST OF TABLES

1. INTRODUCTION

1.1 General

Drought occurs as a result of a prolonged deficiency in precipitation in a certain region and it can be intensified by other natural processes and anthropogenic activities (Chan et al., 2021; Sundararajan et al., 2021). The effects of drought-related processes transferred due to the non-linearity and unevenness, lead to numerous environmental and socioeconomic concerns that might happen simultaneously or chronologically. Therefore, these processes have allured the attentiveness of the scientific community to quantify and predict droughts and anticipate their environmental and socioeconomic impacts (Chan et al., 2021). Meteorological, agricultural, and hydrological droughts are the main three types of physical droughts. Meteorological drought occurs due to the reduction of infiltration, runoff, percolation, and groundwater flow that arise as a consequence of precipitation deficit, and it provides information on the level of dryness. Subsequently, these variations result in a shortage of soil water, which then leads to plant water stress, decreased biomass, and decreased production. This phase is referred to as an agricultural drought. The hydrological drought, which is the following stage of the drought, is characterized by decreased streamflow and inflow to reservoirs, lakes, and ponds (Sundararajan et al., 2021). The socio-economic drought category was later acquainted by the US Geological Survey, and it describes the perspective of society on the impacts of physical droughts (Alahacoon & Edirisinghe, 2022).

Drought can be introduced as the most complicated and highly uncertain natural hazard, which is interconnected with a variety of land-based, atmospheric, and ocean processes (Shelton et al., 2022). On the other hand, the complexity and indeterminacy of these underlying processes will be further aggravated in the future as a consequence of climate change (Tramblay et al., 2020). Despite the objectives outlined in the Paris Agreement to limit global warming to a 1.5°C increase relative to the pre-industrial period of 1850–1900, the sixth assessment report from the Intergovernmental Panel on Climate Change (IPCC) indicates that there is a likelihood of surpassing this target during the 21st century, particularly under scenarios involving intermediate, high, and very high greenhouse gas emissions. On the other hand, with each degree of global warming, the risk of drought and the associated social consequences are predicted to rise, and it has been predicted that the incidence of extreme agricultural droughts would increase by 150% to 200% at 2°C and by over 200% at 4°C in Eurasia (IPCC, 2019). Therefore, it is important to assess the effect of climate change on the occurrence of droughts to plan proactive measures.

In 2019, Sri Lanka, Puerto Rico, and Dominica have been identified as the most affected nations according to the Global Climate Risk Index (CRI), a tool introduced by Germanwatch to assess the impact of extreme climatic events. Sri Lanka is therefore

highly exposed to the effects of climate change (Eckstein et al., 2019). On the other hand, a in regard to the number of affected people and the provided assistance (Abeysingha & Rajapaksha, 2020). Therefore, drought monitoring with possible extents of climate change impacts is very important in the Sri Lankan context. Moreover, agro-based industries are directly impacted by agricultural droughts resulting from prolonged periods of meteorological drought. Conversely, hydrological droughts result in causing restrictions on domestic water availability due to prolonged deficiency of water in basins (Abeysingha et al., 2020). Therefore, it is crucial to identify and monitor both meteorological and hydrological droughts, especially in the river basin scale to manage the water resource efficiently.

1.2 Background

Sri Lanka is a tropical island, and the Southwest monsoon and Northeast monsoon primarily affect the rainfall of the island seasonally. Precipitation stands out as a prominent factor contributing to the seasonal and spatial fluctuations in climate patterns. Sri Lanka has been categorized into three climatic zones, namely, the wet zone, dry zone, and intermediate zone based on total annual rainfall (Chaminda et al., 2016). When precipitation falls below average levels over a prolonged period of time, nearly all climate zones naturally experience drought (Abeysingha & Rajapaksha, 2020). Further, as a result of fluctuating rainfall patterns caused by the southwest monsoon, Sri Lanka has endured severe droughts once every three years (Aadhar & Mishra, 2017). Therefore, it is important to monitor droughts and predict the occurrence of droughts and their consequent impacts to plan proactive solutions.

In general, agriculture in the intermediate and dry zones of Sri Lanka predominantly relies on diverse irrigated or semi-rain-fed small reservoirs, which are crucial for the agricultural productivity of the country. Simultaneously, the dry zone plays a pivotal role, accounting for 70% of the paddy cultivation of the country, with the success of this cultivation highly dependent on irrigated water. In essence, paddy cultivation relies significantly on a sophisticated water management system oriented around river basins in the area (Withanachchi et al., 2014). Therefore, paddy cultivation is substantially impacted by prolonged drought. For instance, the paddy yield experienced a 46% decline from 2016 to 2017 due to sustained drought, marking the lowest recorded paddy yield in Sri Lanka over the last decade (Shelton et al., 2022). Consequently, the early identification of agricultural droughts is crucial for planning effective measures to allocate sufficient irrigated water in advance. Given that the cascade of physical droughts follows a distinct pattern, commencing with meteorological droughts, the monitoring and forecasting of meteorological droughts become imperative to proactively plan for subsequent agricultural and hydrological droughts (Zhao et al., 2014).

Furthermore, in recent decades, numerous studies have been carried out to monitor drought conditions in Sri Lanka, primarily utilizing location-specific rainfall data and

Standardized Precipitation Index (SPI)-based drought analyses. However, these investigations have largely overlooked the mapping of spatial-temporal patterns and the assessment of drought hazards. As a result, the spatial distribution of drought has not been adequately represented, given that these studies relied solely on data specific to particular locations. Consequently, there exists a timely and imperative need to undertake a comprehensive drought analysis that effectively captures the spatial distribution of drought (Alahacoon et al., 2021). Therefore, this study aims to present the spatial distribution of meteorological droughts to identify the vulnerable locations within the selected basins in the future.

On the other hand, while hydrological drought occurs at the final stage of the physical drought cascade, the impacts of hydrological drought are significant and widespread, as it leads to reduced water supplies, deteriorated water quality, limited irrigation water supply, and various other economic and social consequences (Tabari et al., 2013). Hence, the monitoring of hydrological droughts is paramount for efficiently managing basin water resources. Additionally, the assessment and forecasting of the temporal distribution of hydrological droughts are imperative to plan and adopt timely measures, ensuring a reliable water supply for irrigation and other purposes.

To mitigate the impact of drought, it is crucial to monitor it considering various characteristics such as the time of occurrence, duration, severity, and spatial extent (Alahacoon & Edirisinghe, 2022). Drought indices can be introduced as useful tools for monitoring and assessing various types of droughts as they enable the dissemination of climatic anomalies to a wide range of user audiences (Abeysingha et al., 2020). Simultaneously, there is a need to conduct an assessment of the monitoring and forecasting of meteorological and hydrological droughts at the river basin scale. This proactive approach is essential for promptly identifying agricultural droughts and managing water resources efficiently.

Hence, this study focuses on monitoring and predicting the occurrence of meteorological and hydrological droughts, illustrating the spatial and temporal distribution of these droughts, respectively, using selected drought monitoring indices. Simultaneously, the study specifically opts for two Shared Socio-economic Pathway-Representative Concentration Pathway (SSP-RCP) scenarios, denoted as SSP1-2.6 and SSP5-8.5, to assess the impact of climate change on the occurrence of meteorological and hydrological droughts in the future. The prediction of droughts is essential for efficiently managing water resources, supporting irrigation-based agriculture, promoting recreational tourism, conducting environmental monitoring, and maintaining ecosystem health (Alawsi et al., 2022).

1.3 Problem Statement

In the context of escalating global climate change, the dry zone basins of Sri Lanka emerge as critical regions susceptible to altered hydroclimatic dynamics and increased

drought occurrences. Notably, the absence of drought predictions considering climate change further highlights the urgency of the situation. If droughts persist for a certain period, it causes the soil moisture to decrease and exposes the plant to water stress, which in turn leads to the lowering of biomass and yield. Additionally, it will have an impact on the hydrological condition of the area by decreasing streamflow, inflow to reservoirs, and diminishing wetlands, which in turn will escalate the demand for water resources. Conversely, comprehensive predictions concerning these impending drought events are currently unavailable at the river basin scale. Therefore, forecasting drought at the river basin scale both in temporal and spatial scales is crucial for effective water resource management in order to plan solutions in advance.

1.4 Significance of the Research

As a consequence of prolonged meteorological droughts, soil droughts ensue, leading to a loss of crops and, subsequently, agricultural droughts. Agricultural droughts notably impact agro-based industries, as highlighted by Abeysingha et al. (2020). Conversely, the economy of Sri Lanka heavily relies on agriculture, with 25.5% of the workforce engaging in agriculture or agriculture-related livelihoods (Wickramasinghe et al., 2021). Implementing proactive measures to mitigate agricultural droughts resulting from prolonged meteorological droughts is crucial for effective management. Simultaneously, monitoring hydrological droughts remains paramount, although with a comparatively longer response time, given the constraints on water availability for domestic demand and irrigation when focusing on comprehensive perspectives of future water security (Abeysingha et al., 2020; Wickramasinghe et al., 2021).

Furthermore, the research also delves into the significant impact of climate change on drought occurrences. The escalating ambient temperature, influenced by climate change, exacerbates evapotranspiration, diminishing groundwater recharge and soil moisture. Consequently, communities residing in the dry zone of Sri Lanka and similar localities elsewhere face amplified challenges from water scarcity, with severe impacts, as highlighted by Wickramasinghe et al. (2021). Therefore, effective management of water resources in the dry zone basins, which serve as crucial sources for irrigational purposes, becomes imperative.

This study is primarily focused on monitoring and predicting meteorological and hydrological droughts in the Maduru Oya and Kirindi Oya dry zone basins in Sri Lanka, which are pivotal for the agricultural productivity of the country. The study employs designated drought monitoring indices to assess the vulnerability of the selected basins to meteorological and hydrological droughts under both current climatic conditions and future climatic conditions. Simultaneously, the research aims to map the spatial distribution of meteorological droughts in these basins. At the same time, the occurrence of hydrological droughts in the future under two selected projected scenarios on a temporal basis is presented in this study. The findings of this

analysis are of significant importance, providing insights for agricultural planning, disaster management, and the formulation of effective drought mitigation strategies in the selected dry zone basins.

1.5 Main and Specific Objectives

1.5.1 Main objective

The main objective of the research is to analyze the impact of climate change on the temporal and spatial distribution of meteorological and hydrological droughts in the selected dry zone basins through drought monitoring and forecasting with the aid of selected drought monitoring indices.

1.5.2 Specific objectives

The specific objectives of the study are elaborated as follows:

1. To select suitable drought indices and estimate drought conditions using relevant climatic and other variables to monitor meteorological and hydrological droughts.
2. To estimate future streamflow data using an appropriate modelling technique and investigate the applicability of employing a machine learning approach in developing models for the estimation of predicted streamflow based on downscaled future climate data.
3. To forecast the occurrence of meteorological and hydrological droughts in the selected basins based on downscaled future climate data and predicted streamflow.
4. To graphically present the spatial distribution of meteorological droughts in selected basins under current and future climate scenarios.
5. To propose recommendations for drought impact mitigation and effective water resource management perspectives in the future based on the results.

2. LITERATURE REVIEW

2.1 Climate Change and Hydroclimatic Variability in Sri Lanka

Natural climate variability gives rise to numerous instances of hydroclimatic extremes. The implications of climate change are expected to bring about drought conditions in almost all parts of Sri Lanka. The prevailing influence of two primary monsoonal winds, specifically the Southwest monsoon and the Northeast monsoon, significantly shapes the climatic regime in Sri Lanka. At the same time, the shifts between these prevailing monsoons are characterized by two intermediary phases known as the first inter-monsoon and the second inter-monsoon. In parallel, the climatic dynamics are distinctly impacted by the El Niño-Southern Oscillation (ENSO) phenomenon (Naveendrakumar et al., 2018). Consequently, both ENSO and the South Asian monsoon emerge as paramount factors driving hydroclimatic variability within the context of Sri Lanka.

Moreover, a noticeable long-term increase in annual temperatures has been noted. The trends in mean monthly minimum and maximum temperatures reveal increases of 2.6 ℃ and 1.7 ℃ per 100 years, respectively. A substantial warming trend is observed in most districts of Sri Lanka, aligning with the broader context of climate change impacts on temperature patterns (Naveendrakumar et al., 2018).

On the other hand, anticipated adverse impacts on water resources due to greenhouse warming further underscore the complex interplay of climate change on hydroclimatic conditions. The accelerated hydrologic cycle brings about alterations in precipitation patterns, runoff volume, timing, and the frequency and severity of droughts and floods. Elevated temperatures also accelerate evapotranspiration, modify infiltration rates, and influence soil moisture. Changes in runoff primarily result from variations in precipitation and evaporation, with runoff elasticities showing higher sensitivity to changes in precipitation and temperature, particularly in arid climates (Frederick & Major, 1997).

Frederick and Major (1997) have projected that, under climate conditions equivalent to those of 1990, water availability in Sri Lanka may diminish by 2050. This reduction is further compounded by variations in water availability across a spectrum of scenarios. Consequently, the implications of climate change on water resources and subsequent availability necessitate comprehensive research for a thorough understanding of potential impacts.

2.1.1 El Niño-Southern Oscillation (ENSO)

The ENSO can be introduced as the preeminent climate mode that impacts global climate extremes. This phenomenon naturally transpires across the tropical Pacific region, oscillating between periods of unusually elevated temperatures (El Niño) and decreased temperatures (La Niña). The two phases are connected to the Walker

Circulation, which arises from the pressure gradient force stemming from the regional high-pressure system positioned above the eastern Pacific Ocean and the low-pressure system located over Indonesia (Dadson et al., 2019).

A considerable impact of ENSO has been detected on precipitation and temperature patterns in Sri Lanka. During El Niño events, precipitation increases approximately from October to December, while it declines during the periods of January to March and July to August. Consequently, a substantial decrease in river flow is observed from January to September during El Niño occurrences. Moreover, rice cultivation output during the Yala season (April–August) experiences a significant reduction in the El Niño periods (Zubair et al., 2008).

2.1.2 South Asian monsoon

The monsoon circulation is driven by disparities in temperature between land and sea, coupled with the intensity of atmospheric circulation and humidity levels in the air. These factors determine the extent and duration of monsoon precipitation. Additionally, topography and the influence of ENSO contribute to this phenomenon. Among the various regional monsoon systems, the South Asian monsoon stands out as the most influential, impacting approximately half of the global population (Dadson et al., 2019). It frequently gives rise to hazardous extreme weather events such as floods, landslides, and droughts. In the context of Sri Lanka, the hydroclimate is intensely affected by the South Asian monsoon wind system (Chaminda et al., 2016).

2.1.3 ETCCDI climate change indices

Climate indices serve as valuable tools for assessing and quantifying fluctuations in climate as well as the corresponding patterns. The climatic indices formulated by the Expert Team on Climate Change Detection and Indices (ETCCDI), constitute a fundamental collection of climate indicators utilized to observe instances of temperature and precipitation extremes and altogether 27 temperature and rainfall indices have been developed (Panda et al., 2016). The introduction of the ETCCDI core set of indices was driven by the aim to facilitate consistent calculations of these indices by individuals, countries, and regions. This uniform approach ensures that their analyses integrate smoothly into the global context (Yosef et al., 2021). Table 2.1 presents the list of rainfall indices used in this study.

Table 2.1: List of selected rainfall indices

Index	Definition	Unit
RX1day	Maximum 1-day rainfall	mm
RX5day	Maximum 5-day rainfall	mm
CWD	Maximum number of consecutive wet days	Days
CDD	Maximum number of consecutive dry days	Days
R10	Number of days with rainfall 10 mm or more	Days
R20	Number of days with rainfall 20 mm or more	Days
Rnn	Number of days with rainfall 64.5 mm or more	Days
PRCPTOT	Total rainfall on wet days	mm
SDII	Simple daily intensity index	mm/day

Note. A wet day is defined as a day with rainfall of 1 mm or more

Source: (Panda et al., 2016)

2.2 Concepts of Drought Characterization

Drought is a phenomenon that can be characterized through three primary aspects, namely intensity, duration, and spatial coverage. The intensity of drought refers to the severity of the deficit in rainfall, soil moisture, or water storage, which may also encompass the severity of the resulting impacts. The duration of drought is defined as the period during which the drought persists, ranging from several months to several years, with the possibility of extreme droughts occurring. Lastly, spatial coverage describes the geographical extent of the drought and can vary from small, localized areas to entire regions or even continents (Balti et al., 2020). In addition to these primary aspects, several other characteristics can be used to further characterize drought. These include frequency, magnitude, predictability, rate of onset, and timing (Zargar et al., 2011).

2.2.1 Drought types

Primarily droughts can be categorized as meteorological, hydrological, and agricultural droughts based on their physical characteristics. In addition to that, mainly the agricultural drought impacts the economy and society considerably. These impacts are referred to as socio-economic droughts (Sundararajan et al., 2021). Therefore, according to Balti et al. (2020), droughts can be generally classified into four types, namely, meteorological, hydrological, agricultural, and socio-economic droughts. The origin and flow of physical droughts are presented in Figure 2.1.

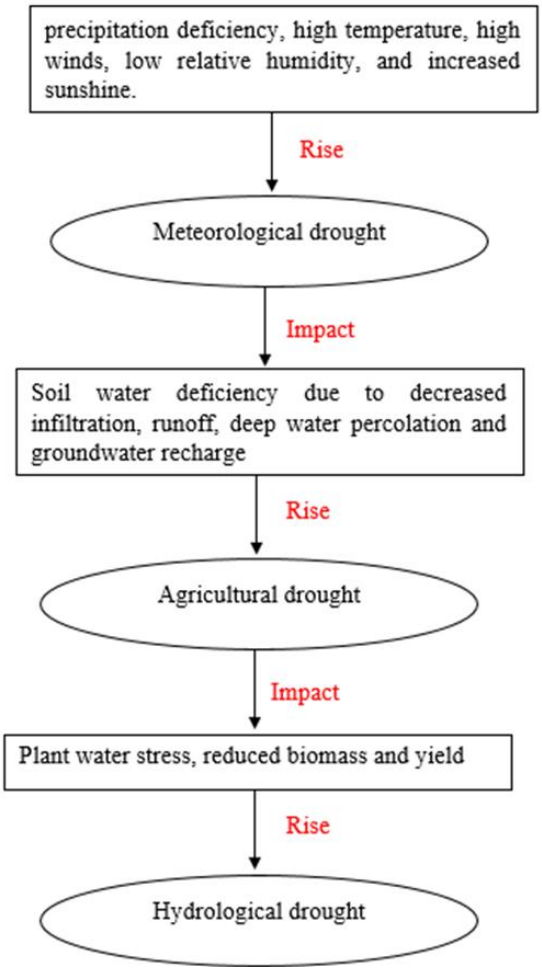

Figure 2.1: Origin and flow of physical droughts

Source: (Zargar et al., 2011)

2.2.2 Drought indicators

In addition to precipitation deficit, drought is also characterized by other variables such as evapotranspiration and streamflow, which are used to provide a more comprehensive understanding of drought conditions (Zargar et al., 2011). In order to derive a drought index, various models like water balance or hydrological models use

these different indicators or variables in combination. These indicators can fall into three categories: meteorological (such as precipitation and cloud cover), hydrological (such as streamflow and groundwater level), or related to water supply and demand (such as reservoir storage). However, certain indicators like precipitation, potential evapotranspiration, and soil and vegetation characteristics are more commonly used indicators and at the same time, they have a greater impact in practice (Loukas et al., 2008; Tsakiris, Pangalou, et al., 2007).

2.2.3 Characterization of droughts using drought indices

Drought indices are useful tools for monitoring and assessing the different types of droughts since they enable the dissemination of climate anomalies to a wide range of user audiences (Abeysingha et al., 2020). On the other hand, drought indices afford a more comprehensive understanding in contrast to raw data derived from individual indicators. Furthermore, over 150 different drought indices have been formulated for the purposes of aiding drought monitoring and assessing possible impacts (Zargar et al., 2011).

2.3 Drought Monitoring Indices

Indices serve as a means of measuring and assessing the severity of droughts. It is crucial to emphasize that these indices function as indicators in addition to quantifying droughts and their intensity (Yihdego et al., 2019). Table 2.2 presents the drought-type classification and suitable drought monitoring indices.

This study primarily focuses on meteorological and hydrological droughts. The Standardized Precipitation Index (SPI) is the predominant drought monitoring tool, acknowledged by the World Meteorological Organization as a benchmark for other indices. However, SPI solely relies on precipitation data and does not consider temperature, a vital factor for assessing the water balance of a region. This limitation becomes evident when comparing events with similar SPI values but different temperature conditions, making such comparisons more challenging. Due to the tropical island climate in Sri Lanka, temperature fluctuations are minor, and there is minimal spatial variation in temperature within small river basins. Consequently, the Standardized Precipitation Index (SPI) is well-suited for application in these smaller basins in Sri Lanka. Therefore, SPI was selected as the preferred index for monitoring meteorological droughts in this research (Abeysingha et al., 2020).

Globally, various hydrological drought indices are utilized, including the streamflow drought index (SDI), which shares similarities with SPI (Abeysingha et al., 2020; Tsakiris, Pangalou, et al., 2007). Building upon SPI concepts, Nalbantis and Tsakiris (2009) developed SDI for characterizing hydrological drought. Consequently, this study employed SDI to assess hydrological drought in the selected dry zone basins.

Table 2.2: Drought type classification

Drought Type	Definition	Monitoring Indices
Meteorological drought	Related to the prolonged deficiency in precipitation in a region (Balti et al., 2020).	PDSI (Palmer, 1965), SPI (Mckee et al., 1993), SPEI (Vicente-Serrano et al., 2010)
Hydrological drought	Occurs when flow of rivers and water accumulation in aquifers, ponds, or reservoirs reduce below usual levels (Balti et al., 2020).	PHDI (Palmer, 1965), SSI, SWSI (Zargar et al., 2011)
Agricultural drought	Refers to long-term soil moisture decline and consequent bio-mass and yield reduction (Balti et al., 2020).	Computed Soil Moisture (CSM), Z-index (Dai, 2011; Faghmous & Kumar, 2014)
Socio-economic drought	Links droughts with the supply and demand of water for economic goods (Balti et al., 2020).	Drought Area Index (DAI), Drought Severity Index (DSI)(Madani et al., 2016; Zargar et al., 2011)

Note. PDSI-Palmer Drought Severity Index, SPI-Standardized Precipitation Index, SPEI- Standardized Precipitation–Evapotranspiration Index, PHDI-Palmer Hydrological Drought Index, SSI- Standardized Streamflow Index, SWSI-Surface Water Supply Index.

2.4 Future Climate Data

The crucial aspect of comprehensive drought management for any region lies in the ability to anticipate plausible future drought scenarios and implement effective response measures. On the other hand, both quantitative and qualitative analyses of drought projections play a vital role in endorsing and formulating effective drought countermeasures (Zhai et al., 2020). Global Climate Models (GCMs) that encompass complex geo-bio-chemical processes are essential tools for accurately forecasting future climate changes (Zhu et al., 2021). The Coupled Model Inter-comparison Project (CMIP), established under the World Climate Research Program, constitutes a structured framework designed for comparing and evaluating GCMs. This project encompasses several distinct phases, each facilitating comprehensive assessments of the performance of models and their ability to simulate and project future climate patterns (Hamed et al., 2022).

Moreover, the outcomes generated by GCMs participating in the CMIP have proven highly valuable in the assessment of forthcoming climatic hazards, such as droughts.

The sixth phase of the CMIP (CMIP6) framework has been specifically developed to meet the growing needs of the scientific community and to address the limitations identified in the previous CMIP5 framework. This new phase aims to enhance and expand the scope of climate modeling capabilities, providing more comprehensive and accurate insights into climate-related phenomena for scientific research and policy formulation (Kumar et al., 2021). Hence, in this study the Global Climate Model (GCM) projections obtained from the latest phase of the Coupled Model Inter-comparison Project (CMIP6) will be used. This approach is aimed at evaluating and quantifying the potential impacts of future climate changes on the exposure of the population to drought conditions with improved accuracy and relevance.

The CMIP6 incorporates nearly 30 enhanced Global Climate Model (GCM) outputs, contributed by multiple modelling centres. From this pool of available models, the analysis for this study has specifically chosen six GCM models to be included in the examination and the details of the selected models are presented in Table 2.3. These improved GCM outputs encompass various emission scenarios, each following distinct forcing trajectories. The Scenario Model Intercomparison Project (ScenarioMIP) forms the core of the 6^{th} phase, focusing on designing and assessing these different emission scenarios to facilitate comprehensive climate model intercomparisons. The newly introduced scenario framework in the recent phase, denoted as SSPs-RCPs, has been formulated by integrating exposure and vulnerability concepts in the context of a changing climate. This integration effectively connects the representative concentration pathways (RCPs) with shared socioeconomic pathways (SSPs). This integrated approach enables the projection of future pathways considering both climate changes and their potential impacts on exposure and vulnerability factors (Kumar et al., 2021).

With careful consideration of the impacts of climate change and various policies, a set of five new shared socioeconomic pathways (SSPs) has been devised. These pathways delineate plausible and alternative transformations in various societal dimensions, encompassing demographic, economic, technological, social, governance, and environmental aspects (Mondal et al., 2021). The SSPs encompass sustainability (SSP1), a middle-of-the-road approach with historical trends (SSP2), fragmentation (SSP3), inequality (SSP4), and growth-oriented development (SSP5) (O'Neill et al., 2017). The scenarios used in this study, namely SSP1-2.6 and SSP5-8.5, are representative of low and high emission trajectories, respectively. These scenarios have been selected to effectively represent different levels of greenhouse gas emissions and their potential impacts on future climate and socioeconomic conditions, providing a robust framework for analysis and assessment.

Table 2.3: List of CMIP6 models selected for the study

No.	Model Name	Country	Horizontal Resolution (Lon. × Lat. in degrees)
1	ACCESS-CM2	Australia	1.9°× 1.3°
2	BCC-CSM2-MR	China	1.1°× 1.1°
3	CAMS-CSM1-0	China	1.1°× 1.1°
4	CESM2	USA	1.3°× 0.9°
5	CNRM-CM6-1-HR	France	0.5°× 0.5°
6	CNRM-ESM2-1	France	1.4°× 1.4°

2.4.1 Downscaling of climate projections from GCMs

The outputs derived from Global Climate Models (GCMs) necessitate post-processing, involving bias correction and downscaling before being used in studies assessing the impacts of climate change. This post-processing step becomes imperative due to biases against observed data and the insufficient spatial resolution present in the original GCM outputs. This necessary adjustment ensures that the GCM data aligns more accurately with observed measurements and meets the requirements of the spatial resolution demands of a specific study (Wang et al., 2016).

The process of climatic downscaling can be classified into two main categories namely, dynamic approaches, which involve explicit solving of physical dynamics, and empirical methods, also known as "statistical downscaling". Dynamic downscaling aims to extract local-scale information from the large-scale Global Climate Model (GCM) data, and this objective is accomplished through the utilization and development of limited-area models (LAMs) or regional climate models (RCMs) (Xu, 1999). On the other hand, the computationally demanding characteristics of dynamical downscaling pose challenges when attempting to conduct multi-decade simulations involving multiple Global Climate Models (GCMs) and/or greenhouse gas scenarios. The complex computational requirements make it difficult to efficiently carry out such extensive simulations using dynamical downscaling techniques (Wang et al., 2016).

On the contrary, statistical downscaling methods demonstrate computational efficiency and sufficient flexibility, enabling their direct application in climate change impact studies. Particularly in situations where cost-effective and expeditious evaluations of localized climate change impacts are needed, statistical downscaling currently stands out as the more promising and favourable option (Wilby & Dawson, 2007; Xu, 1999). Among the assortment of statistical downscaling methods, a category known as 'empirical downscaling methods' or 'empirical scaling methods' is gaining

popularity, particularly in situations where the analysis demands multi-GCM projections. These methods are designed to mitigate biases in climate model outputs and have become increasingly favored in climate change impact studies. The simplicity of their application contributes to their widespread utilization among the various statistical methodologies discussed in the literature (Chen et al., 2013; Wang et al., 2016).

Empirical statistical downscaling methods can be categorized into two types namely, Bias Correction (BC) and Change Factor (CF) approaches (Chen et al., 2013). In this study, the Bias Correction (BC) approach was chosen as the selected method. Table 2.4 provides an overview of bias-correction methods that can be utilized for empirical statistical downscaling.

Table 2.4: Bias correction methods

Method	For precipitation	For temperature
Mean-based method	$X_o' = X_M' \times \frac{\mu_O}{\mu_M}$	$X_O' = X_M' + (\mu_O - \mu_M)$
Variance-based method	$X_O' = \left(\frac{X_M' - \mu_M}{\sigma_M}\right) \times \sigma_O + \mu_O$	$X_O' = \left(\frac{X_M' - \mu_M}{\sigma_M}\right) \times \sigma_O + \mu_O$
Quantile mapping	$X_O' = F_O^{-1}[F_M(X_M')]$	$X_O' = F_O^{-1}[F_M(X_M')]$
Quantile correcting	$X_O' = X_M' \times \frac{F_O^{-1}[F_{M'}(X_M')]}{F_M^{-1}[F_{M'}(X_M')]}$	$X_O' = X_M' + F_O^{-1}[F_{M'}(X_M')] - F_M^{-1}[F_{M'}(X_M')]$
Transfer function	$X_O' = a \times X_M'^b$	$X_O' = a \times X_M' + b$

Source: (Wang et al., 2016)

2.5 Machine Learning Methods for Streamflow Simulations

In the context of this study, it is required to obtain future streamflow data for the purpose of estimating the Streamflow Drought Index (SDI). This estimation is essential for monitoring the occurrence of hydrological droughts in the future. The calculation of SDI relies solely on streamflow values and is analogous to the Standardized Precipitation Index (SPI) (Nalbantis & Tsakiris, 2009).

The process of streamflow is complex and inherently unpredictable, influenced by multiple parameters such as precipitation, temperature, evapotranspiration, and land use. Moreover, the connection between streamflow and the characteristics of the watershed is nonlinear, adding to the intricacy of the process (Adnan et al., 2019). Models for predicting streamflow can be broadly categorized into physically based models and data-driven models. Physically based models rely on extensive data and

necessitate various factors, encompassing rainfall amount, intensity, distribution, as well as physiographic features of the watershed, land use, and anthropogenic activities (Parisouj et al., 2020). However, ensuring consistent model performance universally is challenging, as it depends on the specific study area and intended purpose. Obtaining accurate and sufficient data for numerous watersheds presents difficulties, often resulting in suboptimal model outcomes (Ragettli et al., 2014).

In contrast, data-driven models have gained prominence owing to their minimal data requirements, rapid development, simplicity, and accuracy in streamflow predictions. (Karran et al., 2014). Machine learning can also be introduced as a statistical approach characterized by data-driven and self-adaptive features (Liu et al., 2020). This study uniquely focuses on the application of data-driven models for streamflow prediction. Conventional data-driven predictions of streamflow have historically relied on statistical models such as multiple linear regression (MLR) and autoregressive integrated moving average (ARIMA) models. While these methods have demonstrated relatively satisfactory performance in long-term forecasting, both are constrained by their fundamental assumption of linearity in the data. Subsequently, non-linear models utilizing machine learning methods like Artificial Neural Networks (ANNs), Support Vector Machines (SVMs), and Random Forest (RF) have become widely adopted for hydrologic predictions (Karran et al., 2014).

2.5.1 Prediction of streamflow using a neural network employing deep learning techniques

As a subfield within machine learning techniques, deep neural networks have been increasingly employed in predictive research in recent years, facilitated by the abundance of observational data and enhanced computing power. The majority of deep learning architectures are derived from neural networks (NNs), which consist of layers including input, output, and hidden layers and neurons. At the same time, they possess the ability to handle temporal structures within time series data efficiently, promptly capturing temporal dependencies. As a result of this adept handling of sequential information, deep learning algorithms stand out in their ability to construct optimal predictive models, particularly when dealing with non-linear data patterns. The cyclic nature of cells allows them to retain crucial information from preceding time steps (Liu et al., 2020).

The Long Short-Term Memory (LSTM), categorized as a specific type of Recurrent Neural Network (RNN), exhibits an extended memory capacity, enabling it to retain information over a long time. Notably, the LSTM model possesses the capability to selectively forget irrelevant information during the training process, a functionality attributed to the dynamic adjustments within the internal structure of the RNN. This architecture of LSTM contributes to enhanced performance compared to other deep learning structures in the prediction of long-term time series (Liu et al., 2020).

2.5.2 Prediction of streamflow using the ensemble machine learning approach of random forest algorithm

The Random Forest constitutes an ensemble machine learning methodology that makes predictions through an extensive assembly of classification or regression trees, known as CART. Owing to its notable stability and versatility, this approach has found extensive application across various domains such as land subsidence, invasive plant monitoring, groundwater analysis, gully head susceptibility assessment, and forest fire susceptibility prediction. In the process of training regression trees, rules are formulated based on the response variable to sequentially partition observations. This partitioning continues until the resulting predictions reach a minimum threshold of node impurity. The collective outputs derived from individual decision trees form the ultimate output of the Random Forest model (Jibril et al., 2022).

Miller et al. (2018) have developed 120 Random Forest Models to predict observed streamflow at reference sites. The squared correlation coefficient (R^2) and Nash–Sutcliffe coefficient (NSE) have been chosen as the model fit statistics for evaluating performance. The mean R^2 across all models ranged from 0.5 to 0.96 with a median value of 0.85, while the mean NSE ranged from 0 to 0.96 with a median value of 0.87. These findings suggest superior model performance compared to values reported for water balance models. The Random Forest algorithm has frequently been employed for streamflow predictions, consistently demonstrating better model fits. This underscores the suitability of using the Random Forest algorithm for predicting streamflow (Jibril et al., 2022).

3. METHODOLOGY

3.1 General

This chapter outlines the methodology employed to fulfil the primary and specific goals of the study. To effectively achieve the research objectives, it is crucial to identify appropriate drought monitoring indices to assess drought conditions in the designated dry zone basins. Therefore, the Standardized Precipitation Index (SPI) was chosen as the meteorological drought monitoring index, while the Streamflow Drought Index (SDI) was chosen as the hydrological drought monitoring index based on literature and due to their simplicity in evaluating drought conditions within the chosen basins, considering both present and future climate scenarios.

In order to enhance future drought monitoring, the CNRM-CM6-1-HR model was specifically chosen from the six CMIP6 models assessed in this study. This selection was made based on the objective function values obtained during the bias correction process. The CMIP6 dataset utilized in this study was acquired from the official CMIP6 database website (https://esgf-node.llnl.gov/search/cmip6).

Commencing with the need for generating maps illustrating the meteorological drought status in the designated basins, a gridded dataset was imperative. The Climate Hazards Group InfraRed Precipitation with Station data (CHIRPS), boasting a resolution of 25 km^2, was employed for this purpose. Establishing statistical relationships between each grid point and observed data from the nearest station was a monthly endeavour, utilizing baseline data spanning from 1983 to 2015. These developed relationships were subsequently applied to future data, resulting in the creation of a gridded dataset for future projections. Following this, the Standardized Precipitation Index (SPI) was computed at a three-month scale to monitor meteorological drought conditions. The estimated SPI values served as the basis for generating maps delineating the spatial distribution of extreme, severe, and moderate drought conditions in the selected dry zone basins. These maps were crafted for both the historical period (1983-2014) and the future period (2015-2100), taking into account two distinct projection scenarios: SSP1-2.6 and SSP5-8.5.

On the other hand, for future hydrological drought monitoring purposes, it was necessary to predict future streamflow for the two selected gauging stations in the designated dry zone basins. To forecast these streamflow values, machine learning methods were employed due to their ability to handle the nonlinearity inherent in the streamflow process, as compared to conventional physically-based hydrological models. Hydrological drought monitoring was conducted utilizing only one gauging station per basin, considering the available data. The Streamflow Drought Index (SDI) was estimated using historical and future streamflow data. Additionally, the Standardized Precipitation Index (SPI) was calculated for the same locations.

Subsequently, hydrological drought monitoring was conducted based on the calculated SDI and SPI values.

3.2 Methodology Flowchart

Figure 3.1 illustrates the methodology flowchart elaborating on the stepwise approach followed in the study. The tools and methods used in each step are discussed within the corresponding subsections of this chapter.

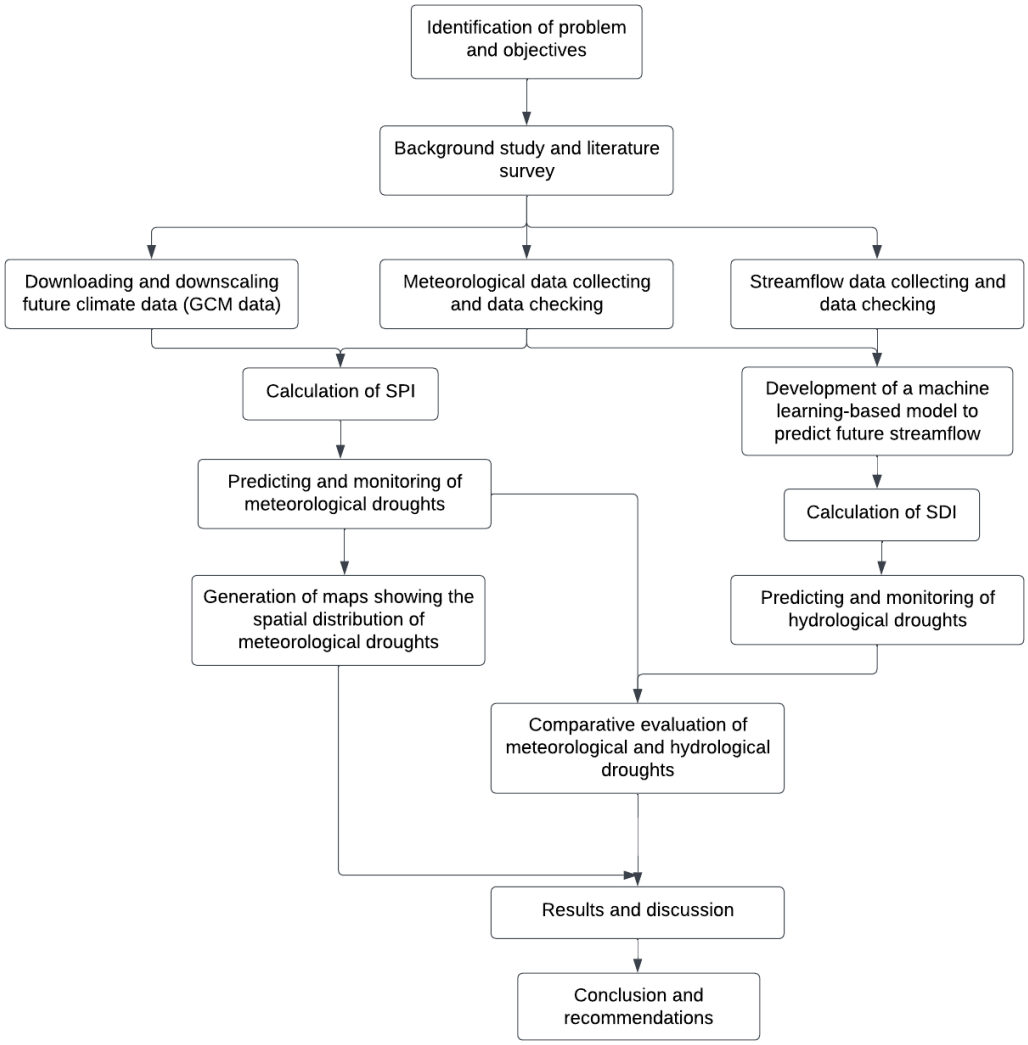

Figure 3.1: Methodology flowchart

3.3 Study Area

Irrigation stands as the predominant water use sector in Sri Lanka, constituting 92% of total water withdrawals, with dry zone alone accounting for 94% of irrigation withdrawals. Furthermore, the dry zone encompasses 91% of the gross irrigated area and a substantial 80% of the gross rice area, with 91% of the irrigated rice area falling

within their bounds. Given these statistics, it is evident that the dry zone regions play a pivotal role in the agricultural landscape of Sri Lanka and water resource utilization (Amarasinghe, 2010).

In light of the aforementioned, this research focuses primarily on two significant dry zone basins in Sri Lanka, the Maduru Oya basin and the Kirindi Oya basin. These basins were meticulously selected as the study area due to their ecological, hydrological, and agricultural significance, which collectively contribute substantially to conservation efforts and food security initiatives in the country.

According to Amarasinghe (2010), the total irrigation withdrawal as a percentage of average runoff varies notably between these two basins. Specifically, the Kirindi Oya basin exhibits a range from 20% to 40%, whereas the Maduru Oya basin demonstrates a significantly higher range from 60% to 90%. This discrepancy underscores the critical importance of assessing water availability, particularly in terms of drought occurrence, within these river basins.

3.3.1 Maduru Oya basin

A substantial portion of the Maduru Oya basin is located in the dry zone, specifically within the Polonnaruwa and Batticaloa administrative districts in the eastern part of the country. It also extends into the intermediate zone of Sri Lanka. The total catchment area of this river basin is 1,541 km² (Kirupacaran, 2020). The Maduru Oya project constitutes one of the five major reservoir projects under the Accelerated Mahaweli Development Program that spanned from the 1980's in Sri Lanka, rendering the Maduru Oya river basin a significant area in the country (Mahenthiran & Rajapakse, 2021). Additionally, Maduru Oya has been identified as a basin with a high hazard level in the drought hazard analysis conducted by Alahacoon and Amarnath (2022). Hence, it is imperative to assess the occurrence of droughts in the Maduru Oya basin.

For the analysis, five rain gauging stations and the Padiyathalawa streamflow gauging station were chosen. Figure 3.2 depicts the study area map and the selected gauging stations. The location coordinates of the chosen rainfall and streamflow gauging stations are provided in Table 3.1 and Table 3.2, respectively.

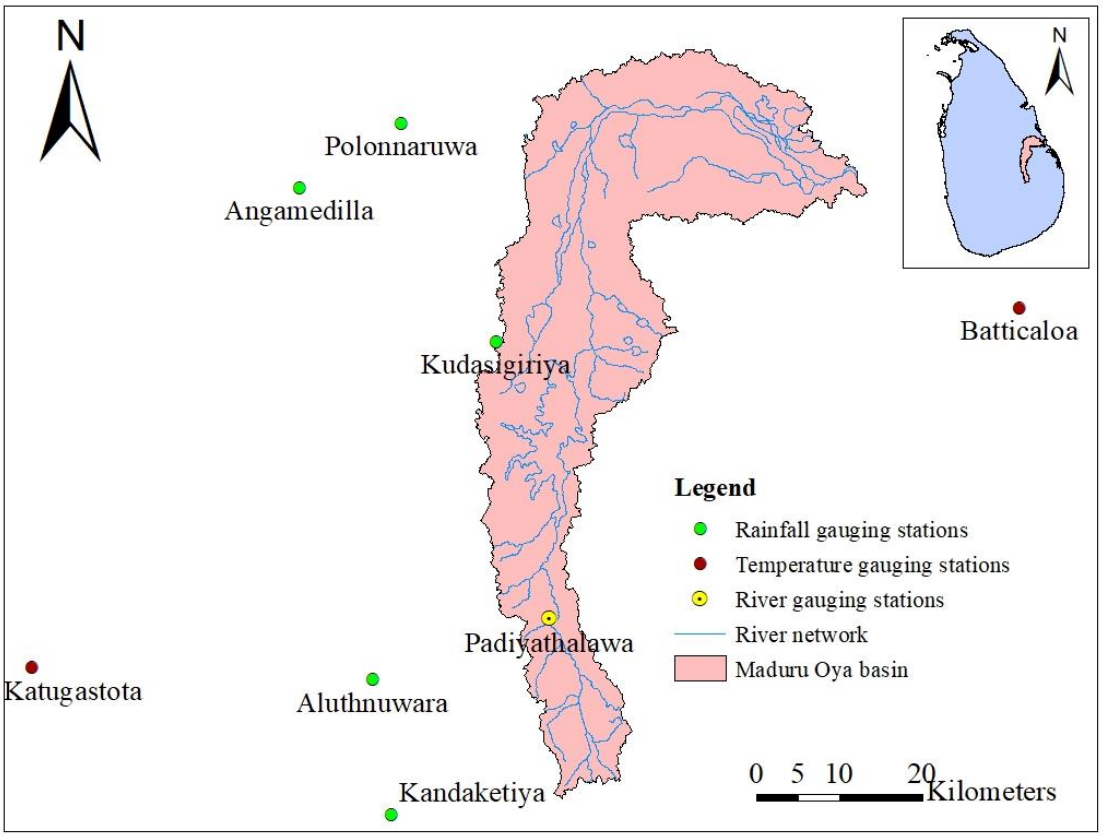

Figure 3.2: Maduru Oya basin and selected gauging stations

Table 3.1: Coordinates of the selected rainfall gauging stations for the Maduru Oya basin

Rainfall Gauging Station	Coordinates	
	Latitude (N)	Longitude (E)
Polonnaruwa Agri	7° 55' 12"	81° 01' 48"
Angamedilla	7° 51' 00"	80° 55' 12"
Aluthnuwara	7° 19' 00"	81° 00' 00"
Kandaketiya	7° 10' 12"	81° 01' 12"
Kudasigiriya	7° 41' 00"	81° 08' 00"

Table 3.2: Coordinates of river gauging station of Maduru Oya basin

River Gauging Station	Coordinates	
	Latitude (N)	Longitude (E)
Padiyathalawa	7° 23' 01"	81° 11' 28"

3.3.2 Kirindi Oya basin

The Kirindi Oya river basin is situated in the dry zone of Sri Lanka, specifically in the southeastern region (refer to Figure 3.3). This river basin encompasses a catchment area of 1,203 km^2 (Abeysingha et al., 2020). The water from Kirindi Oya serves multiple purposes, being utilized by Debera Wewa (Tank), Bandagiriya Wewa, Yoda Wewa, Tissa Wewa, Pannagamuwa Wewa, and Weerawila Wewa (Mahenthiran & Rajapakse, 2021). The basin exhibits distinctive traits, including limited rainfall, elevated ambient temperatures, and reduced relative humidity. Consequently, there is heightened evaporation, surpassing the precipitation for the majority of the months annually. As a result, evaluating drought conditions holds paramount significance for water planning and management within the basin. Furthermore, the assessment of both meteorological and hydrological drought proves valuable for agricultural planning in the region (Abeysingha et al., 2020).

To conduct the analysis, four rain gauging stations and two streamflow gauging stations were chosen. The study area map and the specific gauging stations selected are illustrated in Figure 3.3, while the location coordinates of these selected stations are provided in Tables 3.3 and 3.4.

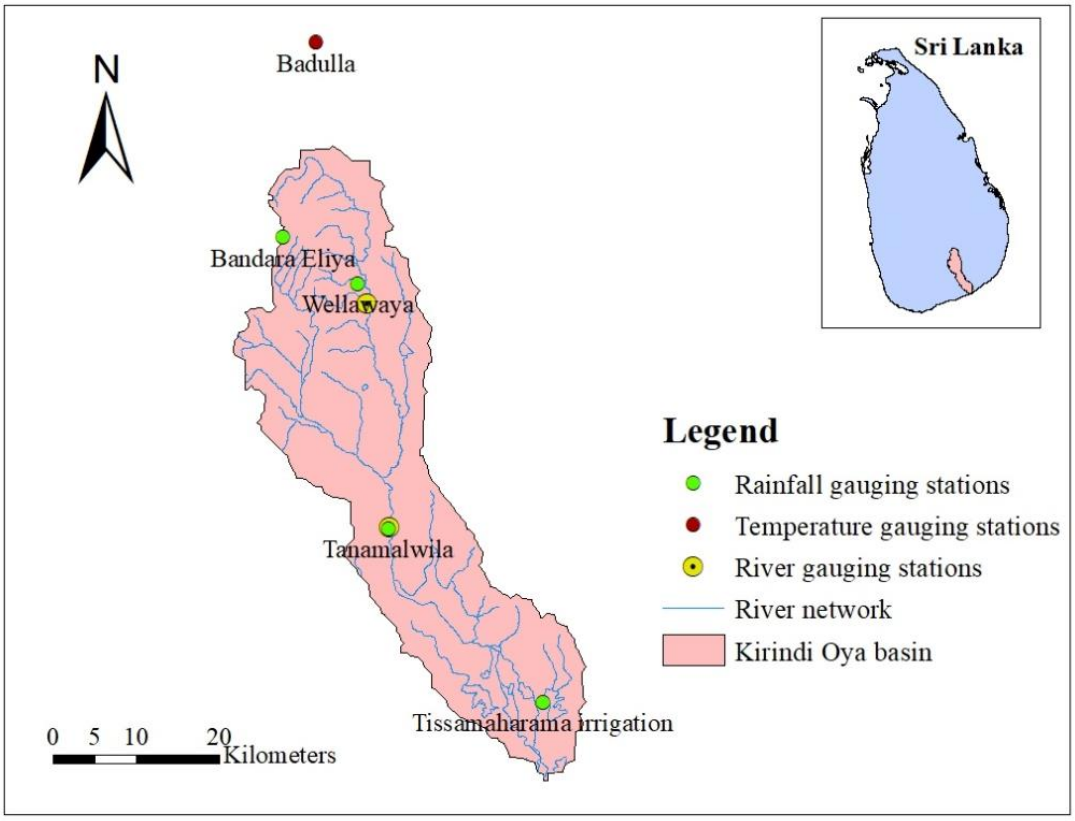

Figure 3.3: Kirindi Oya basin and selected gauging stations

Table 3.3: Coordinates of the selected rainfall gauging stations for the Kirindi Oya basin

Rainfall Gauging Station	**Coordinates**	
	Latitude (N)	**Longitude (E)**
Bandaraeliya	6° 46' 48"	81° 01' 12"
Thissamaharama Irrigation	6° 16' 48"	81° 18' 00"
Wellawaya	6° 43' 48"	81° 01' 12"
Thanamalwila	6° 28' 12"	81° 07' 12"

Table 3.4: Coordinates of river gauging stations of Kirindi Oya basin

River Gauging Station	**Coordinates**	
	Latitude (N)	**Longitude (E)**
Wellawaya	6° 43' 48"	81° 06' 00"

3.4 Data Collection and Data Checking

This study primarily relied on observed rainfall and streamflow data. Table 3.5 presents the data sources and resolution utilized for both the Maduru Oya basin and the Kirindi Oya basin.

Table 3.5: Data sources and resolution

Maduru Oya basin				
Data Type	**Station**	**Selected Period**	**Temporal Resolution**	**Source**
Rainfall	Polonnaruwa Agri	1983-2015	Daily	Dept. of Meteorology
	Angamedilla			
	Aluthnuwara			
	Kandaketiya			
	Kudasigiriya			
Streamflow	Padiyathalawa			Dept. of Irrigation
Kirindi Oya basin				
Data Type	**Station**	**Selected Period**	**Temporal Resolution**	**Source**
Rainfall	Bandaraeliya	1983-2015	Daily	Dept. of Meteorology
	Thissamaharama Irrigation			
	Wellawaya			
	Thanamalwila			
Streamflow	Wellawaya			Dept. of Irrigation

Daily data were collected from the Department of Meteorology and the Department of Irrigation, Sri Lanka. Monthly data were subsequently derived from the collected daily data and used for the analysis since drought assessment typically relies on monthly data, and smaller time intervals do not have a noteworthy impact when using general indices to evaluate drought conditions (Tsakiris, et al., 2007). Data checking procedures encompassed visual observation, as well as the analyses of single mass curve and double mass curve, to assess and scrutinize the daily precipitation and streamflow data, ensuring the integrity, uniformity, and consistency of the data (Punsara & Rajapakse, 2021).

The process of visual data checking involves generating a graphical representation that illustrates the relationship between rainfall and streamflow. Discrepancies in the

patterns of rainfall and streamflow can be identified in a preliminary manner through this visual analysis. Visual data checking was conducted for each water year from the water year 1984/1985 to the water year 2014/2015 for both basins. Figure 3.4 illustrates rainfall-runoff graphs for the Padiyathalawa gauging station in the Maduru Oya basin from the water year 2010/2011 to the water year 2011/2012. The observed inconsistencies have been marked as red circles. It can be observed that in October 2011 and September 2012, although a considerable amount of rainfall has been recorded, the streamflow response has shown comparatively low values.

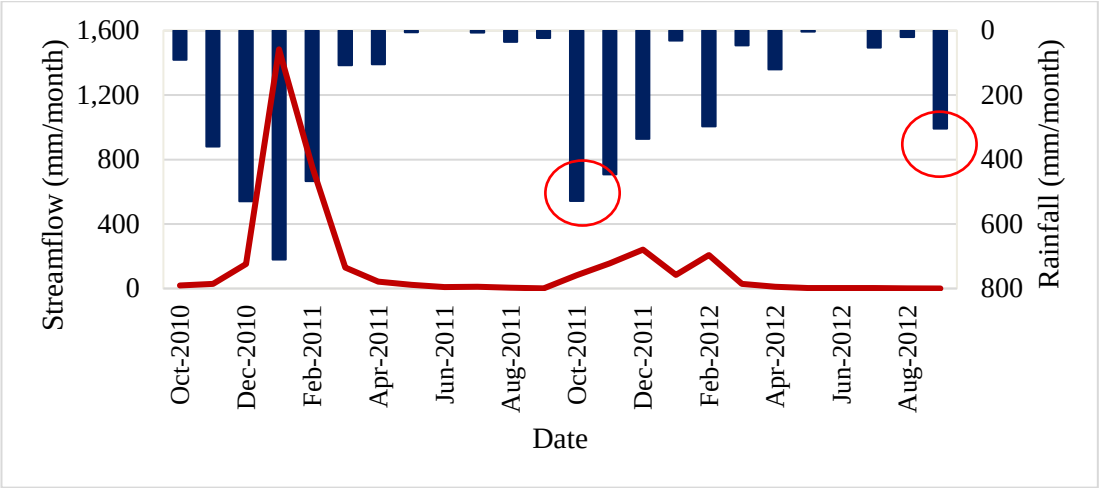

Figure 3.4: Padiyathalawa streamflow response with rainfall from 2010/2011 to 2011/2012

Figure 3.5 illustrates rainfall-runoff graphs for the Wellawaya gauging station in the Kirindi Oya basin from the water year 2004/2005 to the water year 2005/2006.

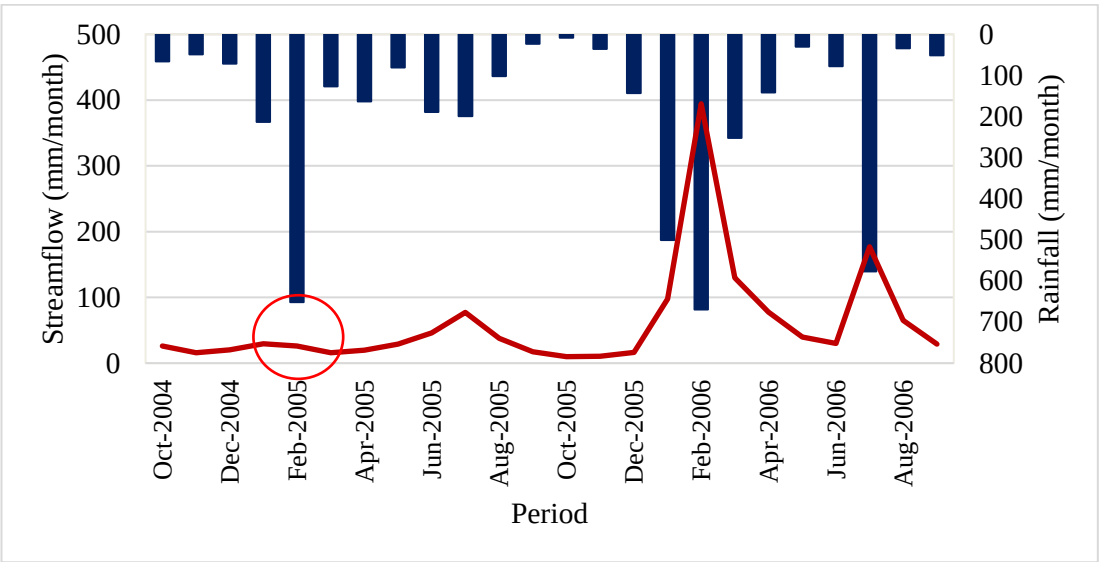

Figure 3.5: Wellawaya streamflow response with rainfall from 2004/2005 to 2005/2006

A considerable discrepancy can be observed in February 2005, where the streamflow response is significantly lower compared to the recorded rainfall.

To address missing data, the closest station patching method was applied, following the approach outlined by Punsara and Rajapakse (2021) where the missing data percentage was less than 10%.

3.4.1 Single mass curve

The analysis of temporal trends in rainfall stations can be facilitated by using single mass curves, which are plotted for each specific rainfall station (Punsara & Rajapakse, 2021). The single mass curves, depicting the temporal trends of the selected rain gauging stations of the Maduru Oya basin and Kirindi Oya basin, are presented in Figure 3.6 and Figure 3.7, respectively. In order to make effective use of rainfall records obtained from a specific station, it is important to thoroughly examine the data for consistency and continuity. Similarly, for the purpose of efficiently monitoring drought conditions, it is essential to possess a comprehensive dataset that does not contain any missing values. As a result, it becomes crucial to estimate the missing data prior to conducting the analysis.

For the purpose of estimating and imputing missing data, the closest station patching method was utilized as outlined by Punsara and Rajapakse (2021). In accordance with this approach, the initial step involved extracting the necessary data from a neighbouring gauging station exhibiting a comparable trend to the station with missing data. Subsequently, the extracted data were multiplied by the ratio of the slope of the single mass curve of the station with missing data to that of the neighbouring station, which provided the substituted data. Finally, the missing values were filled with the calculated value obtained through this procedure.

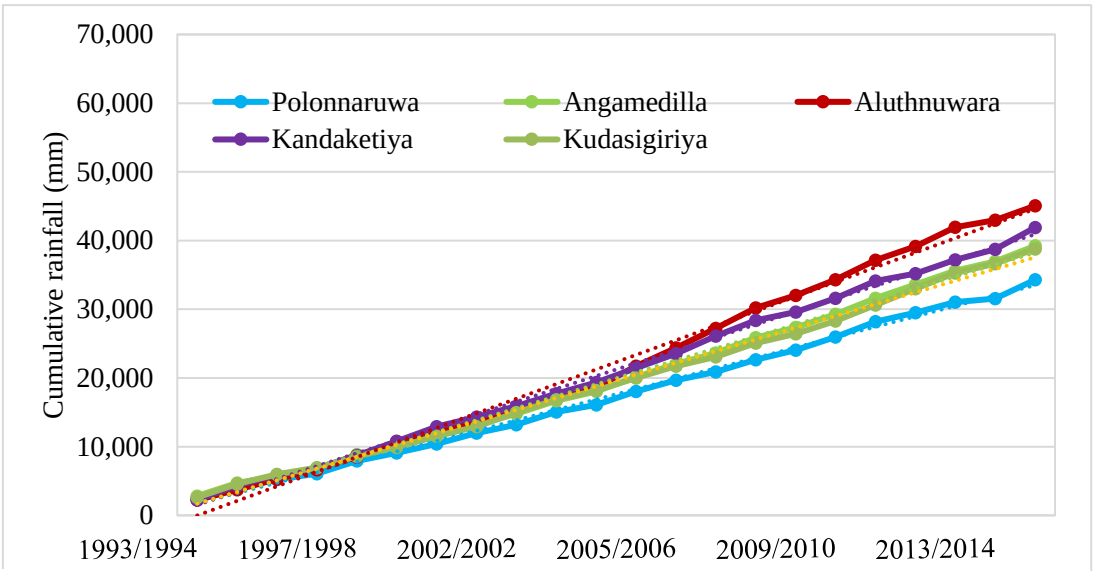

Figure 3.6: Single mass curves for the Maduru Oya basin

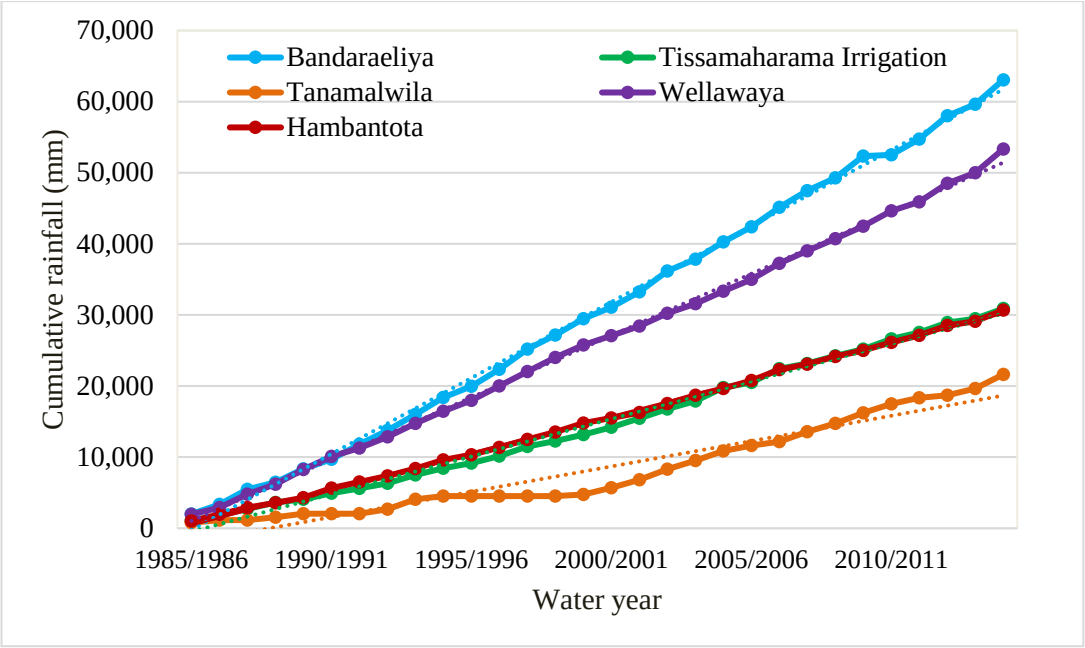

Figure 3.7: Single mass curves for the Kirindi Oya basin

In the single mass curve plotted for the Thanamalwila rain gauging station within the Kirindi Oya basin, noteworthy discontinuities are particularly visible during the period spanning from the 1994/1995 water year to the 1999/2000 water year. These discontinuities are ascribed to a significant proportion of total missing data, accounting for 38.9%. Consequently, the adoption of the closest station patching method may not be regarded as an advantageous approach for the supplementation of the missing data. To address this data gap at the Thanamalwila station, data from the Hambantota station were employed, as both stations are positioned within the same isohyetal layer. The choice of utilizing data from stations within the same isohyetal layer is grounded in the presumption that they experience analogous precipitation patterns. Despite the approximate distance of 45 km between the two gauging stations, Harischandra et al. (2016) state that Thanamalwila and Hambantota belong to the arid zone and share similar climatic conditions.

3.4.2 Double mass curve

The double mass curve methodology serves as a tool for scrutinizing the consistency of hydrological or meteorological records obtained from multiple locations. Simultaneously, double mass curves can be employed for temporal trend analysis of hydro-meteorological data. It involves the comparison of data from an individual station with a pattern derived from data collected across several other stations within the same geographic area. A straight-line graph that illustrates the cumulative data of one variable against the cumulative data of a related variable, indicates a consistent ratio relationship between the two variables. Disruptions in the graph may arise due to various factors, including alterations in the measurement instrumentation or changes

in the observation procedures (Jayadeera, 2016). There is no significant inconsistency observed in the rainfall data, as indicated by the straight-line nature of the plotted graphs for all stations. The double mass curves for the Polonnaruwa station in the Maduru Oya basin and the Bandaraeilya station in the Kirindi Oya basin are illustrated in Figure 3.8 and Figure 3.9, respectively. The corresponding plots for rainfall stations at other locations are provided in Appendix A.

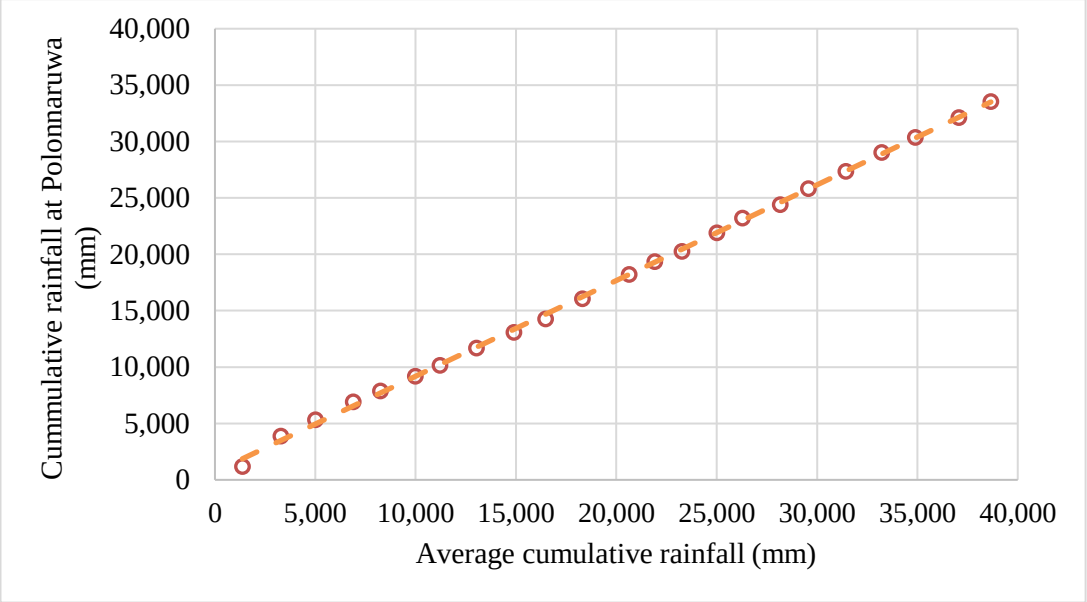

Figure 3.8: Double mass curve for Polonnaruwa rainfall station (Maduru Oya river basin)

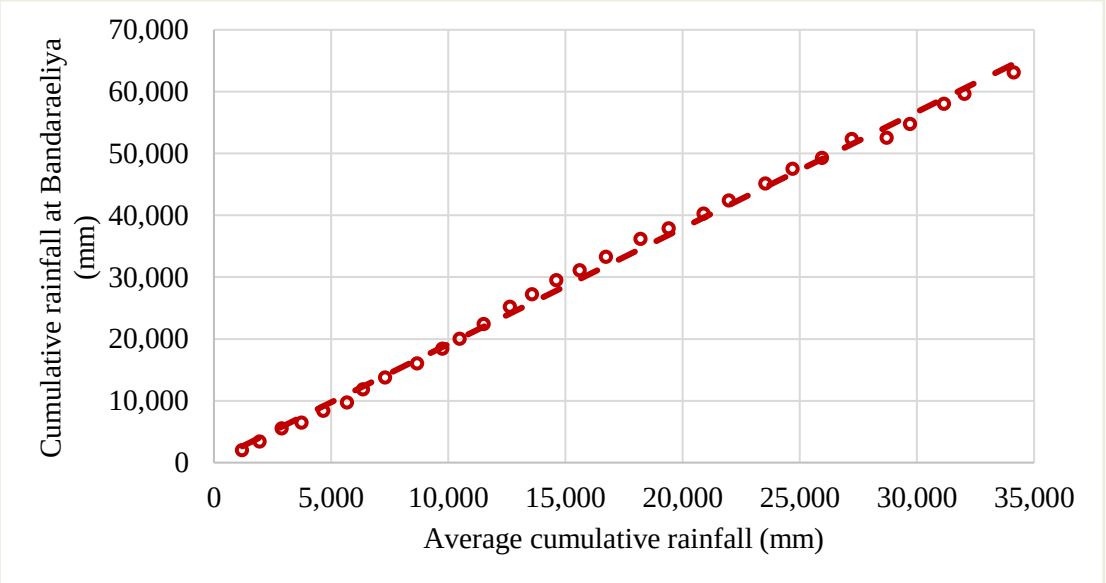

Figure 3.9: Double mass curve for Bandaraeliya rainfall station (Kirindi Oya river basin)

3.5 Calculation of ETCCDI Climate Change Indices

The 11 selected rainfall Climate Change Indices (ETCCDI) were computed using the RStudio software, and Climate Hazards Group InfraRed Precipitation (CHIRPS) daily data from 2000 to 2020 were utilized for the analysis. The maps, illustrating the values of the indices for each year from 2000 to 2020, are presented in Chapter 4. Additionally, the maximum consecutive wet days and maximum consecutive dry days were estimated using the Thiessen average rainfall of the basin, calculated from the observed dataset spanning from 1985 to 2015. The results of these analyses are also presented in Chapter 4.

3.6 Bias Correction of GCM Output

Firstly, comparative plots were created to assess the similarity between the raw data extracted from the six selected models and the observed data. These plots aimed to identify any shared trend patterns within the observed time series. Figure 3.10 presents the time series plots for the chosen models and observed data, focusing specifically on the data collected at the Thissamaharama Irrigation gauging station. Markedly a consistent pattern was evident among all the models, except for the two models, BCC-CSM2-MR and CESM2, across all the gauging stations. Subsequently, the bias correction was performed by computing bias correction factors using the mean-based method and variance-based method. Firstly, historical data spanning from 1983 to 2015 were extracted to estimate bias-correction factors. The coefficient of determination (R^2) was selected as the objective function to assess the performance of the selected climate models. The R^2 is defined as in Equation 3.1,

$$R^2 = \frac{n\sum_{i=1}^{n} O_i S_i - \sum_{i=1}^{n} O_i \sum_{i=1}^{n} S_i}{\sqrt{[n\sum_{i=1}^{n} O_i^2 - (\sum_{i=1}^{n} O_i)^2] - [n\sum_{i=1}^{n} S_i^2 - (\sum_{i=1}^{n} S_i)^2]}} \quad (3.1)$$

where *Oi* and *Si* are observed rainfall (mm) and model rainfall (mm), respectively. The recommended ranges for the coefficient of determination (R^2) are tabulated in Table 3.6.

Table 3.6: Recommended ranges for R^2

Performance Rating	R^2
Very good	$0.75 < R^2 \leq 1.0$
Good	$0.65 < R^2 \leq 0.75$
Satisfactory	$0.5 < R^2 \leq 0.75$
Unsatisfactory	$R^2 \leq 0.5$

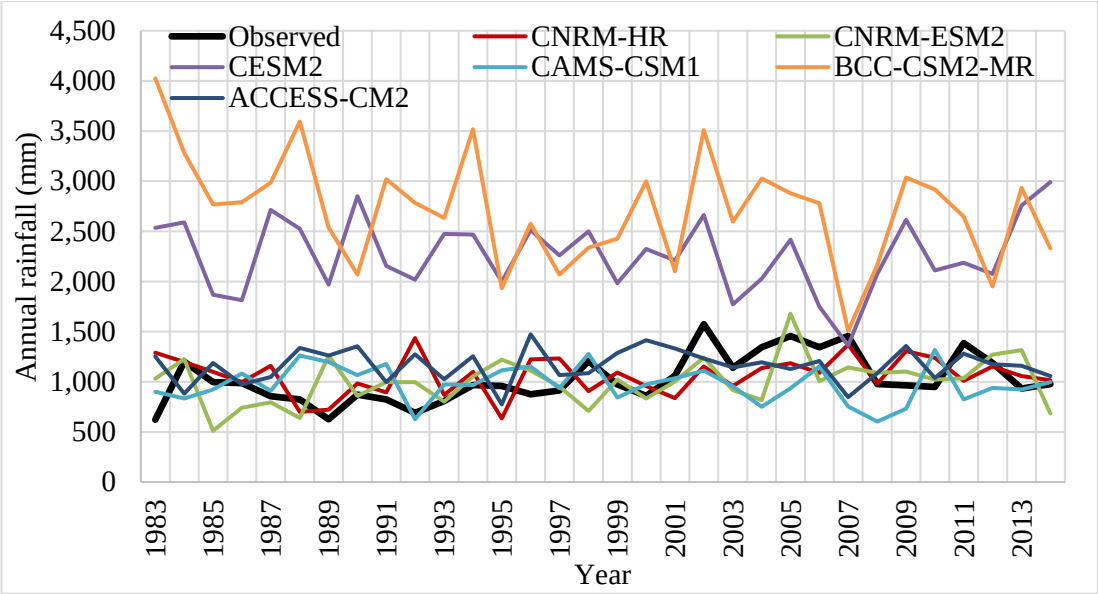

Figure 3.10: Variation of the annual rainfall of selected GCM models

3.7 Generation of Maps showing the Probability of Occurrence of Different Drought Categories

Firstly, a future gridded dataset was developed with the aid of observational data and Climate Hazards Group InfraRed Precipitation (CHIRP) satellite data. Subsequently, the Standardized Precipitation Index (SPI) was estimated for all grids at a 3-month scale to monitor meteorological drought conditions. Following this, maps were generated based on the frequency of occurrence for different SPI drought categories for both present and future climatic scenarios.

3.7.1 Development of a future gridded rainfall data set

To provide an accurate representation of the meteorological drought conditions in the Kirindi Oya and Maduru Oya basins and to forecast their future drought susceptibility, obtaining a dataset with high resolution is of paramount importance. This fine-resolution dataset is critical for conducting precise interpolations, enabling a comprehensive depiction of the drought status across the Maduru oya and Kirindi oya basins in an effective manner. In order to achieve this objective, the study utilized the Climate Hazards Group InfraRed Precipitation satellite (CHIRPS) data, known for its ability to generate high-resolution, satellite-based estimates in both space and time. The selection of CHIRPS data was made to facilitate accurate and detailed assessments of meteorological drought conditions and future drought susceptibility within the selected basins. The CHIRPS dataset encompasses a broad latitudinal range, spanning from 50° S to 50° N, and extends across all longitudes. This extensive coverage enables near-real-time monitoring and evaluation of diverse regions with accuracy and efficiency (Goshime et al., 2019).

Initially, the study identified the CHIRP grid points situated within the basin area. Using the Thiessen polygon method, the closest gauging station was determined for each grid point. The locations of the selected grid points for the Maduru Oya and Kirindi Oya basins are depicted in Figure 3.11 and Figure 3.12, respectively. Following this, statistical relationships were established for each month at every grid point, utilizing the monthly rainfall data from the nearest rain gauging station. For this purpose, monthly data spanning the period from 1983 to 2014 was employed.

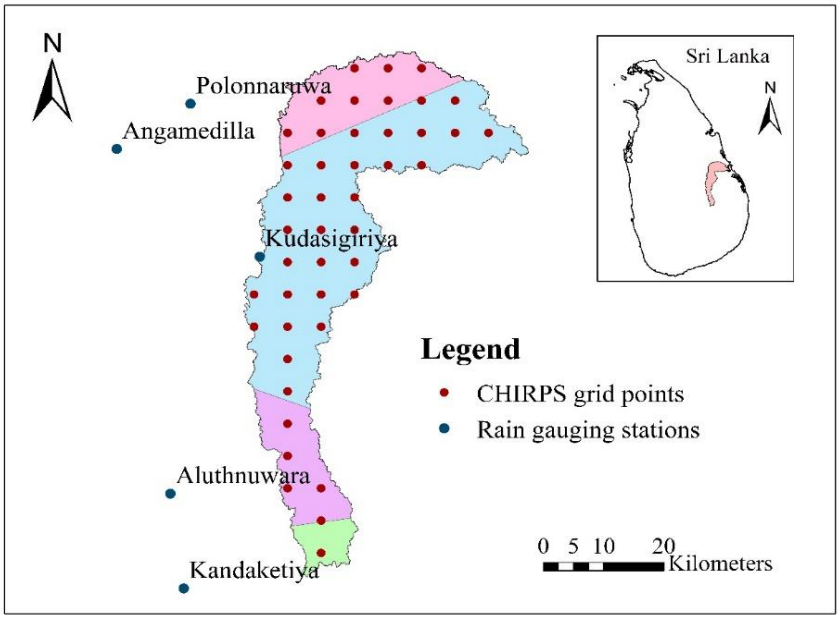

Figure 3.11: Thiessen polygon map (Maduru Oya basin)

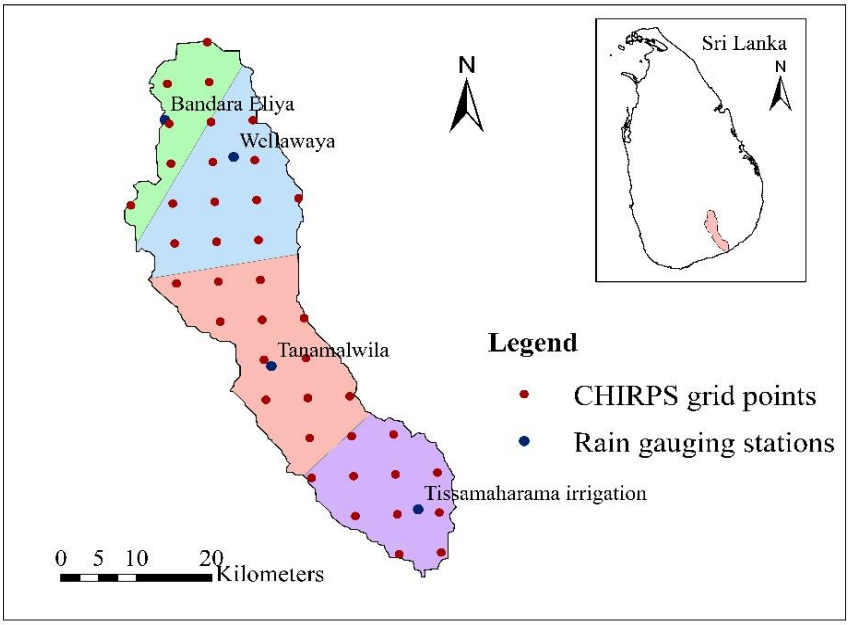

Figure 3.12: Thiessen polygon map (Kirindi Oya basin)

3.7.2 Bias correction of CHIRPS satellite data

This study employed the non-linear power transformation bias correction method to address and correct the bias present in the uncorrected CHIRPS satellite estimate (Goshime et al., 2019). According to Equation 3.2, the bias present in the data was addressed and alleviated, as follows.

$$P_c = xP^y \tag{3.2}$$

The bias correction process for monthly CHIRPS rainfall (*Pc*) involved the application of bias factors (*x* and *y*) to adjust the original CHIRPS rainfall data (*P)*. The determination of these bias factors followed an iterative approach, wherein the observed values were meticulously compared and matched with the corresponding CHIRPS satellite data. To estimate the bias factors, a comprehensive aggregation of complete daily datasets from both data sources was executed for each month within the time frame spanning 1983 to 2014.

The bias factor *y* was computed to align its standard deviation with that of the nearest gauging station data. Subsequently, the bias factor *x* was determined to align with the mean of the observed gauging station data. By employing this methodological approach, monthly bias factors were calculated for all CHIRPS grid points.

3.7.3 Generation of maps based on estimated SPI values

The formulated statistical relationships were employed to acquire prospective gridded rainfall data. Subsequently, the derived dataset underwent bias correction by employing the estimated bias factors unique to each grid point. Following the completion of the bias correction process, the Standardized Precipitation Index (SPI) was computed specifically for the three-month time scale. The selection of this time scale was made based on its acknowledged suitability for monitoring the onset of drought conditions (Manesha et al., 2015).

The SPI formulated by Mckee et al. (1993) initially characterizes the variability of precipitation totals through a gamma distribution, which is subsequently converted into a normal distribution. The probability density function that defines the gamma distribution (Equation 3.3):

$$f_X(x) = \frac{1}{\beta\alpha\Gamma(\alpha)} x^{\alpha-1} e^{\frac{-x}{\beta}} \; for \;\; x > 0 \tag{3.3}$$

where, α and β denote the shape and scale parameters respectively, while *x* represents the precipitation amount, and $\Gamma(\alpha)$ signifies the gamma function.

The estimates for α and β based on the maximum likelihood method are as follows:

$$\alpha = \frac{1}{4\gamma}\left[1 + \sqrt{1 + \frac{4\gamma}{3}}\right],\ \beta = \frac{\bar{x}}{\alpha}, \text{where } \gamma = (\overline{x}) - \frac{\sum ln(x)}{n} \tag{3.4}$$

where, n = Number of observed rainfall values

The derived parameters are subsequently employed to calculate the cumulative probability of an observed precipitation event for the specified month and time scale at the relevant location. Given that the gamma function lacks a definition for x = 0 and precipitation distributions might include zeros, the cumulative probability is expressed as follows (Equation 3.5):

$$G(x) = p + (1 - p)H(x) \tag{3.5}$$

In this context, p represents the probability of zero precipitation, and $H(x)$ signifies the cumulative probability derived from the incomplete gamma function. Subsequently, the cumulative probability, denoted as $G(x)$, is converted into the standard normal random variable z with a mean of zero and a variance of one. This transformed value of z corresponds to the SPI (Tigkas et al., 2015).

This research specifically opted for two Shared Socio-economic Pathway-Representative Concentration Pathway (SSP-RCP) scenarios, denoted as SSP1-2.6 and SSP5-8.5, with the explicit purpose of evaluating the potential future drought conditions within the river basin. The SSP1-2.6 scenario embodies a juxtaposition of reduced societal vulnerability and low emission levels. On the other hand, SSP5-8.5 characterizes elevated emissions leading to substantial mitigation efforts and limited adaptation capabilities (IPCC, 2021, Chapter 4). The probability of occurrence for each drought category was estimated based on the SPI values for both the historical period (1983-2014) and the projected period (2015-2100). Subsequently, the computed percentage values were used to create maps depicting drought occurrences. The map generation process was carried out using the Inverse Distance Weighted (IDW) spatial analyst tool, which is available within the ArcGIS (ESRI Inc, USA) software.

3.8 Streamflow Prediction

This study specifically focuses on the application of machine learning methods for predicting future streamflow. In the development of these models, monthly rainfall data served as the input, while monthly streamflow values were utilized as the output. Various methodologies were employed, and their performance in predicting monthly streamflow values was primarily evaluated based on metrics such as coefficients of determination (R^2), the Nash–Sutcliffe coefficient (NASH), and Percent Bias (PBIAS) (Al-Sudani et al., 2019; Karran et al., 2014). The selected objective functions are defined as,

$$R^2 = \frac{n\sum_{i=1}^{n} O_i S_i - \sum_{i=1}^{n} O_i \sum_{i=1}^{n} S_i}{\sqrt{[n\sum_{i=1}^{n} O_i^2 - (\sum_{i=1}^{n} O_i)^2] - [n\sum_{i=1}^{n} S_i^2 - (\sum_{i=1}^{n} S_i)^2]}} \tag{3.6}$$

$$NASH = 1 - \frac{\sum_{i=1}^{n}(S_i - O_i)^2}{\sum_{i=1}^{n}(O_i - O_{mean})^2} \tag{3.7}$$

$$PBIAS = \frac{\sum_{i=1}^{n}(O_i - S_i)}{\sum_{i=1}^{n} O_i} \quad (3.8)$$

where O_i and S_i are observed streamflow (m^3/s) and simulated streamflow (m^3/s), respectively, while O_{mean} is the mean observed streamflow (m^3/s).

The Wellawaya subbasin of the Kirindi Oya basin and the Padiyathalawa subbasin of the Maduru Oya basin were chosen for analysis. Thiessen average rainfall data were used as the input for both models, while the streamflow values at the Wellawaya and Padiyathalawa stations served as the output data for the models developed for the Kirindi Oya and Maduru Oya basins, respectively. Figure 3.13 and Figure 3.14 depict the selected subbasins and Thiessen polygon maps for the Maduru Oya basin and Kirindi Oya basin, respectively. Monthly data from the 1984/1985 year to the 2014/2015 water year were employed for the study. During the model development process, 80% of the data was dedicated to training the models, and the remaining 20% was allocated for testing. The primary models employed for predicting monthly streamflow at the selected observed streamflow gauging station in each river basin were based on Long Short-Term Memory (LSTM) Recurrent Neural Networks (RNN) and Random Forest. The selection of these model types was informed by their documented suitability for streamflow prediction in existing literature.

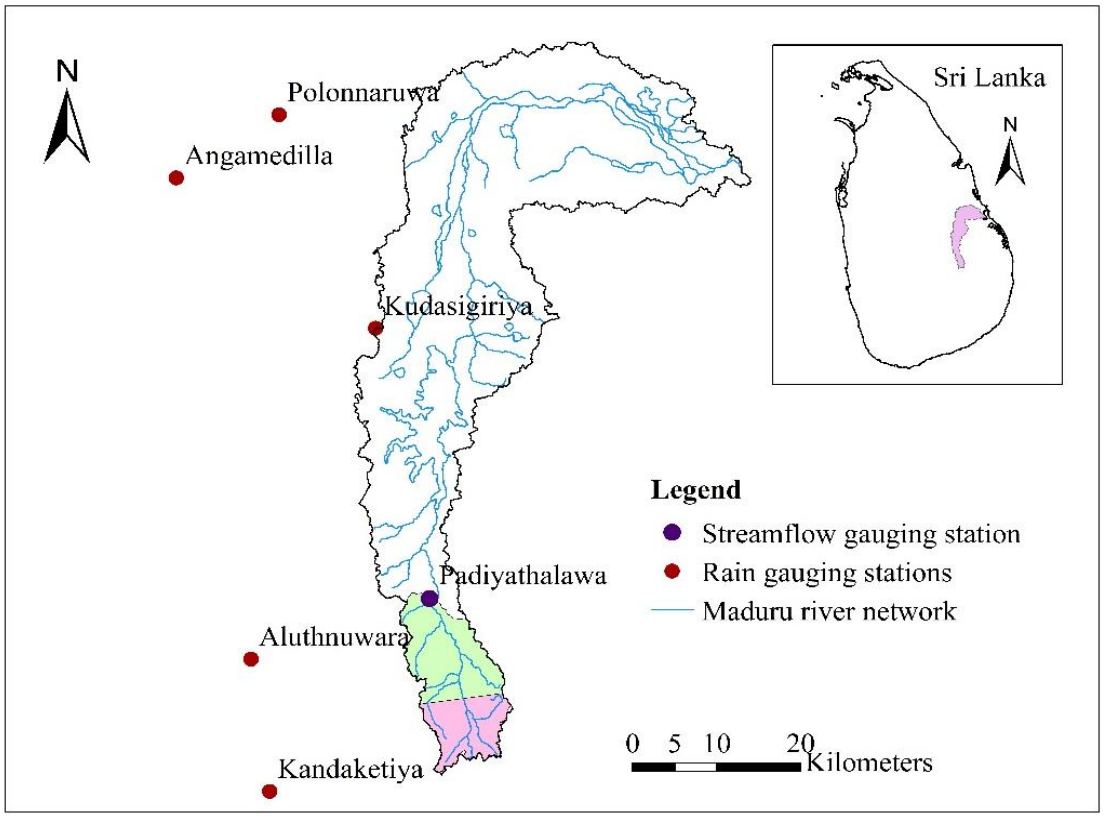

Figure 3.13: Padiyathalawa subbasin of the Maduru Oya basin

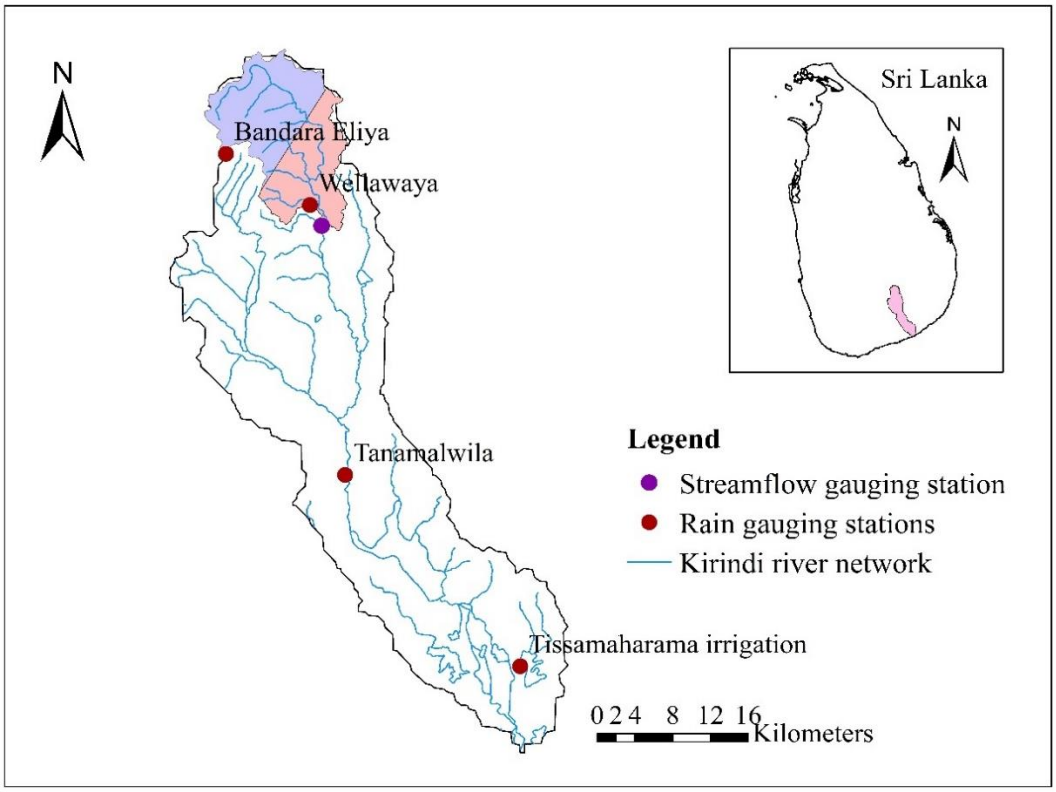

Figure 3.14: Wellawaya subbasin of the Kirindi Oya basin

When training the LSTM model, the Back-Propagation Through Time (BPTT) algorithm was employed. This algorithm possesses the capability to iteratively develop the network and update the weights across each time step, facilitating effective learning. Furthermore, the Rectified Linear Unit (ReLU) function was chosen as the activation function for the RNN models. This decision stems from the observation that the ReLU function offers improved gradient propagation in comparison to other activation functions (Liu et al., 2020).

The best models among the developed RNN and RF models were chosen based on the values obtained for the selected objective functions to evaluate model performance. Subsequently, the selected models were employed to predict future monthly streamflow, incorporating future monthly rainfall under SSP1-2.6 and SSP5-8.5 scenarios.

3.9 Estimation of the Streamflow Drought Index (SDI)

In this study, SDI was selected as the hydrological drought monitoring index. The calculation algorithm of SDI is explained below.

If the time series of monthly streamflow values are available (S_{ij}), where i indicates the hydrological year and j indicates the month within the hydrological year, the cumulative streamflow (R_{ik}) can be expressed by the following Equation 3.9 (Nalbantis & Tsakiris, 2009).

$$R_{ik} = \sum_{j=1}^{3k} S_{ij} \quad \text{i} = 1, 2, 3, \ldots, \text{j} = 1, 2, 3, \ldots, 12\,, \ \text{k} = 1, 2, 3, 4 \tag{3.9}$$

R_{ik} represents the total cumulative streamflow volume for the i[th] hydrological year and the k[th] reference period. Specifically, k takes on different values: k = 1 corresponds to the period from October to December, k = 2 corresponds to October to March, k = 3 corresponds to October to June, and k = 4 corresponds to October to September.

Derived from the cumulative streamflow volumes R_{ik}, the Standardized Drought Index (SDI) is formulated for each reference period k within the i[th] hydrological year in the following manner:

$$SDI_{ik} = \frac{R_{ik} - \overline{R_{\imath k}}}{s_k} \ \text{i} = 1, 2, 3, \ldots, \ \text{k} = 1, 2, 3, 4 \tag{3.10}$$

where $\overline{R_{\imath k}}$ and s_k denote the mean and standard deviation, respectively, of cumulative streamflow volumes for reference period k, calculated over an extended timeframe. In this definition, the threshold level is established at $\overline{R_{\imath k}}$, although alternative values could be considered.

In the case of small basins, the probability distribution of streamflow often exhibits skewness and can be effectively approximated using the family of Gamma distribution functions. Subsequently, this distribution is transformed into a normal distribution. Utilizing the two-parameter log-normal distribution, where normalization involves simply taking the natural logarithms of streamflow, the SDI index is formulated as:

$$SDI_{ik} = \frac{T_{ik} - \overline{T_{\imath k}}}{S_{Tk}} \ \text{i} = 1, 2, 3, \ldots, \ \text{k} = 1, 2, 3, 4 \tag{3.11}$$

Here, T_{ik} represents the natural logarithms of cumulative streamflow, characterized by a mean T_{ik} and standard deviation S_{Tk}, with these statistical parameters derived from a long-term estimation (Tigkas et al., 2015).

This study employed hydrological drought classifications as outlined by Nalbantis and Tsakiris (2009), as detailed in Table 3.7.

Table 3.7: Drought categorization based on SDI values

Category	**SDI Values**
Non-drought	SDI ≥ 0.0
Mild drought	–1.0 ≥ SDI < 0.0
Moderate drought	–1.5 ≥ SDI < –1.0
Severe drought	–2.0 ≥ SDI < –1.5
Extreme drought	SDI < –2.0

In this study, the software tool known as the Drought Indices Calculator (DrinC) was used for the computation of SDI (Tigkas et al., 2015).

4. RESULTS AND ANALYSIS

4.1 General

In this chapter, a comprehensive exposition is provided regarding the obtained results and the applied analysis methods, as outlined in the methodology presented in Chapter 3. The presented results encompass the bias correction of GCM data, developed statistical relationships between CHIRPS grid points and station data, bias-correction of CHIRPS data, generated maps showing the meteorological drought status in the selected basins, streamflow predictions based on machine learning approaches and hydrological drought monitoring assessment based on the estimated Streamflow Drought Index (SDI) values at three-month (October-December), six-month (October-March) and twelve-month (October-September) time scales.

4.2 Bias Correction of GCM Output

The evaluation of the six selected GCM models was conducted using both the mean-based approach and the variance-based approach. Figure 4.1 and Figure 4.2 illustrate the coefficient of determination (R^2) values obtained for each gauging station of the Maduru Oya basin and Kirindi Oya basin, respectively. The mean-based method evaluation based on the results of the objective function values obtained for both basins ($R^2 > 0.5$) revealed that the CNRM-CM6-1-HR model exhibited the highest performance among all the models. Consequently, the CNRM-CM6-1-HR model was selected as the preferred climate model for generating future predictions, and mean based method was selected as the bias-correction method.

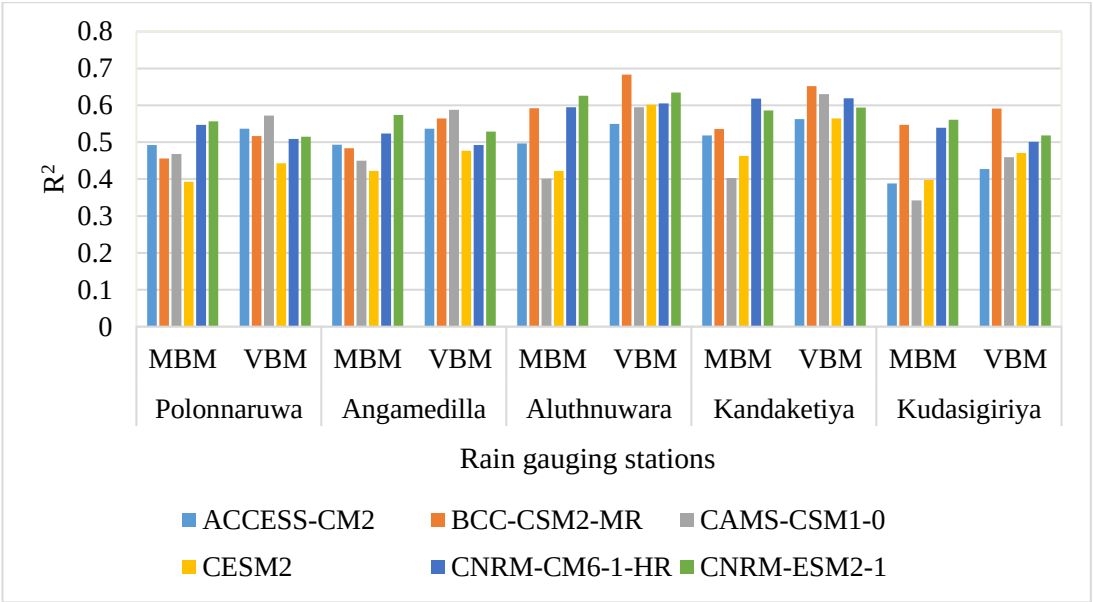

Figure 4.1: Objective function values (Maduru Oya basin)

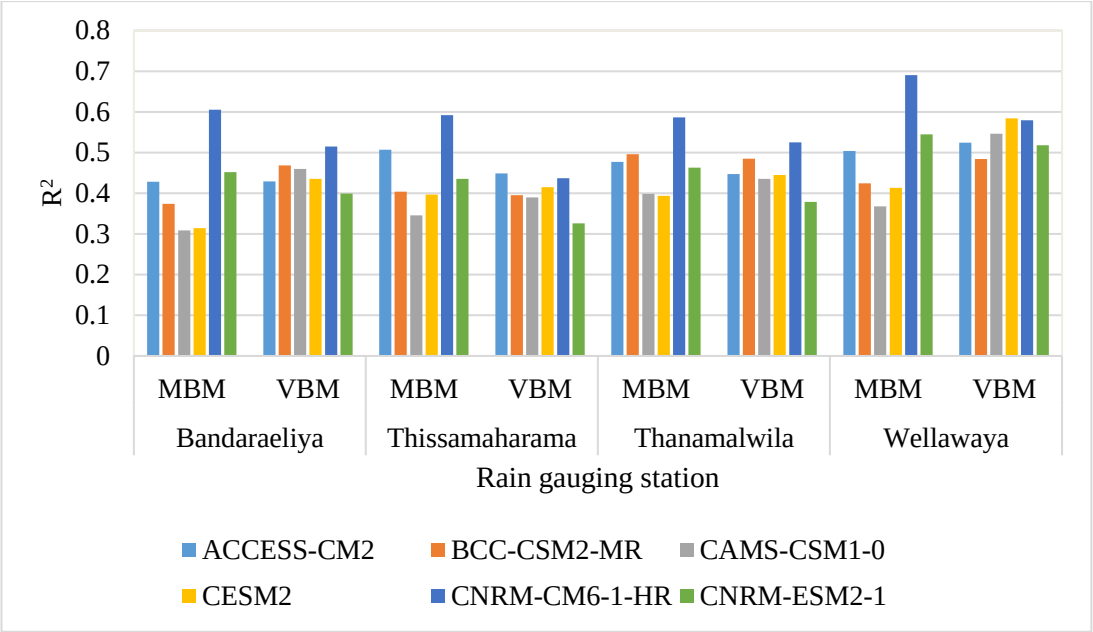

Figure 4.2: Objective function values (Kirindi Oya basin)

Figure 4.3 and Figure 4.4 visually represent the relationship between the bias-corrected CNRM-CM6-1-HR model data and the observed data at the Kandaketiya gauging station of the Maduru Oya basin and Wellawaya gauging station of the Kirindi Oya basin, respectively.

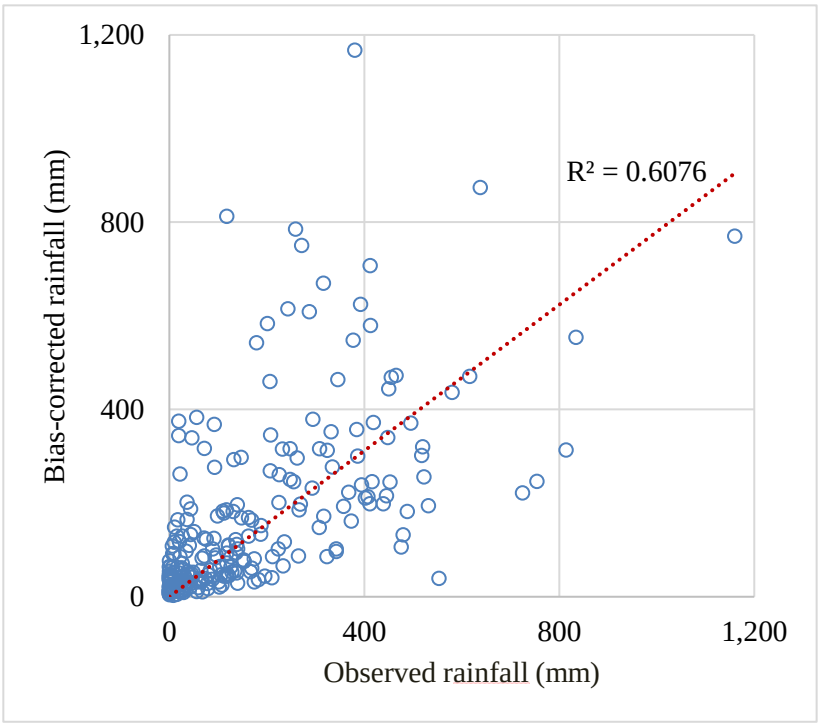

Figure 4.3: Variation of bias-corrected data with observed data at the Kandaketiya station

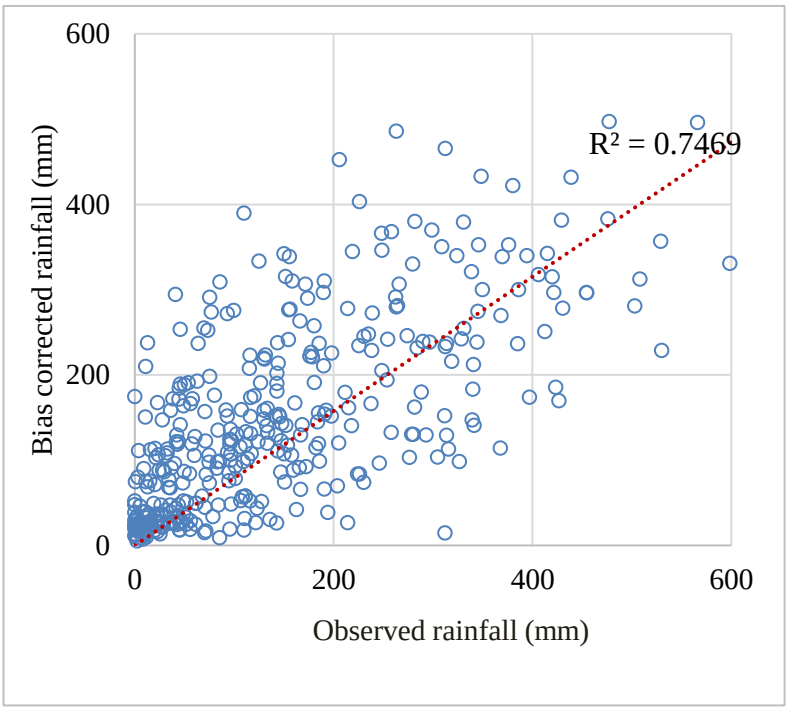

Figure 4.4: Variation of bias-corrected data with observed data at the Wellawaya station

Figure 4.5 and Figure 4.6 depict rainfall time series for both the observed data and the bias-corrected data recorded at the Thissamaharama Irrigation station in the Kirindi Oya basin and the Polonnaruwa station in the Maduru Oya basin, respectively.

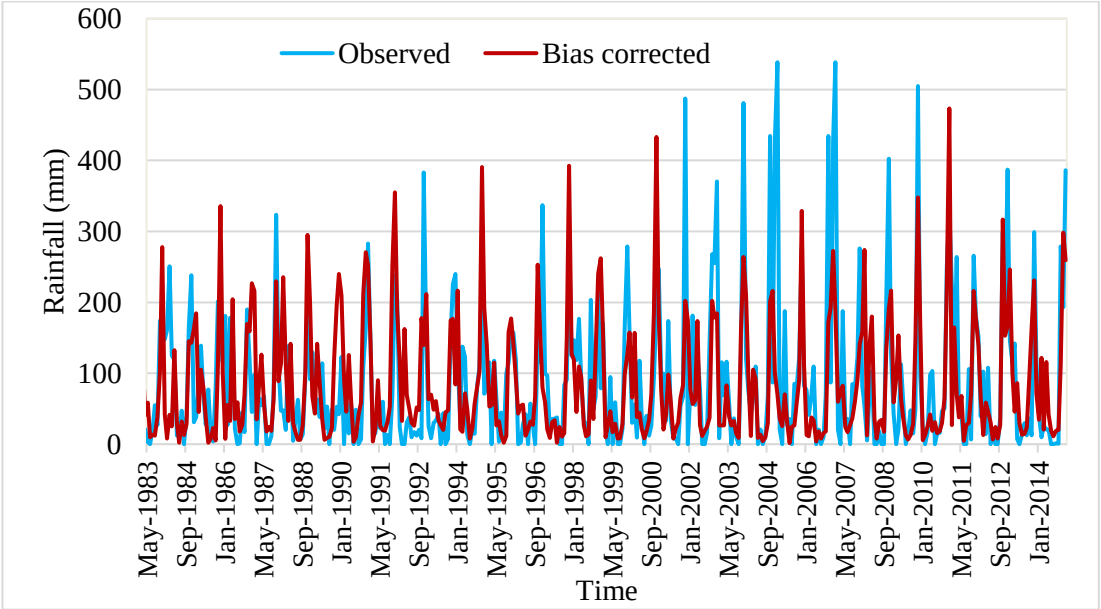

Figure 4.5: Thissamaharama Irrigation gauging station (Kirindi Oya basin) rainfall time series

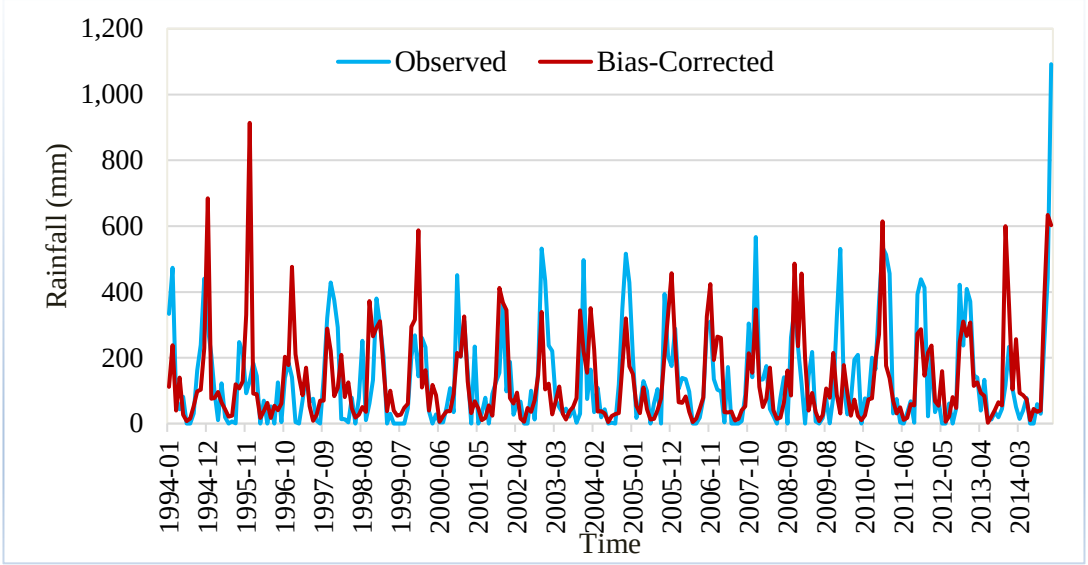

Figure 4.6: Polonnaruwa gauging station (Maduru Oya basin) rainfall time series

However, despite the improved performance indicated by the bias-corrected CNRM-CM6-1-HR model data, as evidenced by an R^2 exceeding 0.5, it is suggested that an alternative method such as quantile mapping may provide better results when compared to the mean-based approach. This perspective has been elaborated upon in the Discussion chapter (Chapter 5).

4.3 ETCCDI Climate Change Indices

The ETCCDI Climate Change Indices, the maximum consecutive wet days (CWD) and maximum consecutive dry days (CDD) for the Kirindi Oya basin were computed using the Thiessen average rainfall. Figure 4.7 illustrates the variation in maximum consecutive wet days and dry days in the Kirindi Oya basin from 1985 to 2015. Additionally, maps showing the values of the total rainfall on wet days (PRCPTOT) for the Maduru Oya and Kirindi Oya basins, generated using CHIRPS data, are illustrated in Figures 4.8 and 4.9, respectively.

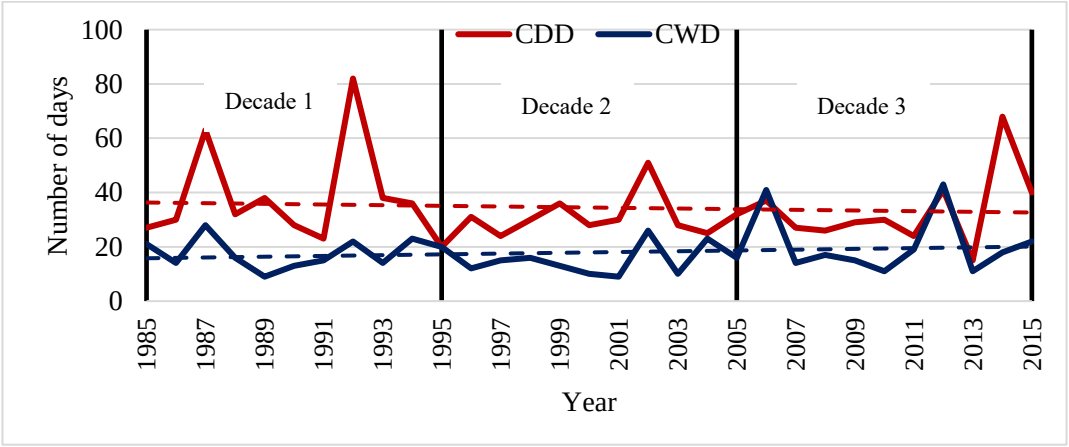

Figure 4.7: Variation of CWD and CDD from 1985 to 2015 in the Kirindi Oya basin

The dataset has been divided into three decades. Based on the observed variation, the maximum number of consecutive wet days (CWD) has shown an increase in the last ten years compared to the other two decades. In other words, CWD exhibits an increasing trend, while the maximum number of consecutive dry days (CDD) demonstrates a decreasing trend. The record for the maximum number of consecutive dry days (82 days) was in the year 1992. According to Shelton et al. (2022), droughts have been documented in Sri Lanka in 1987, 1992, and 2014, particularly in the intermediate zone and dry zone. Therefore, the higher CDD values recorded in those years clearly represent drought conditions.

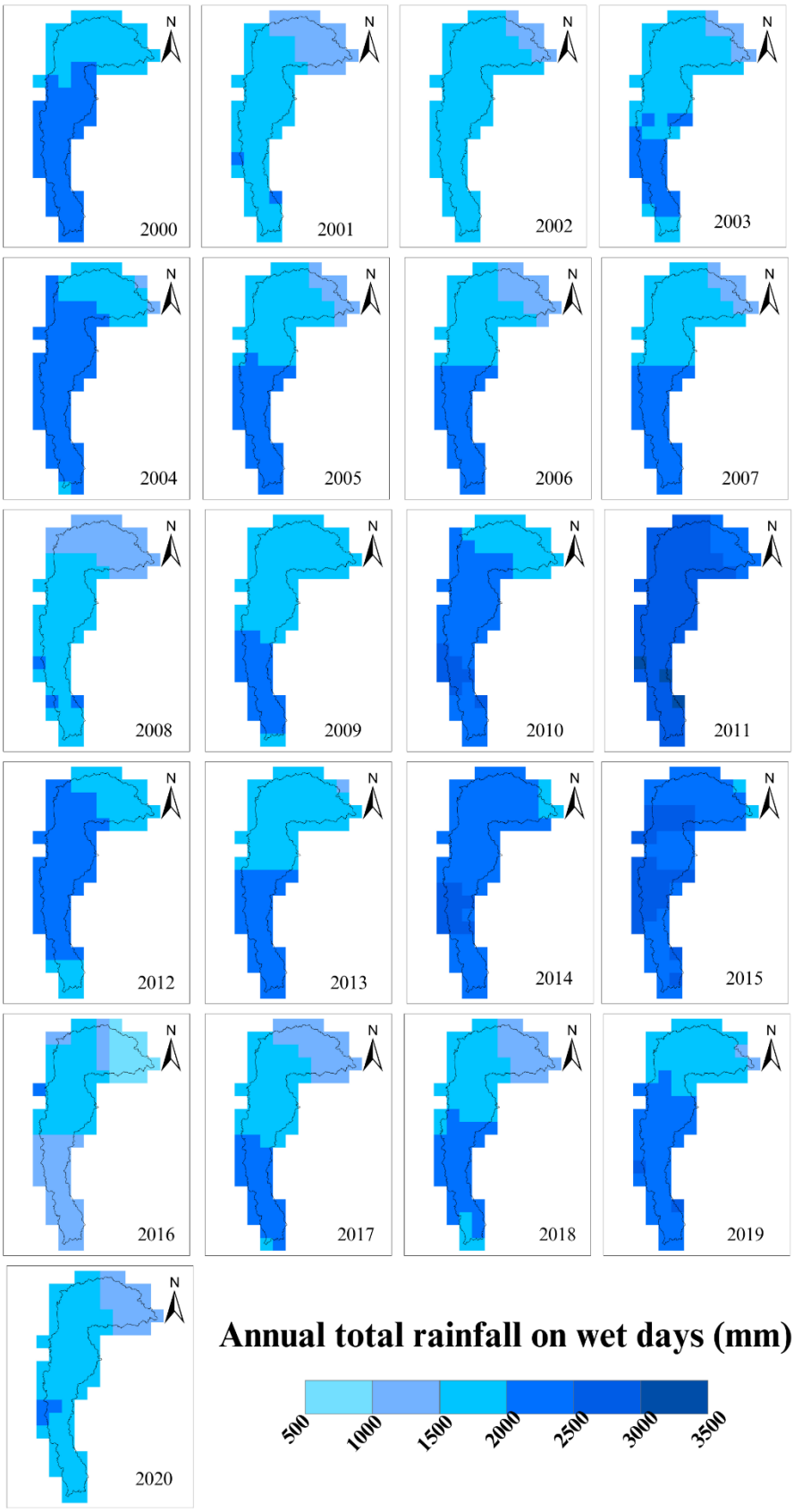

Figure 4.8: Annual total rainfall on wet days recorded in the Maduru Oya basin

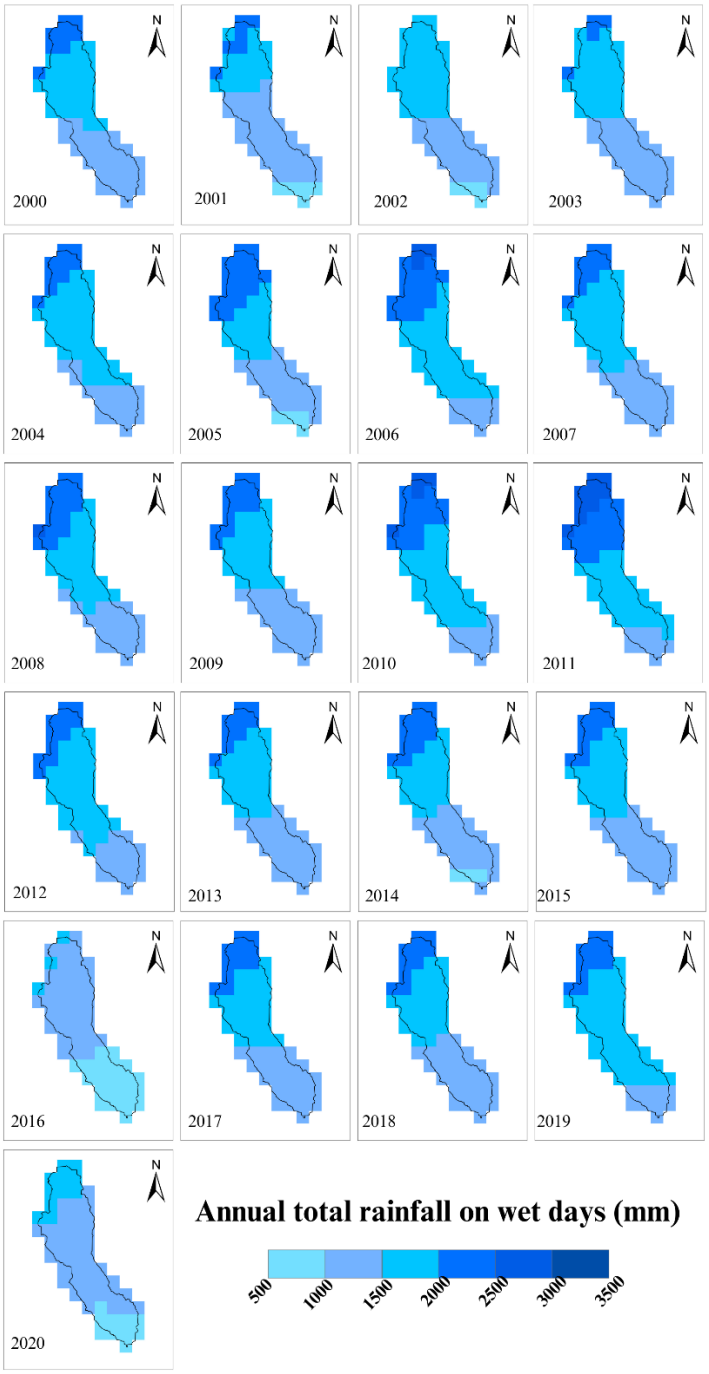

Figure 4.9: Annual total rainfall on wet days recorded in the Kirindi Oya basin

According to the results, the highest total precipitation on wet days was recorded in 2011 in both river basins. Conversely, the minimum total precipitation on wet days was recorded in 2016. As stated by Lokuhetti et al. (2017), a drought condition in Sri Lanka persisted throughout the entirety of 2016. Hence, this condition may have contributed to the reduction in the annual total precipitation on wet days in 2016. The maps illustrating the computed values of other selected rainfall indices are presented in Appendix B.

4.4 Statistical Relationship Between CHIRP Satellite Data and Observed Data

In order to develop a statistical relationship between CHIRPS data and observed precipitation data, the grid points lying within the basin were identified as the first step. Accordingly, 41 and 44 grid points were located within the Kirindi Oya basin and Maduru Oya basin, respectively. Then the closest station to each grid point was identified using the Thiessen polygon method. After identifying the closest station, y = mx graphs were plotted for all months of each grid point. Then the gradients of the best-fitted curve of each month were estimated for every grid point. The estimated gradients were used to develop future gridded data sets for the study area. Figure 4.10 illustrates the gradient obtained for the month of December at Grid No. 39 of the Kirindi Oya basin, with the Bandaraeliya station identified as the nearest station.

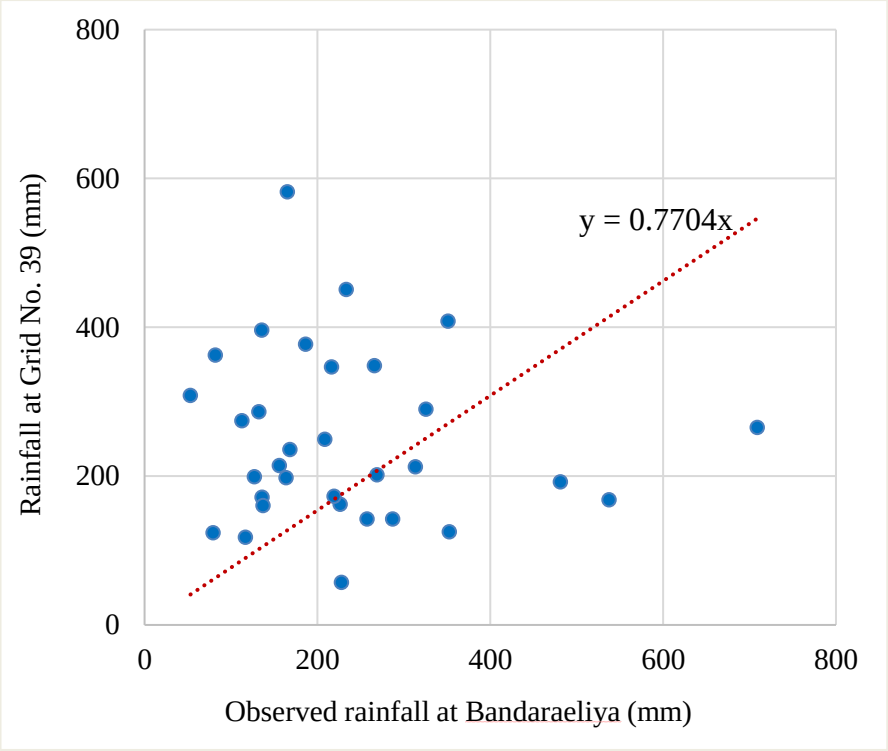

Figure 4.10: Variation of rainfall at Grid No. 39 of Kirindi Oya basin with Observed rainfall at Bandaraeliya station

4.5 Bias Correction of CHIRPS Satellite Data

The bias-correction process employed a non-linear power transformation method. Figure 4.11 exhibits hydrographs illustrating the observed data at Wellawaya station alongside the bias-corrected data at Grid No. 32. The bias-corrected data series have displayed a significantly elevated level of correlation with the observed variation in the nearest station data across all grid points. This is evident through correlation coefficients ranging from 0.80 to 0.98.

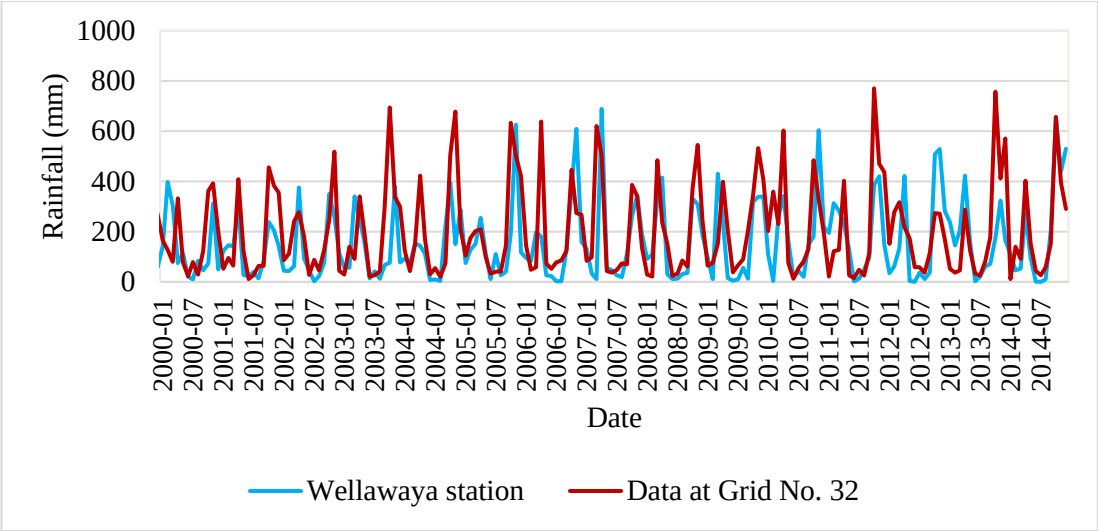

Figure 4.11: Hydrographs of the observed data at Wellawaya station and bias corrected data at Grid No. 32

4.6 Generation of Maps

Using the calculated SPI-3 values, the occurrence percentages of extreme, severe, and moderate droughts were determined for each grid point (Edossa et al., 2010). The respective SPI ranges corresponding to each drought category are presented in Table 4.1. Maps were generated to visually represent the spatial distribution of drought occurrences during both the historical and projected periods, considering the two selected scenarios, SSP1-2.6 and SSP5-8.5. The resulting maps of the Maduru basin, portraying the historical and projected periods under the two scenarios are presented in Figure 4.12.

Table 4.1: Drought categorization based on SPI values

SPI Range	Drought Category
≤ -2	Extreme drought
$(-2.0, -1.5]$	Severe drought
$(-1.5, -1.0]$	Moderate drought
$(-1, 0]$	Mild drought
≤ 0	Mild and above

According to the results, the occurrence percentages of moderate droughts at the upstream part of the Maduru Oya basin are significant (8-10%) in the historical period compared to the two projected scenarios. Under the SSP1-2.6 scenario, the occurrence of extreme, severe, and moderate droughts shows percentage increases of 18%, 16%, and -6%, respectively, in comparison to the historical period. The occurrence of moderate droughts has shown a considerable increase in the downstream part of the

basin. Conversely, for the SSP5-8.5 scenario, the percentage increments for extreme, severe, and moderate drought conditions are 31%, 2%, and -4%, respectively.

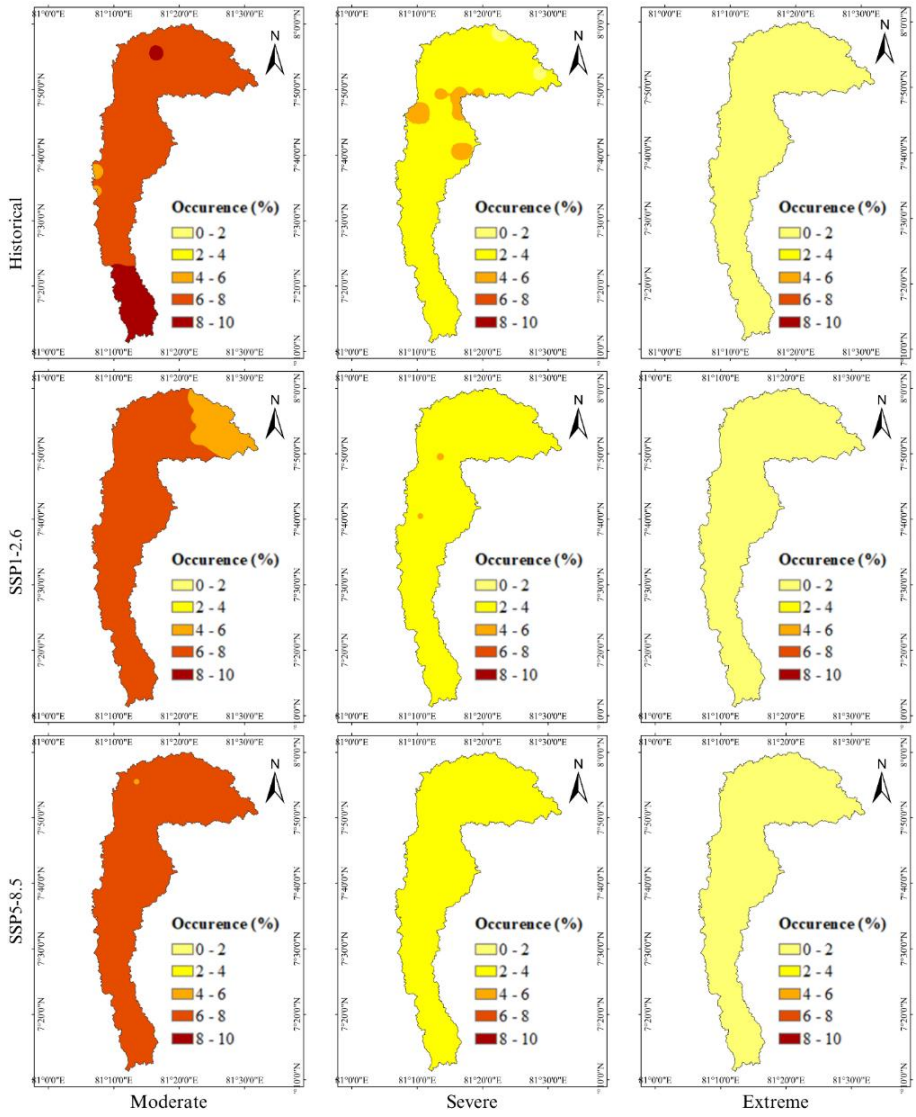

Figure 4.12: Occurrence of extreme, severe, and moderate droughts in the Maduru Oya basin

The resulting maps of the Kirindi Oya basin, portraying the historical and projected periods under the two scenarios are presented in Figure 4.13. The results elaborate that the occurrence percentages of moderate droughts exhibit relatively higher values across all three scenarios in comparison to the occurrence percentages of extreme and severe droughts. On the other hand, the occurrence percentages of moderate droughts at some locations are significant (8-10%) in the historical period compared to the two projected scenarios. Furthermore, the vulnerability of the Kirindi Oya basin to moderate drought conditions has been reduced under the SSP5-8.5 scenario compared to the SSP1-2.6 scenario.

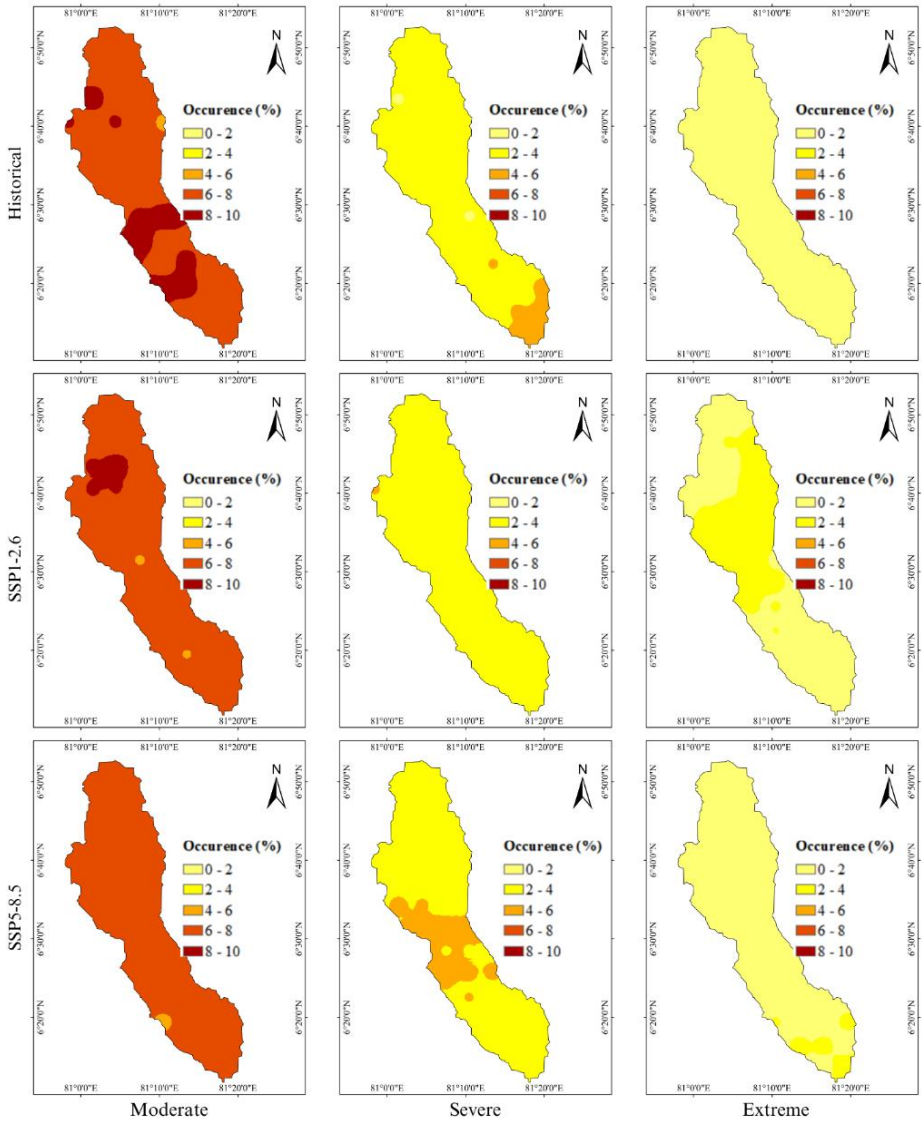

Figure 4.13: Occurrence of extreme, severe, and moderate droughts in Kirindi Oya basin

Additionally, the analysis reveals that, in the Kirindi Oya basin, under the SSP1-2.6 scenario, the occurrence of extreme, severe, and moderate droughts shows percentage increases of 49%, -8%, and 8%, respectively, in comparison to the historical period. Conversely, for the SSP5-8.5 scenario, the percentage increments for extreme, severe, and moderate drought conditions are 37%, -5%, and 4%, respectively. Importantly, it is noteworthy that the occurrence of extreme meteorological droughts is projected to surge by more than 35% under both projection scenarios. On the other hand, the occurrence of severe droughts is expected to decline, while the occurrence of moderate droughts is predicted to show a marginal increase in comparison to the historical period.

4.7 Streamflow Prediction based on Selected Machine Learning Approaches

This study mainly employed Long Short-Term Memory (LSTM), Recurrent Neural Networks (RNN), and Random Forest algorithm to predict future streamflow. Estimated Thiessen average monthly rainfall data spanning from the 1984/1985 water year to the 2014/2015 water year served as the input data for predicting monthly streamflow. The RNN models were trained using various configurations, including different hidden layers, LSTM units, activation functions, learning rates, batch sizes, and epoch numbers, to identify the model with better performance. The evaluation of model performance employed key metrics, including the coefficient of determination (R^2), Nash Sutcliffe coefficient (NASH), and the root mean square error (RMSE). This assessment focused on two distinct models developed for the Padiyathalawa sub-basin of the Maduru Oya basin and the Wellawaya subbasin of the Kirindi Oya basin.

Table 4.2 presents the values obtained for the selected objective functions for the RNN model, while Table 4.3 presents the objective function values obtained for the random Forest (RF) model. Based on the acquired values for the objective functions, the RF models developed for the two subbasins were deemed as the preferred models. This decision was made since the trained RNN models did not demonstrate satisfactory performance when compared to the RF models. This observation is evident in the hydrographs obtained for the training dataset (80 % of the data) of the Padiyathalawa subbasin of the Maduru Oya basin and the Wellawaya subbasin of the Kirindi Oya basin, as illustrated in Figure 4.14 and Figure 4.15, respectively, which highlights the subpar performance of the RNN model.

Table 4.2: Objective function values obtained for the developed RNN model

Sub basin	Process	R^2	NASH	RMSE
Padiyathalwa (Maduru)	Training	0.378	-0.791	7.747
	Testing	0.427	0.252	5.343
Wellawaya (Kirindi)	Training	0.513	-0.046	2.787
	Testing	0.447	0.019	2.693

Table 4.3: Objective function values obtained for the developed RF model

Sub basin	Process	R^2	NASH	RMSE
Padiyathalwa (Maduru)	Training	0.928	0.915	2.859
	Testing	0.898	0.888	2.350
Wellawaya (Kirindi)	Training	0.903	0.889	1.347
	Testing	0.865	0.859	1.279

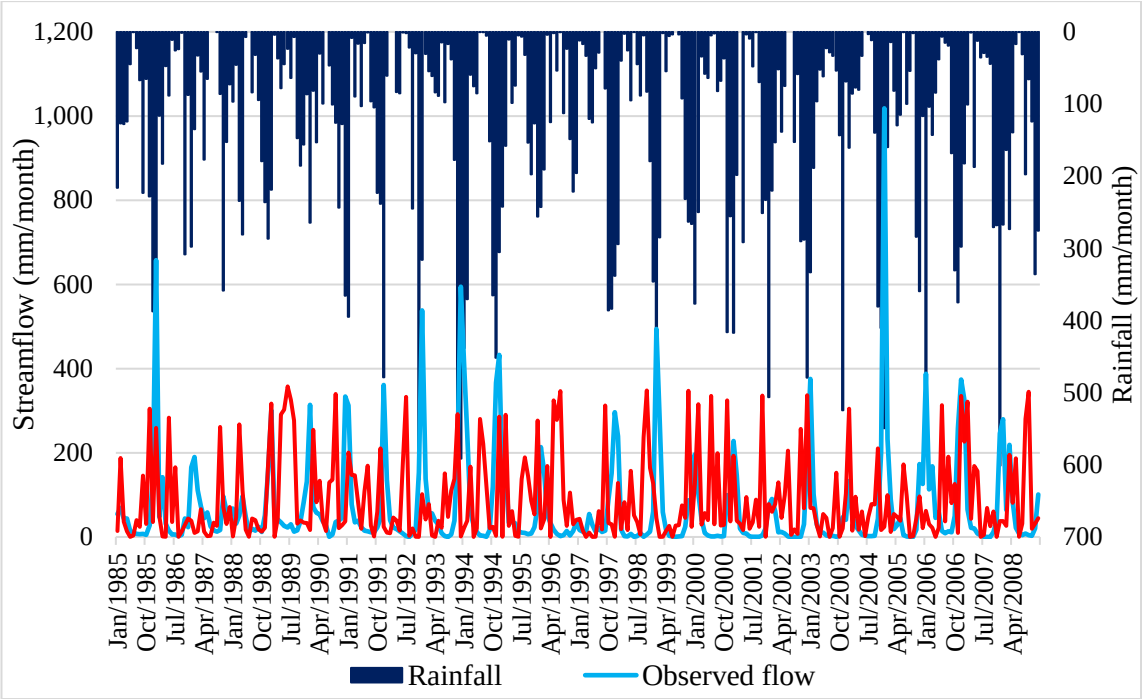

Figure 4.14: Hydrographs obtained from the RNN model developed for the Padiyathalawa subbasin

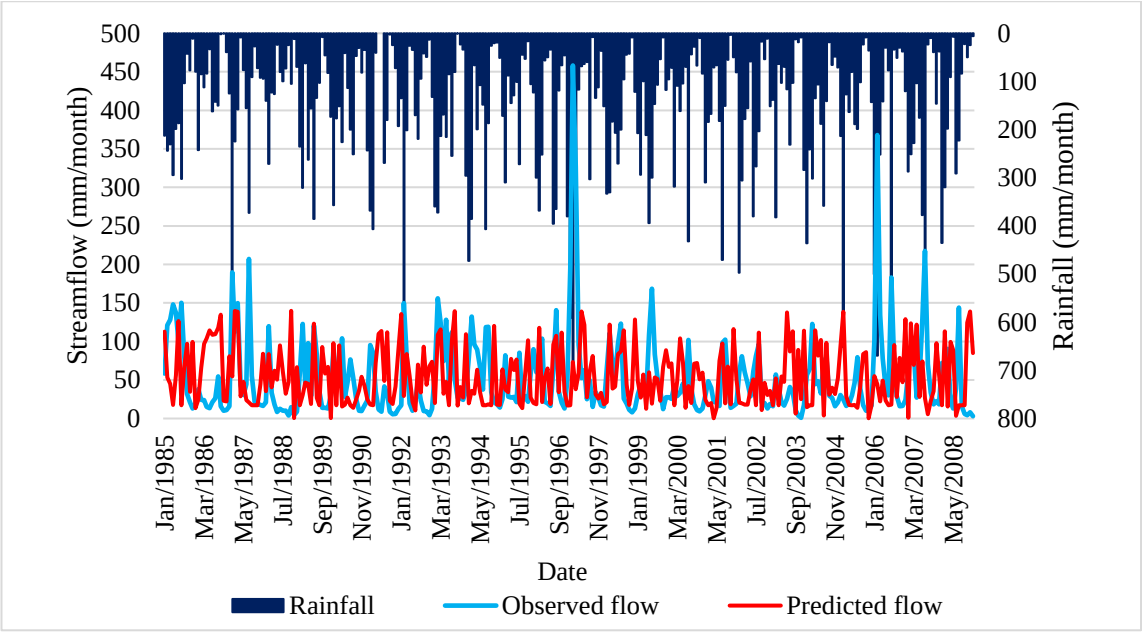

Figure 4.15: Hydrographs obtained from the RNN model developed for the Wellawaya subbasin

In both RNN models, the prediction of peak and troughs values has not been accurate, significantly impacting the overall goodness of fit and resulting in very low values for the Nash-Sutcliffe Coefficient.

4.7.1 Streamflow prediction using the random forest algorithm

Eighty percent (80%) of the dataset was utilized for training the Random Forest models, with the remaining 20% allocated for testing (validation). Figures 4.16 and 4.17 depict the scatter plots and hydrographs obtained for the training data set of the model developed for the Padiyathalawa subbasin of the Maduru Oya basin, respectively.

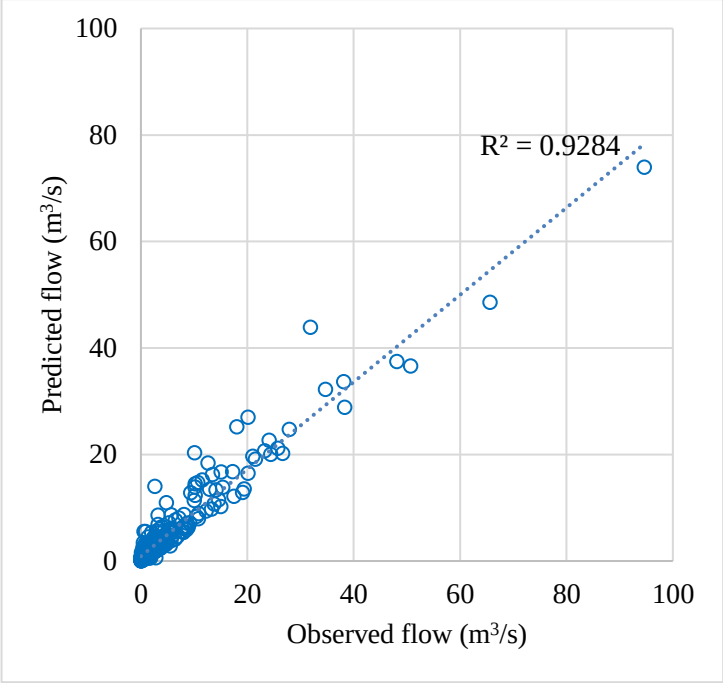

Figure 4.16: Scatter plots obtained from the RF model developed for the Padiyathalawa sub-basin (Training period)

Figure 4.18 illustrates the flow duration curves plotted for the observed and simulated streamflow at the Padiyathalawa gauging station of the Maduru Oya basin for the training period. The flow duration curves demonstrate the superior performance of the model in simulating high flows compared to low flows. However, the simulated low flows have shown higher values compared to the observed values, which remains a limitation of machine learning-based models. This limitation is further elaborated in the discussion section.

Subsequently, Figures 4.19 and 4.20 illustrate the scatter plots and hydrographs obtained for the testing dataset of the model developed for the Padiyathalawa sub-basin, respectively. Figure 4.21 depicts the flow duration curves plotted for the testing period of the model developed for the Padiyathalawa sub-basin. The testing period has also shown similar behavior to the training period when predicting low flows at the Padiyathalawa gauging station.

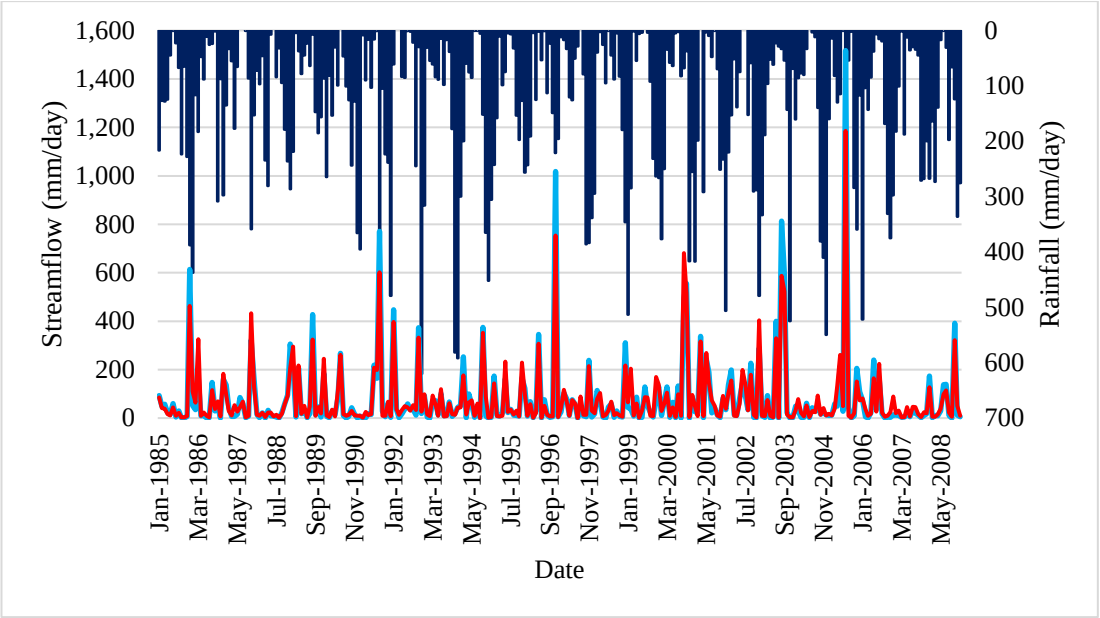

Figure 4.17:Hydrographs obtained from the RF model developed for the Padiyathalawa sub-basin (training period)

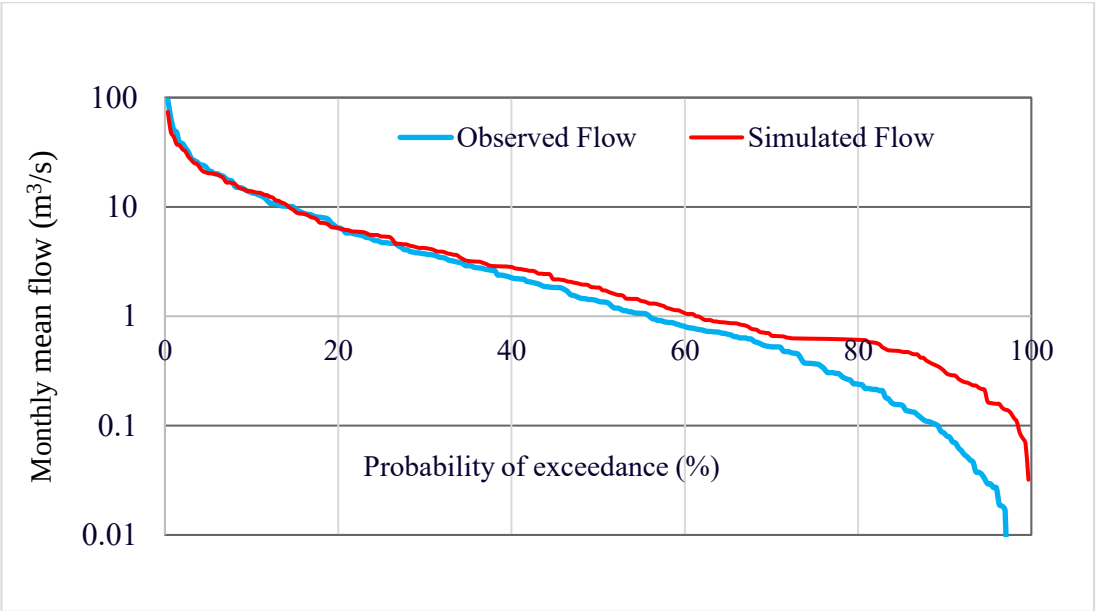

Figure 4.18: Flow Duration Curves obtained for the training period for the Padiyathalawa sub-basin

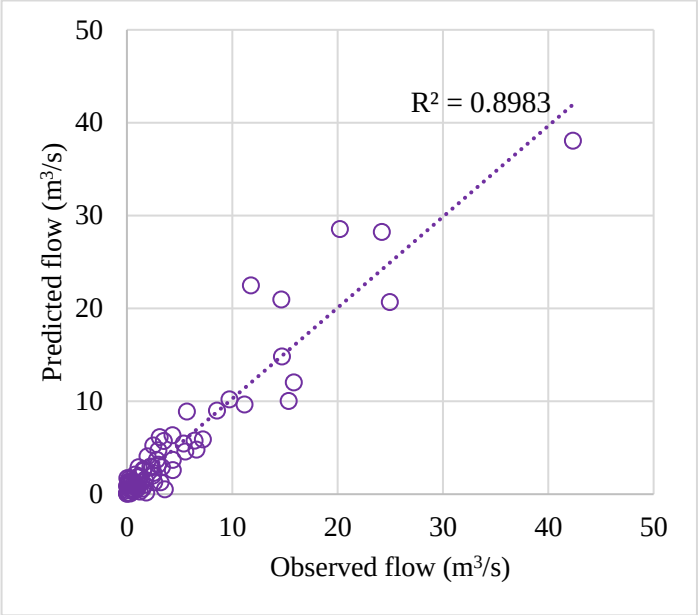

Figure 4.19: Scatter plots obtained from the RF model developed for the Padiyathalawa sub-basin (Testing period)

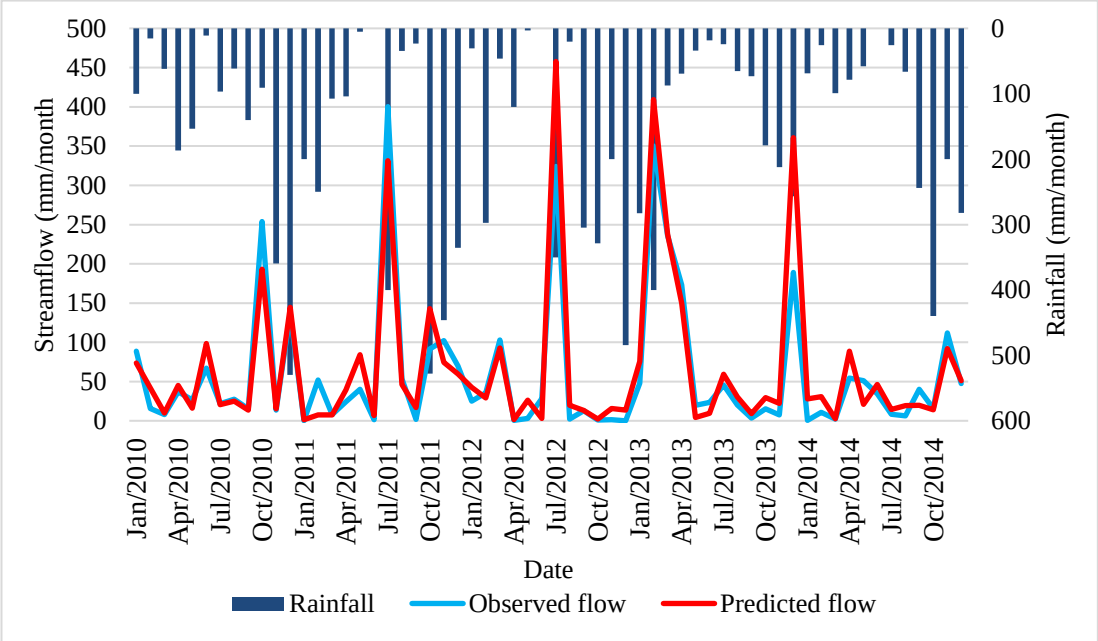

Figure 4.20: Hydrographs obtained from the RF model developed for the Padiyathalawa sub-basin (Testing period)

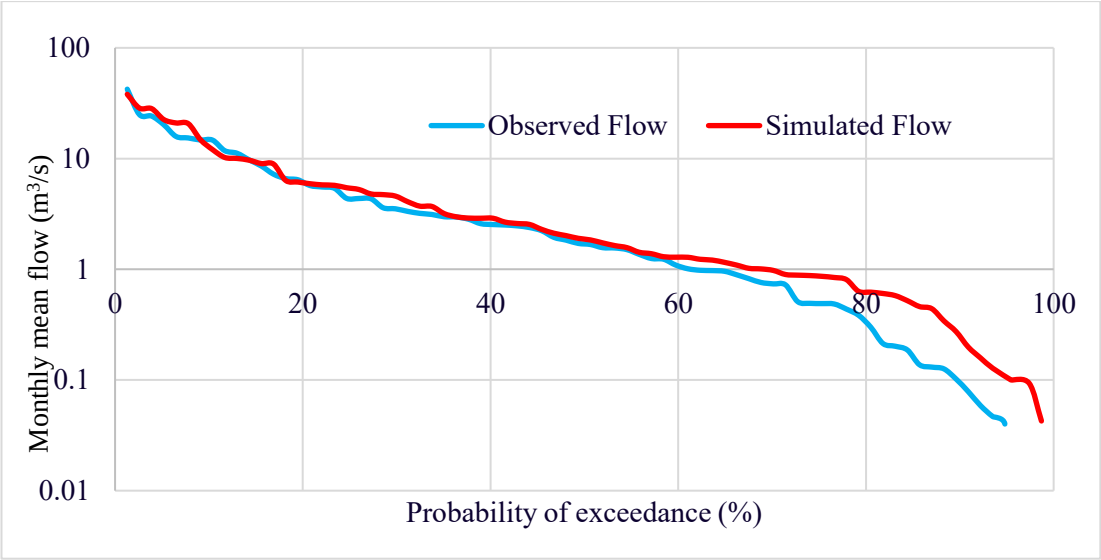

Figure 4.21: Flow Duration Curves obtained for the testing period for the Padiyathalawa sub-basin

Furthermore, Figures 4.22 and 4.23 showcase the scatter plots and hydrographs obtained for the training data set of the model developed for the Wellawaya sub-basin of the Kirindi Oya basin, respectively. Figure 4.24 depicts the flow duration curves plotted for the training period of the model developed for the Wellawaya sub-basin. Simultaneously, Figures 4.25 and 4.26 display the scatter plots and hydrographs obtained for the testing data set of the model developed for the Wellawaya sub-basin, respectively, while Figure 4.27 depicts the flow duration curves plotted for the testing period of the model developed for the Wellawaya sub-basin.

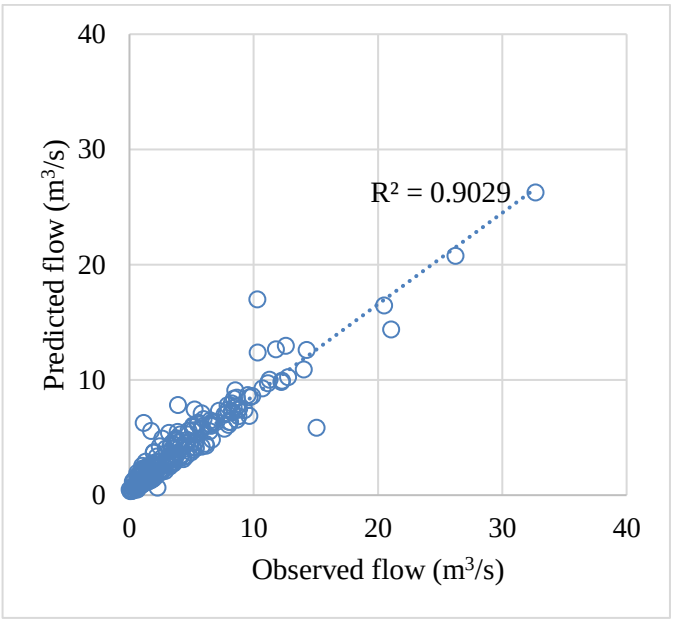

Figure 4.22: Scatter plots obtained from the RF model developed for the Wellawaya sub-basin (Training period)

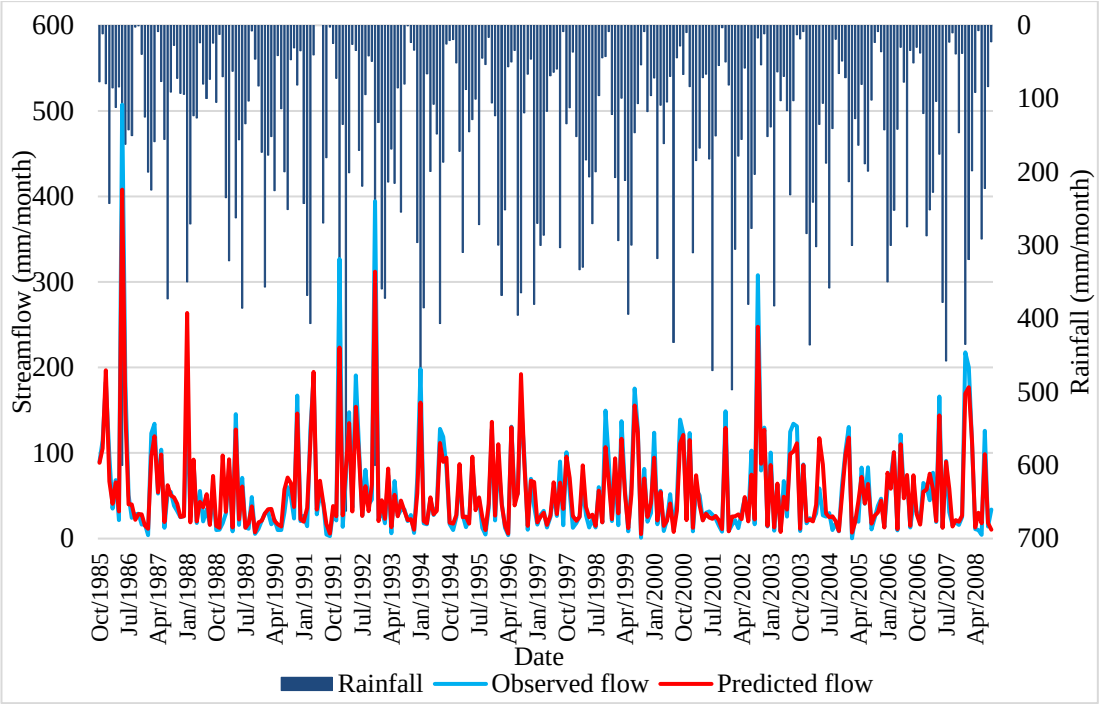

Figure 4.23: Hydrographs obtained from the RF model developed for the Wellawaya sub-basin (training period)

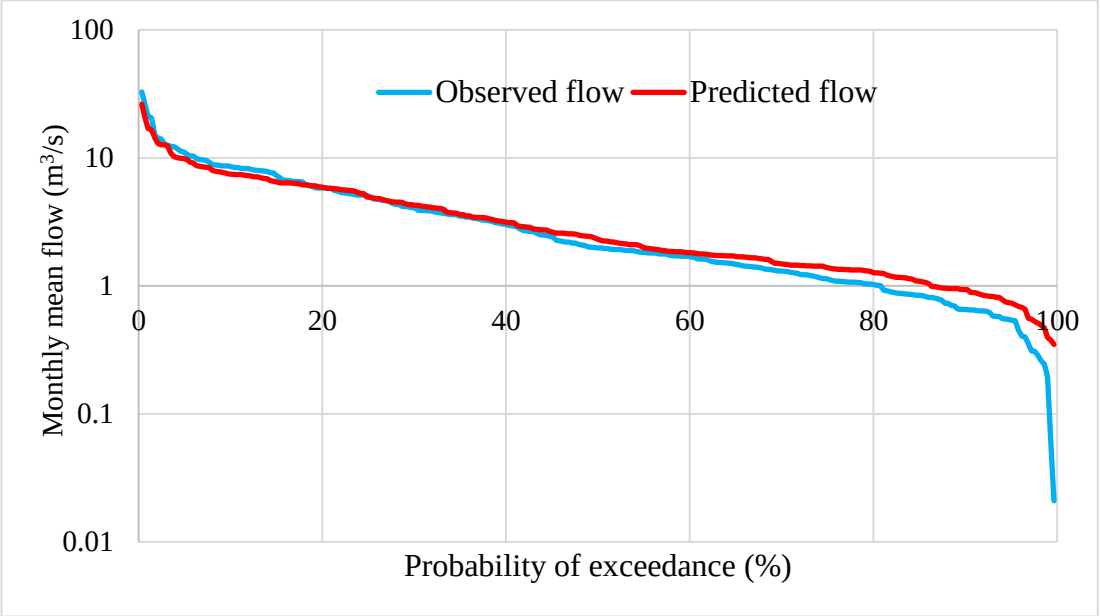

Figure 4.24: Flow Duration Curves obtained for the training period for the Wellawaya sub-basin

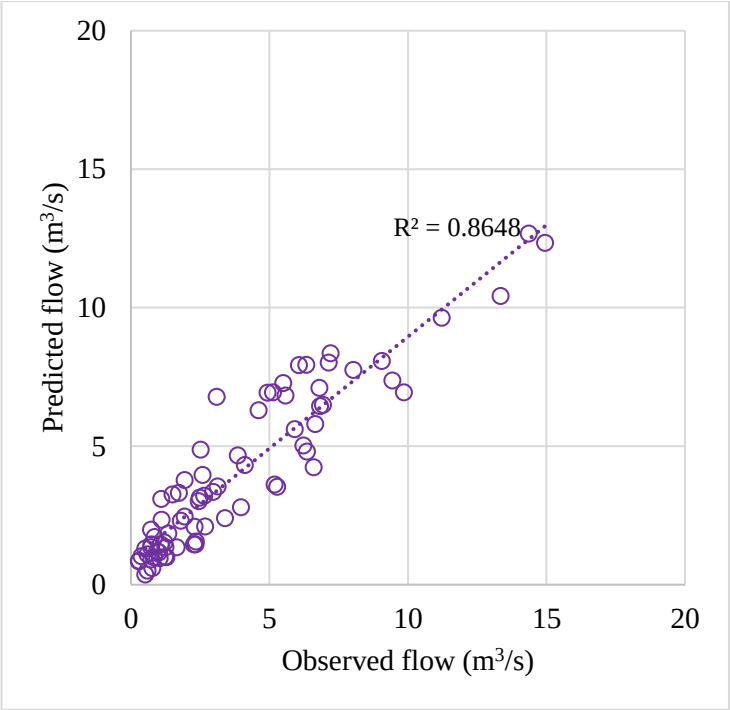

Figure 4.25: Scatter plots obtained from the RF model developed for the Wellawaya sub-basin (Testing period)

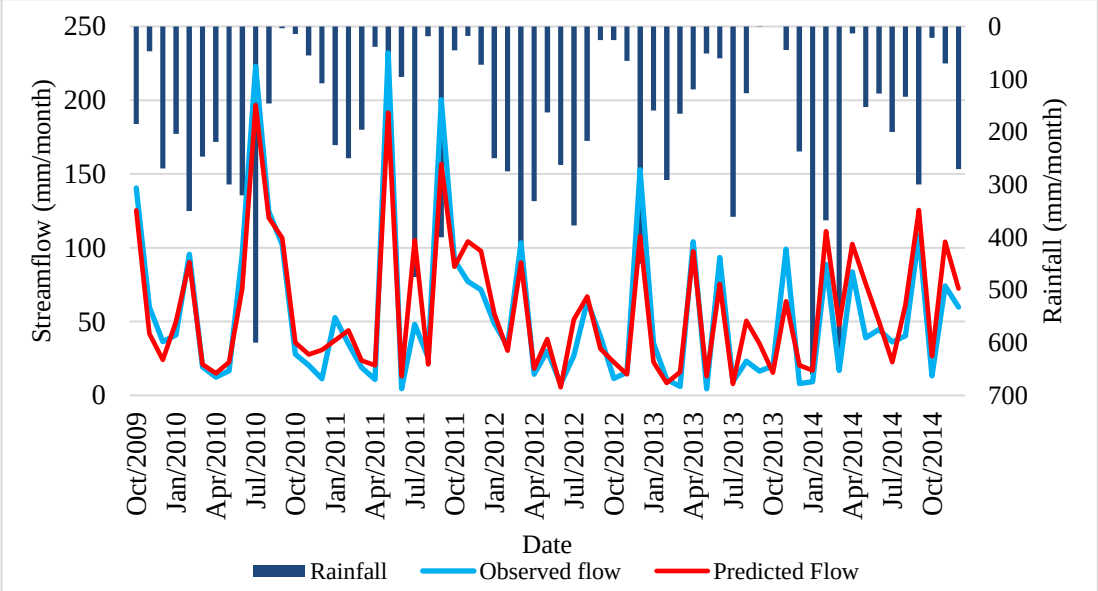

Figure 4.26: Hydrographs obtained from the RF model developed for the Wellawaya sub-basin (testing period)

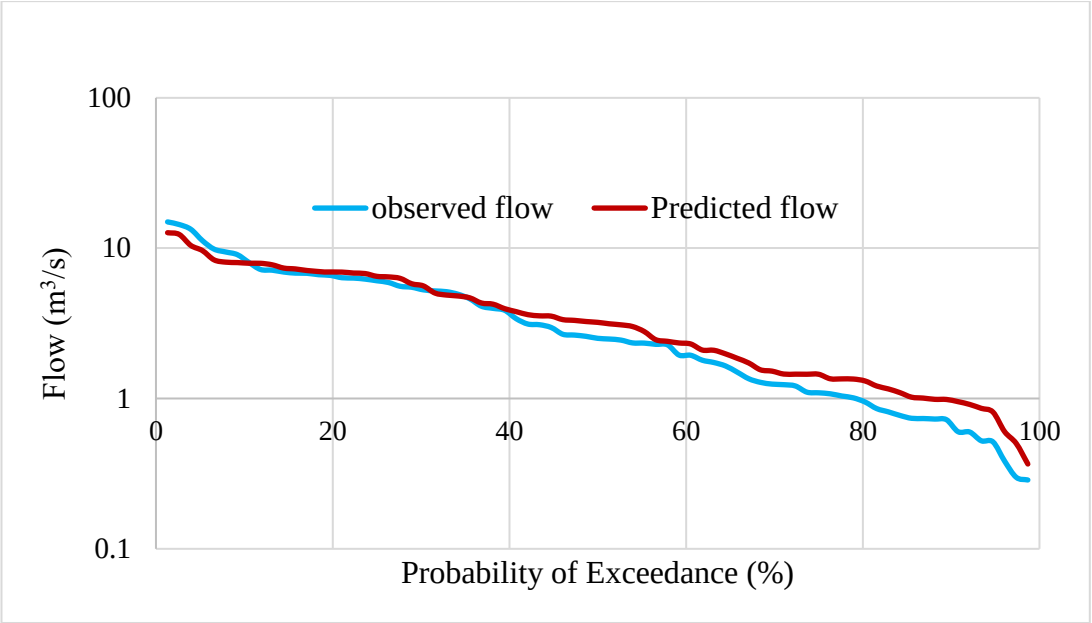

Figure 4.27: Flow Duration Curves obtained for the testing period for the Wellawaya sub-basin

The low flow simulation of the model developed for the Wellawaya sub-basin has exhibited better performance compared to the model developed for the Padiyathalawa sub-basin, although the similar deviation of overestimation can be observed.

4.8 Hydrological Drought Assessment Based on SDI

The Streamflow Drought Index (SDI) was estimated using the monthly mean streamflow for three selected time scales (3-month, 6-month, and 12-month) at Padiyathalawa and Wellawaya gauging stations of the Maduru Oya basin and Kirindi Oya basin, respectively. This estimation was conducted for both current and future climate scenarios.

Figures 4.28 and 4.29 illustrate the variation of the Streamflow Drought Index (SDI) for different time scales from the 1985/1986 water year to the 2014/2015 water year (historical period) in the Padiyathalawa sub-basin and Wellawaya sub-basin, respectively.

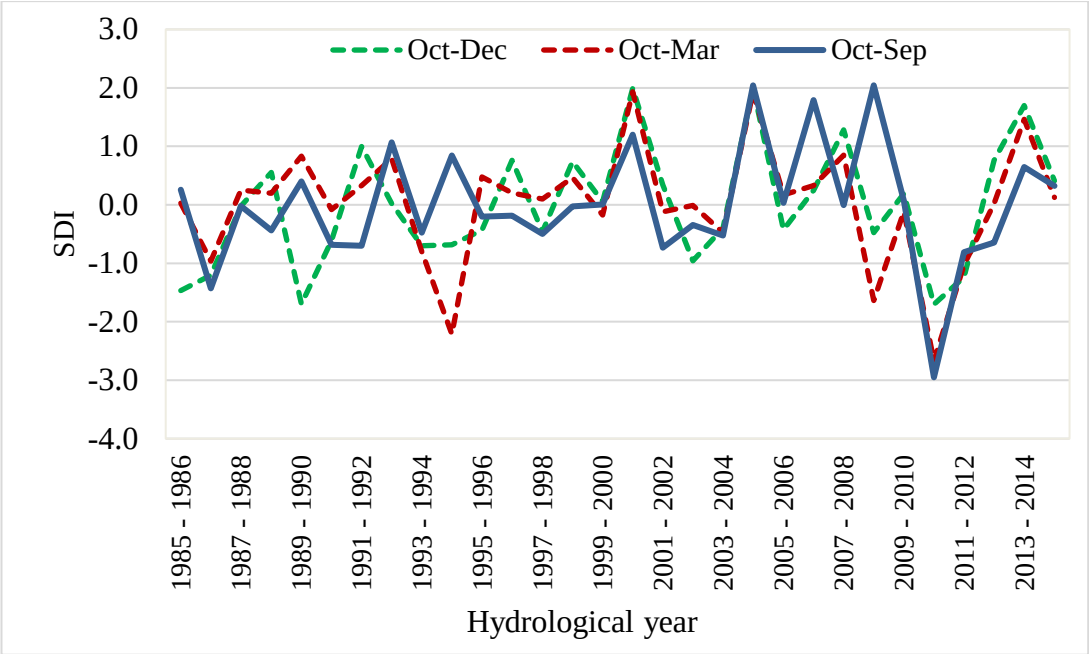

Figure 4.28: Variation of Streamflow Drought Index (SDI) during the historical period at different time scales at the Padiyathalawa gauging station

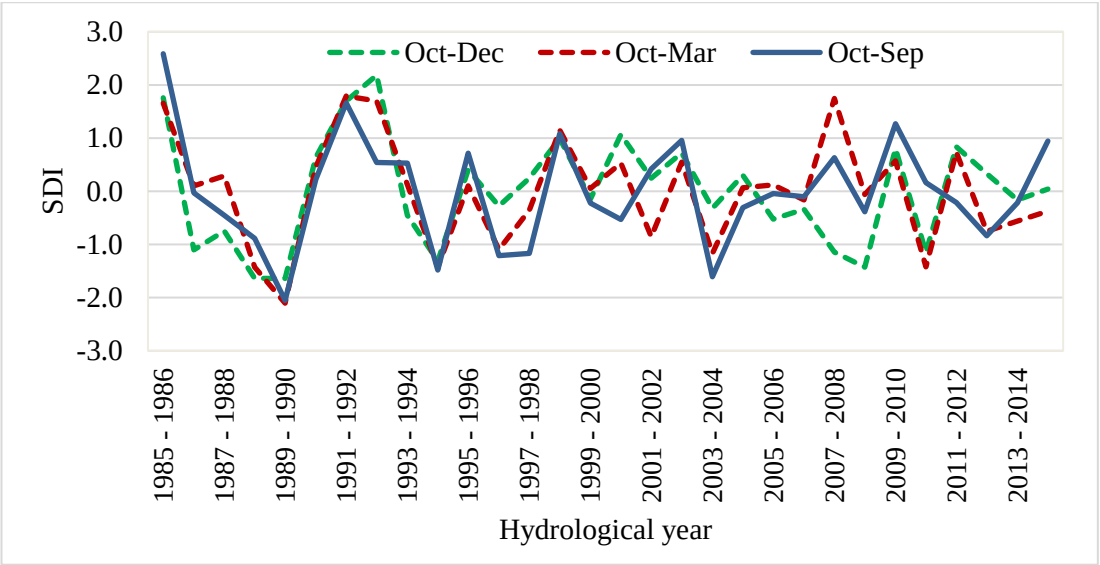

Figure 4.29: Variation of Streamflow Drought Index (SDI) during the historical period at different time scales at the Wellawaya gauging station

At the Padiyathalawa gauging station, the hydrological years of 1989/1990 and 2010/2011 exhibited two drought events at the three-month time scale (October to December). Additionally, the years 1986/1987 and 2010/2011 manifested drought conditions at all three time scales. Conversely, the water years 1994/1995 and 2008/2009 indicated drought conditions at the six-month time scale (October to March). At the Wellawaya gauging station, the hydrological years of 1989/1990,

2008/2009, and 2010/2011 exhibited drought events at the three-month time scale (October to December). The drought event of 1989/1990 was observed at all three time scales, while the drought event of 2010/2011 was noted at the three-month and six-month scales.

At the Padiyathalawa gauging station of the Maduru Oya basin, the drought event observed in the year 2010/2011, manifested across all three time scales, is characterized as an extreme drought event (SDI ≤ -2). In contrast, it is classified as a moderate drought event (-1.5 ≥ SDI < –1.0) for the Wellawaya Gauging station of the Kirindi Oya basin at both three-month and six-month time scales. The drought event of 1989/1990 observed at the Wellawaya station is identified as an extreme drought event. Additionally, it is evident at the Padiyathalawa station at the three-month scale, exhibiting a severe drought condition (–2.0 ≥ SDI < –1.5). Therefore, the two drought events noted in the 1989/1990 and 2010/2011 water years hold significant importance. Moreover, the drought event noticed in 1986/1987 is also noteworthy, as significant agricultural losses were recorded in the dry zone of Sri Lanka due to the drought prevailing in the year 1987 as stated in the Sri Lanka National Report on Disaster Risk, Poverty and Human Development Relationship.

Figures 4.30 and 4.31 depict the variation of SDI at the Padiyathalawa gauging station in the Maduru Oya basin for the future under SSP1-2.6 and SSP5-8.5 scenarios, respectively. The SDI values were estimated based on the predicted streamflow for the projected period from 2015 to 2100. According to the results, under SSP1-2.6, although the Padiyathalawa sub-basin will not be vulnerable to frequent extreme droughts in the future, it will be susceptible to severe droughts more frequently. The water years 2031/2032, 2058/2059, and 2090/2091 show drought events at all time scales. On the other hand, the year 2087/2088 exhibits an extreme drought condition at the three-month (October-December) time scale. Most importantly, the sub-basin is more vulnerable to moderate droughts under the SSP1-2.6 scenario. This vulnerability was also evident in the meteorological drought assessment using SPI.

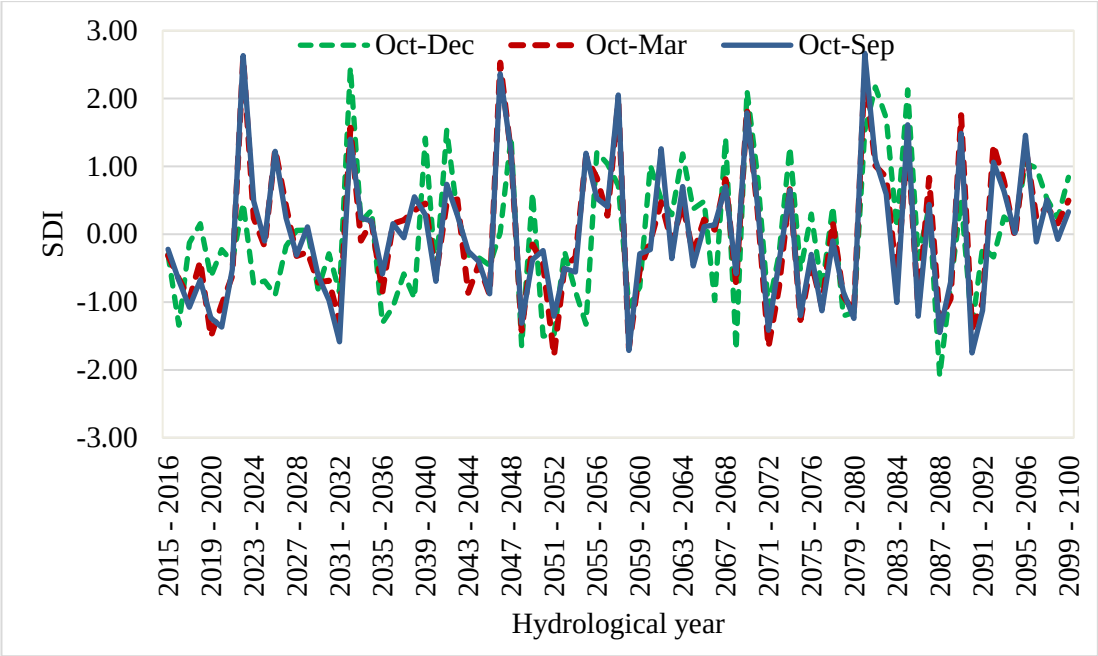

Figure 4.30: Variation of SDI at the Padiyathalawa gauging station in the Maduru Oya basin for the future under SSP1-2.6

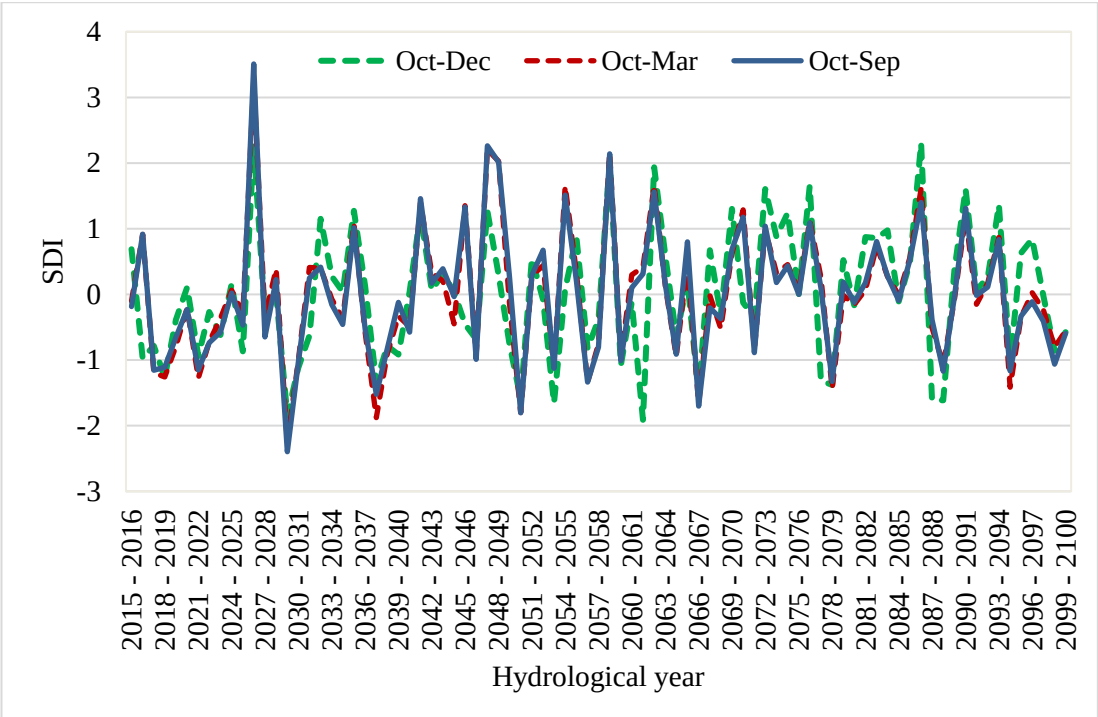

Figure 4.31: Variation of SDI at the Padiyathalawa gauging station in the Maduru Oya basin for the future under SSP5-8.5

The Padiyathalawa sub-basin is more vulnerable to frequent severe droughts under the SSP5-8.5 scenario as well. On the other hand, the 2029/2030 year demonstrates an extreme drought event at the six-month (October to March) and twelve-month

(October to September) scales, while at the three-month (October to December), a severe drought condition is depicted. Simultaneously, the years 2050/2051 and 2066/2067 indicate severe drought conditions at all three time scales. Moreover, under this scenario, the basin is more vulnerable to moderate droughts compared to other drought categories.

Figures 4.32 and 4.33 depict the variation of SDI at the Wellawaya gauging station in the Kirindi Oya basin for the future under SSP1-2.6 and SSP5-8.5 scenarios, respectively.

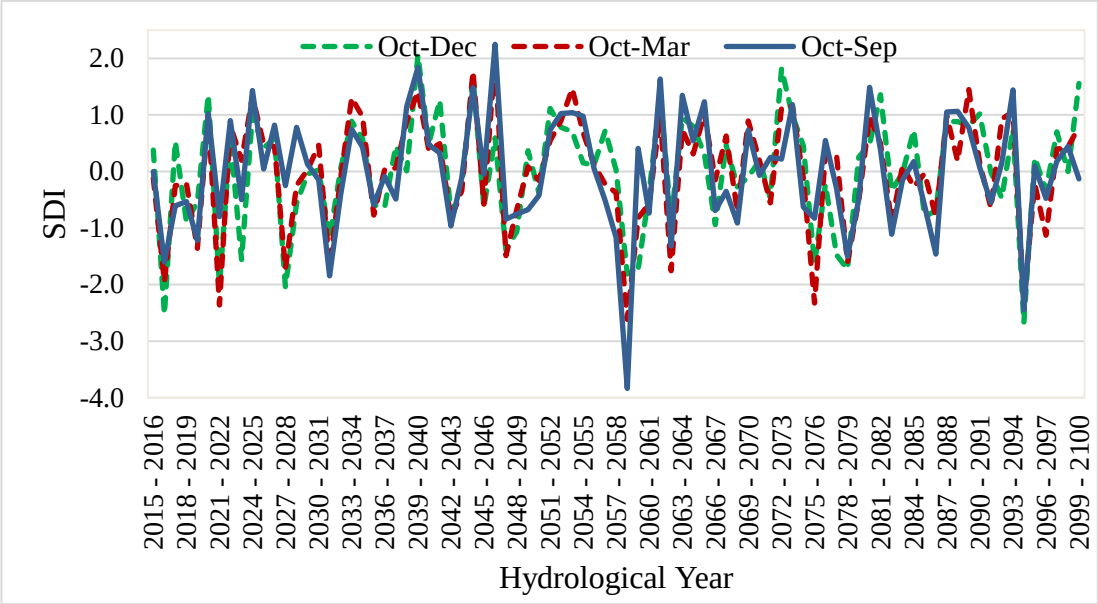

Figure 4.32: Variation of SDI at the Wellawaya gauging station in the Kirindi Oya basin for the future under SSP1-2.6

Under the SSP1-2.6 scenario, the year 2094/2095 demonstrates extreme hydrological drought conditions at all three time scales, and the 2058/2059 year indicates an extreme hydrological drought event at the 6-month and 12-month scales. The year 2075/2076 also indicates an extreme drought at the six-month scale in the Wellawaya sub-basin of the Kirindi Oya basin. Therefore, the Kirindi Oya basin is more vulnerable to extreme droughts under the SSP1-2.6 scenario during the Maha season (October to March).

Under the SSP5-8.5 scenario, the Wellawaya sub-basin of the Kirindi Oya basin is more vulnerable to extreme droughts at the 3-month scale compared to other time scales. The year 2032/2033 indicates an extreme drought event at the 12-month time scale. More frequent moderate hydrological droughts are demonstrated under the SSP5-8.5 scenario.

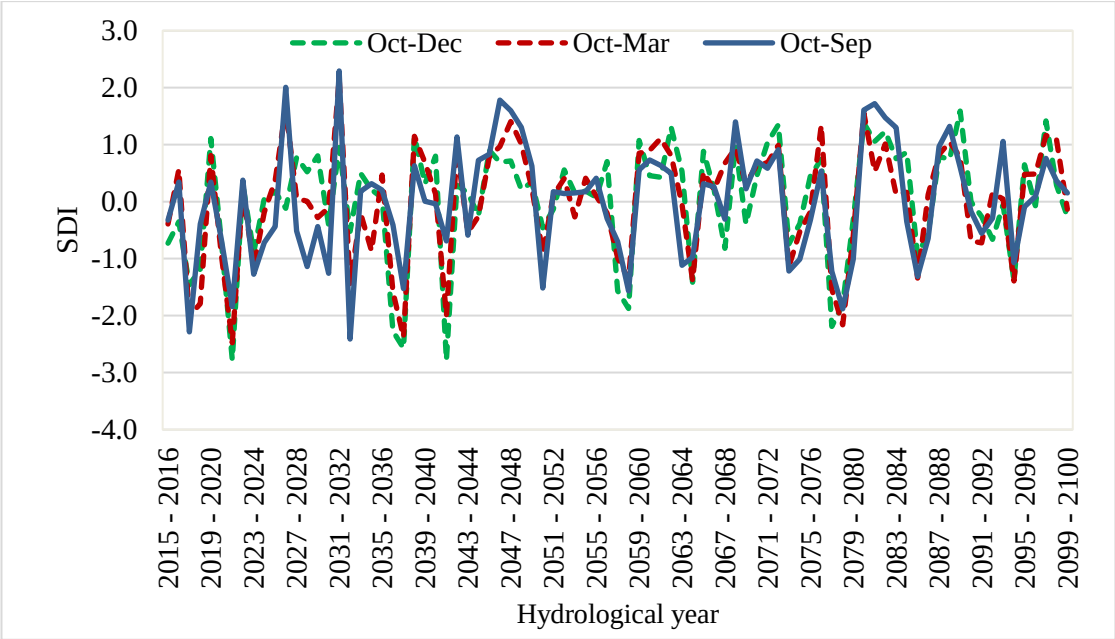

Figure 4.33: Variation of SDI at the Wellawaya gauging station in the Kirindi Oya basin for the future under SSP5-8.5

Tables 4.4, 4.5, and 4.6 present the occurrence percentages of different drought categories based on the frequencies in the historical period (1985-2015), under SSP1-2.6 and SSP5-8.5 for the projected period from 2015 to 2100, respectively. In Tables 4.4, 4.5, and 4.6, the Padiyathalawa subbasin of the Maduru Oya basin and Wellawaya subbasin of the Kirindi Oya basin are denoted as Basin 1 and Basin 2, respectively.

Table 4.4: Occurrence percentages of different drought categories based on SDI in the historical period

Basin	Extreme drought (%)			Severe drought (%)			Moderate drought (%)		
	3-mon	6-mon	12-mon	3-mon	6-mon	12-mon	3-mon	6-mon	12-mon
Basin 1	0	6.45	3.23	6.45	3.23	0	6.45	3.23	3.23
Basin 2	0	3.23	3.23	3.23	0	3.23	12.90	16.13	6.45

Table 4.5: Occurrence percentages of different drought categories based on SDI under the SSP1-2.6 scenario

Basin	Extreme drought (%)			Severe drought (%)			Moderate drought (%)		
	3-mon	6-mon	12-mon	3-mon	6-mon	12-mon	3-mon	6-mon	12-mon
Basin 1	1.16	0	0	3.49	4.65	3.49	9.30	10.46	13.95
Basin 2	4.65	4.65	2.33	4.65	5.81	2.33	3.49	3.49	6.98

Table 4.6: Occurrence percentages of different drought categories based on SDI under the SSP5-8.5 scenario

Basin	Extreme drought (%)			Severe drought (%)			Moderate drought (%)		
	3-mon	6-mon	12-mon	3-mon	6-mon	12-mon	3-mon	6-mon	12-mon
Basin 1	0	1.16	1.16	6.98	3.49	3.49	6.98	9.30	11.63
Basin 2	4.65	5.81	2.33	2.33	3.49	5.81	3.49	8.14	10.47

The highlighted values in Table 4.5 and Table 4.6 represent the drought categories that exhibit increasing trends under the SSP1-2.6 and SSP5-8.5 projection scenarios in comparison to the historical period. It is evident that both Basin 1 (Padiyathalawa sub-basin of the Maduru Oya basin) and Basin 2 (Wellawaya sub-basin of the Kirindi Oya basin) are susceptible to moderate drought conditions under both projection scenarios. Additionally, both basins are prone to extreme drought events at the 3-month (October to December) and 6-month scales (October to March).

When considering the 12-month time scale, the Padiyathalawa sub-basin of the Maduru Oya basin is more vulnerable to moderate droughts under both future scenarios. The occurrence percentages are approximately 14% and 12% under the SSP1-2.6 and SSP5-8.5 scenarios, respectively, representing a significant increase compared to the historical period. This highlights the likelihood of more frequent occurrences of hydrological years with moderate drought conditions, exacerbating water scarcities in the future. Conversely, the occurrence percentage of severe droughts under both scenarios remains unchanged at the 12-month scale. However, no extreme droughts have been recorded under the SSP1-2.6 future scenario. Under the SSP5-8.5 scenario, there is a value of 1.2%, which is relatively small. Therefore, the vulnerability of the subbasin to extreme droughts is not significant in the future. At the 3-month scale, the subbasin is more vulnerable to extreme and moderate hydrological

conditions under the SSP1-2.6 scenario compared to the historical period. However, the vulnerability to moderate droughts remains significant. Moreover, when considering all three time scales, frequent hydrological droughts can be identified under the SSP5-8.5 scenario compared to the historical period.

he Wellawaya sub-basin of the Kirindi Oya basin is also susceptible to frequent moderate hydrological droughts in the future under both projection scenarios, with occurrence percentages of 7% and 10% under SSP1-2.6 and SSP5-8.5, respectively, at the 12-month timescale. Conversely, the sub-basin has exhibited a considerable increase in vulnerability to extreme hydrological droughts at the 3-month and 6-month timescales under both projection scenarios, indicating the likelihood of frequent water scarcities during the Maha season (October to March) in the future. Moreover, an 80% increase in the occurrence of severe hydrological droughts can be observed under the SSP5-8.5 scenario at the 12-month scale, which represents a significant escalation compared to the historical period. Conversely, under the SSP1-2.6 scenario, there is a decrease of 27%. Therefore, the vulnerability of the basin to severe hydrological droughts is notable under the high emission scenario.

5. DISCUSSION

5.1 Bias Correction of GCM Outputs

Currently, significant progress has been achieved in global climate modelling, marked by enhanced spatial resolution and a more comprehensive representation of physicochemical processes, leading to improved accuracy in General Circulation Models (GCMs) (Grillakis et al., 2013). Specifically, the small-scale patterns of daily precipitation exhibit a strong dependence on both model resolution and parameterization. Consequently, they frequently prove unsuitable for direct application in studies evaluating the impacts of climate change (Themeßl et al., 2011). As a result, it is imperative to address the biases inherent in GCM outputs before employing them in investigations related to climate change impacts. In this study, the empirical downscaling method was utilized.

Among the two approaches of empirical downscaling, the bias correction approach was selected. This study selected the statistical bias correction approach, which establishes statistical relationships between observed and simulated precipitation by equalizing key statistical characteristics, including the mean and variance, between modelled and observed precipitation (Grillakis et al., 2013). Two statistical bias correction methods, namely the mean-based and variance-based methods, were employed to calculate monthly bias factors. The selected objective function, the coefficient of determination (R^2), showed satisfactory values. In Chapter 4, Figures 4.1 and 4.2 illustrate the coefficient of determination (R^2) values obtained for each gauging station in the Maduru Oya basin and Kirindi Oya basin, respectively. Notably, the mean-based approach exhibited better performance compared to the variance-based method Notably, the mean-based approach exhibited better performance compared to the variance-based method.

Although R^2 values were greater than 0.5, it is acknowledged that a method like quantile mapping could potentially provide superior results. Quantile mapping, a statistical bias correction technique, establishes statistical relationships between cumulative density functions (CDFs) from a common time frame in observed and simulated precipitation, subsequently applying this method to projected precipitation (Grillakis et al., 2013). Additionally, quantile mapping extends the correction to the entire distribution, including the tails, rendering it suitable for assessing extreme climatic events. This approach addresses biases in the distribution shape and rectifies errors in variability (Miao et al., 2016). Consequently, the utilization of quantile mapping for bias correction may offer enhanced performance compared to other statistical bias correction approaches based on the equalization of statistical characteristics when correcting GCM outputs.

Even though the conventional quantile mapping approach offers a more accurate representation of observed precipitation in comparison to bias correction methods

based on the equalization of statistical characteristics, it operates under the assumption that biases in climate models remain stationary over time. However, the probabilistic structure of climatic variables may undergo changes (Miao et al., 2016). Hence, it is recommended to employ an updated, dynamic cumulative distribution function matching technique for improved GCM output bias correction in future research.

5.2 Streamflow Prediction by Machine Learning Methods

This study primarily utilized two supervised machine learning methods, namely the Recurrent Neural Network (RNN) model and the Random Forest (RF) model. The results indicated that the Long Short-Term Memory (LSTM) RNN models developed for the two basins exhibited inferior performance compared to the RF model, as evident by the values of objective functions presented in Table 4.2 and Table 4.3 in Chapter 4. Additionally, Figures 4.14 and 4.15 present the subpar performance of the developed RNN models. Despite this, literature acknowledges the potency of LSTMs in addressing time series predictions, as they can effectively capture both the periodic and chaotic behaviours of time series data, learning their long-range dependencies with increased accuracy (Wang et al., 2022).

Several researchers have recognized the suitability of LSTMs in rainfall-runoff modelling. However, it is important to note some limitations in this study that may have influenced the subpar performance of LSTM models. In assessing the performance of the models on data not previously encountered, a standard procedure in supervised machine learning involves partitioning the data into three distinct sets. These sets are utilized at various stages in the model creation process.

The model is first trained on a designated training dataset. Subsequently, the trained model is employed to forecast responses for the observations within a second dataset known as the validation dataset. The optimal combination of hyperparameters, determined by the best performance on the validation dataset, is then selected for the machine learning model. Ultimately, an impartial assessment of the final model is conducted using the test dataset.

In this study, monthly rainfall values and streamflow values were employed, resulting in a dataset of 360 values for both model training and testing. Specifically, 80% of the data was allocated for model training, 15% for validation, and the remaining 5% for testing, potentially impacting the performance of the model due to the relatively short data period. The validation and testing datasets are comparatively small, and the trained model exhibited suboptimal performance on these datasets. Sufficient data is essential for effective model training, and the utilization of a more extended data period is preferable.

Conversely, the Thiessen average rainfall for the chosen sub-basin was utilized as the input data based on literature suggesting that gauging stations located within or near the watershed exhibit superior performance when predicting streamflow using LSTM

models (Li et al., 2020). However, it is advisable to incorporate all available rain gauges within and in proximity to the watershed to assess the performance of gauges that align with physical intuition based on statistical tests. Furthermore, the consideration of only rainfall as an input variable may contribute to model limitations. Enhancing the performance of the model could involve incorporating additional factors such as evapotranspiration, humidity, and temperature.

On the other hand, although the random forest models have exhibited better performance compared to LSTM models, indicating superior values for all selected objective functions, an analysis of the plotted flow duration curves for both training and testing periods reveals that the simulated low flow values are comparatively high in relation to the observed streamflow values. While high low flow values are significant in the context of a drought-related study, where the assessment of hydrological drought relies on streamflow values, this discrepancy remains a limitation of the black box model approach. This limitation arises from the inability to adjust only the low flow conditions, as parameters associated with low flow conditions cannot be altered, unlike in physically based hydrological models.

5.3 Vulnerability of the Maduru Oya and Kirindi Oya Basins to Droughts in the Future

In this study, two primary assessments were conducted for drought monitoring. Meteorological drought monitoring was performed using the Standardized Precipitation Index (SPI), while hydrological drought monitoring was based on the Streamflow Drought Index (SDI). Maps were generated to visualize the spatial distribution of meteorological droughts. A comparison of the two results can be undertaken only by considering the upstream parts of the two basins, as the hydrological drought assessment was conducted solely for the two upstream sub-basins.

According to the results, the upstream part of the Maduru Oya basin exhibits greater vulnerability to moderate meteorological droughts during the historical period compared to the two future scenarios. Additionally, based on the hydrological drought assessment, the Padiyathalawa sub-basin, which constitutes the upstream portion of the Maduru Oya basin, demonstrates increased vulnerability to moderate droughts under the two projected scenarios across all three time scales. As a consequence, the upstream region is rendered more susceptible to moderate meteorological droughts and moderate hydrological droughts. This heightened vulnerability is anticipated to significantly impact water availability downstream as well. Consequently, the Maduru Oya basin emerges as more vulnerable to moderate hydrological droughts in the future.

Furthermore, a significant variation is not apparent in the generated maps depicting the meteorological drought status of the two basins, particularly concerning extreme drought conditions. This holds true for both the historical period and the projection

scenarios, where the occurrence percentages, on average, have exhibited noteworthy increases. In the Maduru Oya basin, the occurrence percentages have shown increments of 18% and 31% under the SSP1-8.5 and SSP5-8.5 scenarios, respectively. Similarly, in the Kirindi Oya basin, percentage increments of 49% and 37% have been observed under the SSP1-2.6 and SSP5-8.5 scenarios, respectively.

On the other hand, the vulnerability of both Kirindi Oya and Maduru Oya basins to moderate meteorological drought conditions has been reduced under the SSP5-8.5 scenario compared to the SSP1-2.6 scenario. According to Zhai et al. (2020), Sri Lanka belongs to the South-East (SE) dryness region among the five homogeneous dryness regions of South Asia. The projections indicate a significant increase in precipitation under the SSP5-8.5 scenario, while there is a considerable decrease rate under the SSP1-2.6 scenario in the SE region, leading to reduced meteorological drought vulnerability under SSP5-8.5 compared to SSP1-2.6. Moreover, the drought frequency per decade projected by CMIP6 models is in the range of 4-6% for Sri Lanka. Therefore, the results can be verified.

Moreover, the Padiyathalawa sub-basin of the Maduru Oya basin is more vulnerable to severe hydrological droughts at the 6-month (October-March) and 12-month scale (October-September) under the two projected scenarios. Therefore, frequent droughts and water scarcities can be expected in the future. On the other hand, the increment in the occurrence of extreme hydrological drought events in the future in the Wellawaya sub-basin of the Kirindi Oya basin is comparatively high at the 3-month and 6-month time scales under both projection scenarios. Therefore, considerable water scarcities can be expected in the Kirindi Oya basin in comparison to the Maduru Oya basin.

The SSP1-2.6 scenario outlines a trajectory characterized by minimal challenges in terms of mitigation and adaptation. This results in a future global landscape where both social and economic development adhere to sustainability goals. In contrast, the SSP5-8.5 scenario assumes a global socio-economic development focus on economic growth, high energy demand, and limited efforts to mitigate climate change. While SSP1-2.6 envisions a future marked by ambitious climate change mitigation efforts, aiming to restrict global warming to levels significantly below 2°C above pre-industrial levels, an assessment of all five scenarios by Working Group I (WGI) of the Intergovernmental Panel on Climate Change (IPCC) indicates a probability exceeding 50% that global warming will attain or surpass 1.5°C in the near term. This likelihood persists even for the very low greenhouse gas emissions scenario (SSP1-2.6) (IPCC, 2023). Consequently, it is evident that both basins will encounter frequent meteorological and hydrological droughts in the future, given their heightened vulnerability to droughts, even under the low emission scenario, which is projected to be surpassed in the near future. Consequently, the susceptibility of the two basins to drought conditions is anticipated to significantly increase in the future.

6. CONCLUSIONS

In summary, the study findings and insights contribute valuable perspectives to the understanding of the effect of climate change on the occurrence of meteorological and hydrological droughts in Maduru Oya and Kirindi Oya dry zone basins, and the following key conclusions emerge.

1. According to the results of the meteorological drought assessment of the Maduru Oya basin, under the SSP1-2.6 scenario, the occurrence of extreme, severe, and moderate droughts shows percentage increases of 18%, 16%, and -6%, respectively, in comparison to the historical period. The occurrence of moderate droughts has shown a considerable increase in the upstream part of the basin.

2. Under the SSP5-8.5 scenario, the percentage increments in the occurrence of meteorological droughts in the Maduru Oya basin for extreme, severe, and moderate drought conditions are 31%, 2%, and -4%, respectively, compared to the historical period (1985-2015). Therefore, the frequency of moderate meteorological droughts in the future is lower compared to the historical period.

3. The results of the meteorological drought assessment for the Kirindi Oya basin elaborate that the occurrence percentages of moderate droughts exhibit relatively higher values across all three scenarios compared to the occurrence percentages of extreme and severe droughts.

4. The analysis reveals that, in the Kirindi Oya basin, under the SSP1-2.6 scenario, the occurrence of extreme, severe, and moderate meteorological droughts shows percentage increases of 49%, -8%, and 8%, respectively, compared to the historical period.

5. For the SSP5-8.5 scenario, the percentage increments of the Kirindi Oya basin for extreme, severe, and moderate meteorological drought conditions are 37%, -5%, and 4%, respectively. Importantly, it is noteworthy that the occurrence of extreme droughts is projected to surge by more than 35% under both projection scenarios.

6. According to the results of the hydrological drought assessment, the Padiyathalawa sub-basin of the Maduru Oya basin is anticipated to experience frequent moderate hydrological droughts. The basin has shown a substantial increase in occurrence percentages under both future scenarios across all three time scales. Particularly noteworthy is the heightened susceptibility observed at the 12-month time scale under both future scenarios, with occurrence percentages of 14% under SSP1-2.6 and 12% under SSP5-8.5. This underscores the likelihood of more frequent occurrences of hydrological years characterized by moderate drought conditions, which in turn exacerbates water scarcities in the future.

7. Additionally, the occurrence percentages of severe droughts remain unchanged at the 12-month scale under both scenarios. Furthermore, no extreme droughts have been recorded under SSP1-2.6, with only a small occurrence (1.2%) observed under SSP5-8.5 in the Padiyathalawa sub-basin.

8. The Wellawaya sub-basin of the Kirindi Oya basin is susceptible to frequent moderate hydrological droughts in the future under both projection scenarios at the 12-month timescale (7% under SSP1-2.6 and 10% under SSP5-8.5). Moreover, an 80% increase in the occurrence of severe hydrological droughts under SSP5-8.5 at the 12-month scale, which represents a significant escalation compared to the historical period, has been indicated.

9. Furthermore, there is a considerable increase in vulnerability to extreme hydrological droughts at the 3-month and 6-month timescales under both scenarios, emphasizing the likelihood of frequent water scarcities during the Maha season (October to March) in the future in the Wellawaya sub-basin of the Kirindi Oya basin.

10. Both river basins are vulnerable to hydrological droughts, with the Kirindi Oya basin being more susceptible to extreme droughts compared to the Maduru Oya basin. Conversely, the Maduru Oya basin is found to be more vulnerable to moderate hydrological drought events in the future.

11. In conclusion, both river basins may experience water scarcities more frequently during the Maha season (October to March), which influences rainfall patterns in the dry zone, thereby increasing susceptibility to water shortages in the subsequent Yala season in the future. Therefore, the findings of this research are crucial for effective water management in these basins. The results are of great significance for decision-making authorities, emphasizing the importance of implementing proactive measures to ensure a reliable water supply for irrigation and domestic purposes.

7. RECOMMENDATIONS

Based on the findings of this research, several recommendations are proposed. It is suggested to implement sustainable water management practices in both the Maduru Oya and Kirindi Oya basins to optimize the utilization of available water resources. According to the meteorological drought assessment, both river basins have indicated an increasing vulnerability to extreme meteorological drought, with increment percentages exceeding 30% under the SSP5-8.5 scenario. Simultaneously, both basins have shown an increasing vulnerability to extreme meteorological droughts under the low emission scenario, which is projected to be surpassed in the near future. Moreover, both river basins are susceptible to hydrological droughts, with the Kirindi Oya basin being more vulnerable to extreme hydrological droughts, with an increasing occurrence percentage of 80% in the future under the SSP5-8.5 scenario. Encouraging the promotion of alternative water supply options, such as rainwater harvesting, groundwater recharge, and the adoption of efficient water storage facilities, is crucial. This initiative aims to ensure a reliable water supply, particularly during the Yala cultivation season, due to the expected frequent water scarcities during the Maha season (Northeast monsoon period), which influences the rainfall patterns of the dry zone.

Furthermore, there is a recommendation to conduct additional research, expanding the dataset to include longer time periods and additional variables such as evaporation, humidity, and temperature. This expansion is anticipated to enhance the accuracy and performance of predictive models.

In addition, fostering collaboration among relevant stakeholders, including governmental agencies, local communities, and research institutions, is encouraged. This collaborative effort aims to collectively address water scarcity challenges and implement sustainable solutions. Given the substantial impact of climate change on watershed hydrology, the insights gained from this research are deemed imperative for proactively devising effective strategies to enhance the efficient management of water resources within the basin. This emphasizes the importance of integrating these findings into future planning initiatives.

BIBILIOGRAPHY

Aadhar, S., & Mishra, V. (2017). *Data Descriptor : High-resolution near real-time drought monitoring in South Asia*. 1–14.

Abdulelah Al-Sudani, Z., Salih, S. Q., sharafati, A., & Yaseen, Z. M. (2019). Development of multivariate adaptive regression spline integrated with differential evolution model for streamflow simulation. *Journal of Hydrology*, *573*, 1–12. https://doi.org/10.1016/j.jhydrol.2019.03.004

Abeysingha, N. S., & Rajapaksha, U. R. L. N. (2020). SPI-Based Spatiotemporal Drought over Sri Lanka. *Advances in Meteorology*, *2020*. https://doi.org/10.1155/2020/9753279

Abeysingha, N. S., Wickramasuriya, M. G., & Meegastenna, T. J. (2020). *Assessment of meteorological and hydrological drought ; a case study in Kirindi Oya river basin in Sri Lanka*. *10*(5), 429–447.

Adnan, R. M., Liang, Z., Trajkovic, S., Zounemat-Kermani, M., Li, B., & Kisi, O. (2019). Daily streamflow prediction using optimally pruned extreme learning machine. *Journal of Hydrology*, *577*. https://doi.org/10.1016/j.jhydrol.2019.123981

Alahacoon, N., & Amarnath, G. (2022). Agricultural drought monitoring in Sri Lanka using multisource satellite data. *Advances in Space Research*, *69*(11), 4078–4097. https://doi.org/10.1016/j.asr.2022.03.009

Alahacoon, N., & Edirisinghe, M. (2022). A comprehensive assessment of remote sensing and traditional based drought monitoring indices at global and regional scale. *Geomatics, Natural Hazards and Risk*, *13*(1), 762–799. https://doi.org/10.1080/19475705.2022.2044394

Alahacoon, N., Edirisinghe, M., & Ranagalage, M. (2021). Satellite-based meteorological and agricultural drought monitoring for agricultural sustainability in Sri Lanka. *Sustainability (Switzerland)*, *13*(6). https://doi.org/10.3390/su13063427

Alawsi, M. A., Zubaidi, S. L., Al-bdairi, N. S. S., Al-ansari, N., & Hashim, K. (2022). *Drought Forecasting : A Review and Assessment of the Hybrid Techniques and Data Pre-Processing*. 1–23.

Amarasinghe, U. A. (2010). Spatial variation of water supply and demand in Sri Lanka. *In Proceedings of the National Conference on Water, Food Security and Climate Change*, 19–35. http://ageconsearch.umn.edu

Balti, H., Ben, A., Mellouli, N., Riadh, I., Sang, Y., & Lamolle, M. (2020). Ecological Informatics A review of drought monitoring with big data : Issues , methods ,

challenges and research directions. *Ecological Informatics*, *60*(July), 101136. https://doi.org/10.1016/j.ecoinf.2020.101136

Chaminda, S. P., Kazama, S., & Komori, D. (2016). Near future climatic impact on seasonal runoff in Sri Lanka.

Chan, S. S., Seidenfaden, I. K., Jensen, K. H., & Sonnenborg, T. O. (2021). Climate change impacts and uncertainty on spatiotemporal variations of drought indices for an irrigated catchment. *Journal of Hydrology*, *601*(August). https://doi.org/10.1016/j.jhydrol.2021.126814

Chen, J., Brissette, F. P., Chaumont, D., & Braun, M. (2013). Performance and uncertainty evaluation of empirical downscaling methods in quantifying the climate change impacts on hydrology over two North American river basins. *Journal of Hydrology*, *479*, 200–214. https://doi.org/10.1016/j.jhydrol.2012.11.062

Climate change and water resources. (n.d.).

Dadson, S. J., Lopez, H. P., Peng, J., & Vora, S. (2019). Hydroclimatic Extremes and Climate Change. *Water Science, Policy, and Management: A Global Challenge*, 11–28.

Dai, A. (2011). Drought under global warming: A review. In *Wiley Interdisciplinary Reviews: Climate Change* (Vol. 2, Issue 1, pp. 45–65). Wiley-Blackwell. https://doi.org/10.1002/wcc.81

Eckstein, D., Hutfils, M., & Winges, M. (2019). Global Climate Risk Index 2019 Who Suffers Most From Extreme Weather Events ? Weather-related Loss Events in 2017 and 1998 to 2017.

Edossa, D. C., Babel, M. S., & Gupta, A. Das. (2010). Drought analysis in the Awash River Basin, Ethiopia. *Water Resources Management*, *24*(7), 1441–1460. https://doi.org/10.1007/s11269-009-9508-0

Faghmous, J. H., & Kumar, V. (2014). *The Climate System: A Data Science Perspective A BIG DATA GUIDE TO UNDERSTANDING CLIMATE CHANGES*.

Goshime, D. W., Absi, R., & Ledésert, B. (2019). Evaluation and bias correction of CHIRP rainfall estimate for rainfall-runoff simulation over Lake Ziway Watershed, Ethiopia. *Hydrology*, *6*(3). https://doi.org/10.3390/hydrology6030068

Grillakis, M. G., Koutroulis, A. G., & Tsanis, I. K. (2013). Multisegment statistical bias correction of daily GCM precipitation output. *Journal of Geophysical Research Atmospheres*, *118*(8), 3150–3162. https://doi.org/10.1002/jgrd.50323

Hamed, M. M., Nashwan, M. S., & Shahid, S. (2022). A novel selection method of CMIP6 GCMs for robust climate projection. In *International Journal of Climatology* (Vol. 42, Issue 8). https://doi.org/10.1002/joc.7461

Harischandra, I. N., Dassanayake, R. S., & De Silva, B. G. D. N. K. (2016). Three sympatric clusters of the malaria vector Anopheles culicifacies e (Diptera: Culicidae) detected in Sri Lanka. *Parasites and Vectors*, *9*(1). https://doi.org/10.1186/s13071-015-1286-3

Intergovernmental Panel on Climate Change (IPCC). (2023). Technical Summary. In *Climate Change 2022 – Impacts, Adaptation and Vulnerability* (pp. 37–118). Cambridge University Press. https://doi.org/10.1017/9781009325844.002

IPCC. (2019). Foreword Technical and Preface. In *Climate Change and Land:* an IPCC special report on climate change, desertification, land degradation, sustainable land management, food security, and greenhouse gas fluxes in terrestrial ecosystems.

Jakob Themeßl, M., Gobiet, A., & Leuprecht, A. (2011). Empirical-statistical downscaling and error correction of daily precipitation from regional climate models. *International Journal of Climatology*, *31*(10), 1530–1544. https://doi.org/10.1002/joc.2168

Karran, D. J., Morin, E., & Adamowski, J. (2014). Multi-step streamflow forecasting using data-driven non-linear methods in contrasting climate regimes. *Journal of Hydroinformatics*, *16*(3), 671–689. https://doi.org/10.2166/hydro.2013.042

Kirupacaran, S. (2020). Analysis of precipitation trend and streamflow sensitivity to precipitation in Maduru Oya river basin with HEC-HMS. July.

Kumar, S., Huang, J., Wang, Y., Su, B., Zhai, J., Tao, H., Wang, G., Fischer, T., Wen, S., & Jiang, T. (2021). Science of the Total Environment Doubling of the population exposed to drought over South Asia : CMIP6 multi-model-based analysis. *Science of the Total Environment*, *771*, 145186. https://doi.org/10.1016/j.scitotenv.2021.145186

Li, W., Kiaghadi, A., & Dawson, C. N. (2020). *High Temporal Resolution Rainfall Runoff Modelling Using Long-Short-Term-Memory (LSTM) Networks*. https://doi.org/10.1007/s00521-020-05010-6

Liu, D., Jiang, W., Mu, L., & Wang, S. (2020). Streamflow Prediction Using Deep Learning Neural Network: Case Study of Yangtze River. *IEEE Access*, *8*, 90069–90086. https://doi.org/10.1109/ACCESS.2020.2993874

Lokuhetti, R., Zubair, L., Visvanathan, J., & Nijamdeen, A. (2017). *Drought Monitoring for Sri Lanka: Spatial Extent and Temporal Evolution during the 2016-17 Drought*.

Loukas, A., Vasiliades, L., & Tzabiras, J. (2008). Climate change effects on drought severity. *Advances in Geosciences*, *17*, 23–29. https://doi.org/10.5194/adgeo-17-23-2008

Madani, K., AghaKouchak, A., & Mirchi, A. (2016). Iran's Socio-economic Drought: Challenges of a Water-Bankrupt Nation. *Iranian Studies*, *49*(6), 997–1016. https://doi.org/10.1080/00210862.2016.1259286

Mahenthiran, B., & Rajapakse, L. (2021). Water resources availability and low flow discharge analysis of two selected river basins in the dry zone under changing climate conditions. *MERCon 2021 - 7th International Multidisciplinary Moratuwa Engineering Research Conference, Proceedings*, 504–509. https://doi.org/10.1109/MERCon52712.2021.9525654

Manesha, S., Vimukthini, S., & Premalal, K. H. M. S. (2015). *Develop Drought Monitoring in Sri Lanka Using Standard Precipitation Index (SPI)*. http://www.desinventar.lk/

Mckee, T. B., Doesken, N. J., & Kleist, J. (1993). The relationship of drought frequency and duration to time scales. In *Eighth Conference on Applied Climatology*.

Miao, C., Su, L., Sun, Q., & Duan, Q. (2016). A nonstationary bias-correction technique to remove bias in GCM simulations. *Journal of Geophysical Research*, *121*(10), 5718–5735. https://doi.org/10.1002/2015JD024159

Miller, M. P., Carlisle, D. M., Wolock, D. M., & Wieczorek, M. (2018). A Database of Natural Monthly Streamflow Estimates from 1950 to 2015 for the Conterminous United States. *Journal of the American water resources association*. https://doi.org/10.1111/1752

M.M Jibril, Aliyu Bello, Ismail I Aminu, Awaisu Shafiu Ibrahim, Abba Bashir, Salim Idris Malami, Habibu M.A, & Mohammed Mukhtar Magaji. (2022). An overview of streamflow prediction using random forest algorithm. *GSC Advanced Research and Reviews*, *13*(1), 050–057. https://doi.org/10.30574/gscarr.2022.13.1.0112

Mondal, S. K., Huang, J., Wang, Y., Su, B., Zhai, J., Tao, H., Wang, G., Fischer, T., Wen, S., & Jiang, T. (2021). Doubling of the population exposed to drought over South Asia: CMIP6 multi-model-based analysis. *Science of the Total Environment*, *771*. https://doi.org/10.1016/j.scitotenv.2021.145186

Nalbantis, I., & Tsakiris, G. (2009). Assessment of hydrological drought revisited. *Water Resources Management*, *23*(5), 881–897. https://doi.org/10.1007/s11269-008-9305-1

Naveendrakumar, G., Vithanage, M., Kwon, H. H., Iqbal, M. C. M., Pathmarajah, S., & Obeysekera, J. (2018). Five decadal trends in averages and extremes of rainfall

and temperature in Sri Lanka. *Advances in Meteorology*, *2018*. https://doi.org/10.1155/2018/4217917

O'Neill, B. C., Kriegler, E., Ebi, K. L., Kemp-Benedict, E., Riahi, K., Rothman, D. S., van Ruijven, B. J., van Vuuren, D. P., Birkmann, J., Kok, K., Levy, M., & Solecki, W. (2017). The roads ahead: Narratives for shared socioeconomic pathways describing world futures in the 21st century. *Global Environmental Change*, *42*, 169–180. https://doi.org/10.1016/j.gloenvcha.2015.01.004

Palmer, W. C. (1965). Meteorological_Drought. *Meteorological Drought*, *Vol. 30*.

Panda, D. K., Panigrahi, P., Mohanty, S., Mohanty, R. K., & Sethi, R. R. (2016). The 20th century transitions in basic and extreme monsoon rainfall indices in India: Comparison of the ETCCDI indices. *Atmospheric Research*, *181*, 220–235. https://doi.org/10.1016/j.atmosres.2016.07.002

Parisouj, P., Mohebzadeh, H., & Lee, T. (2020). Employing Machine Learning Algorithms for Streamflow Prediction: A Case Study of Four River Basins with Different Climatic Zones in the United States. *Water Resources Management*, *34*(13), 4113–4131. https://doi.org/10.1007/s11269-020-02659-5

Punsara, C., & Rajapakse, L. (2021). Water Resources Availability and Low Flow Discharge Analysis of Kelani River Basin in Wet Zone under Changing Climate Conditions. *2021 Moratuwa Engineering Research Conference (MERCon)*, 516–521. https://doi.org/10.1109/MERCon52712.2021.9525721

Ragettli, S., Cortés, G., Mcphee, J., & Pellicciotti, F. (2014). An evaluation of approaches for modelling hydrological processes in high-elevation, glacierized Andean watersheds. *Hydrological Processes*, *28*(23), 5674–5695. https://doi.org/10.1002/hyp.10055

Shelton, S., Ogou, F. K., & Pushpawela, B. (2022a). *Spatial-Temporal Variability of Droughts during Two Cropping Seasons in Sri Lanka and Its Possible Mechanisms*. *2014*, 127–144.

Shelton, S., Ogou, F. K., & Pushpawela, B. (2022b). Spatial-Temporal Variability of Droughts during Two Cropping Seasons in Sri Lanka and Its Possible Mechanisms. *Asia-Pacific Journal of Atmospheric Sciences*, *58*(1), 127–144. https://doi.org/10.1007/s13143-021-00239-0

Sundararajan, K., Garg, L., Srinivasan, K., Bashir, A. K., Ganapathy, G. P., Selvaraj, S. K., & Meena, T. (2021). A Contemporary Review on Drought Modeling Using Machine Learning Approaches. *Computer Modeling in Engineering and Sciences*, *Vol.128, N*, 41. https://doi.org/10.32604/cmes.2021.015528

Tabari, H., Nikbakht, J., & Hosseinzadeh Talaee, P. (2013). Hydrological Drought Assessment in Northwestern Iran Based on Streamflow Drought Index (SDI).

Water Resources Management, *27*(1), 137–151. https://doi.org/10.1007/s11269-012-0173-3

Tigkas, D., Vangelis, H., & Tsakiris, G. (2015). DrinC: a software for drought analysis based on drought indices. *Earth Science Informatics*, *8*(3), 697–709. https://doi.org/10.1007/s12145-014-0178-y

Tramblay, Y., Koutroulis, A., Samaniego, L., Vicente-Serrano, S. M., Volaire, F., Boone, A., Le Page, M., Llasat, M. C., Albergel, C., Burak, S., Cailleret, M., Kalin, K. C., Davi, H., Dupuy, J. L., Greve, P., Grillakis, M., Hanich, L., Jarlan, L., Martin-StPaul, N., … Polcher, J. (2020). Challenges for drought assessment in the Mediterranean region under future climate scenarios. *Earth-Science Reviews*, *210*(August), 103348. https://doi.org/10.1016/j.earscirev.2020.103348

Tsakiris, G., Loukas, A., Pangalou, D., Vangelis, H., Tigkas, D., Rossi, G., & Cancelliere, A. (2007). Drought characterization [Part 1. Components of drought planning. 1.3. Methodological component]. *Drought Management Guidelines Technical Annex*, *58*(58), 85–102. http://om.ciheam.org/om/pdf/b58/00800535.pdf

Tsakiris, G., Pangalou, D., & Vangelis, H. (2007). Regional drought assessment based on the Reconnaissance Drought Index (RDI). *Water Resources Management*, *21*(5), 821–833. https://doi.org/10.1007/s11269-006-9105-4

Vicente-Serrano, S. M., Beguería, S., & López-Moreno, J. I. (2010). A multiscalar drought index sensitive to global warming: The standardized precipitation evapotranspiration index. *Journal of Climate*, *23*(7), 1696–1718. https://doi.org/10.1175/2009JCLI2909.1

Wang, J., Li, X., Li, J., Sun, Q., & Wang, H. (2022). NGCU: A New RNN Model for Time-Series Data Prediction. *Big Data Research*, *27*. https://doi.org/10.1016/j.bdr.2021.100296

Wang, L., Ranasinghe, R., Maskey, S., van Gelder, P. H. A. J. M., & Vrijling, J. K. (2016). Comparison of empirical statistical methods for downscaling daily climate projections from CMIP5 GCMs: A case study of the Huai River Basin, China. *International Journal of Climatology*, *36*(1), 145–164. https://doi.org/10.1002/joc.4334

Wickramasinghe, M. R. C. P., De Silva, R. P., & Dayawansa, N. D. K. (2021). Climate Change Vulnerability in Agriculture Sector: An Assessment and Mapping at Divisional Secretariat Level in Sri Lanka. *Earth Systems and Environment*, *5*(3), 725–738. https://doi.org/10.1007/s41748-021-00206-9

Wilby, R. L., & Dawson, C. W. (2007). *SDSM 4.2-A decision support tool for the assessment of regional climate change impacts User Manual*. http://www.cics.uvic.ca/scenarios/index.cgi?Scenarios

Withanachchi, S. S., Köpke, S., Withanachchi, C. R., Pathiranage, R., & Ploeger, A. (2014). Water resource management in dry zonal paddy cultivation in mahaweli river basin, Sri Lanka: An analysis of spatial and temporal climate change impacts and traditional knowledge. *Climate*, *2*(4), 329–354. https://doi.org/10.3390/cli2040329

Xu, C.-Y. (1999). *From GCMs to river flow: a review of downscaling methods and hydrologic modelling approaches*.

Yihdego, Y., Vaheddoost, B., & Al-Weshah, R. A. (2019). Drought indices and indicators revisited. In *Arabian Journal of Geosciences* (Vol. 12, Issue 3). Springer Verlag. https://doi.org/10.1007/s12517-019-4237-z

Yosef, Y., Aguilar, E., & Alpert, P. (2021). Is it possible to fit extreme climate change indices together seamlessly in the era of accelerated warming? *International Journal of Climatology*, *41*(S1), E952–E963. https://doi.org/10.1002/joc.6740

Zargar, A., Sadiq, R., Naser, B., & Khan, F. I. (2011). A review of drought indices. *Environmental Reviews*, *19*(1), 333–349. https://doi.org/10.1139/a11-013

Zhai, J., Mondal, S. K., Fischer, T., Wang, Y., Su, B., Huang, J., Tao, H., Wang, G., Ullah, W., & Uddin, M. J. (2020). Future drought characteristics through a multi-model ensemble from CMIP6 over South Asia. *Atmospheric Research*, *246*. https://doi.org/10.1016/j.atmosres.2020.105111

Zhao, L., Lyu, A., Wu, J., Hayes, M., Tang, Z., He, B., Liu, J., & Liu, M. (2014). Impact of meteorological drought on streamflow drought in Jinghe River Basin of China. *Chinese Geographical Science*, *24*(6), 694–705. https://doi.org/10.1007/s11769-014-0726-x

Zhu, X., Lee, S. Y., Wen, X., Ji, Z., Lin, L., Wei, Z., Zheng, Z., Xu, D., & Dong, W. (2021). Extreme climate changes over three major river basins in China as seen in CMIP5 and CMIP6. *Climate Dynamics*, *57*(3–4), 1187–1205. https://doi.org/10.1007/s00382-021-05767-z

Zubair, L., Siriwardhana, M., Chandimala, J., & Yahiya, Z. (2008). Predictability of Sri Lankan rainfall based on ENSO. *International Journal of Climatology*, *28*(1), 91–101. https://doi.org/10.1002/joc.1514

APPENDIX A: DOUBLE MASS CURVES

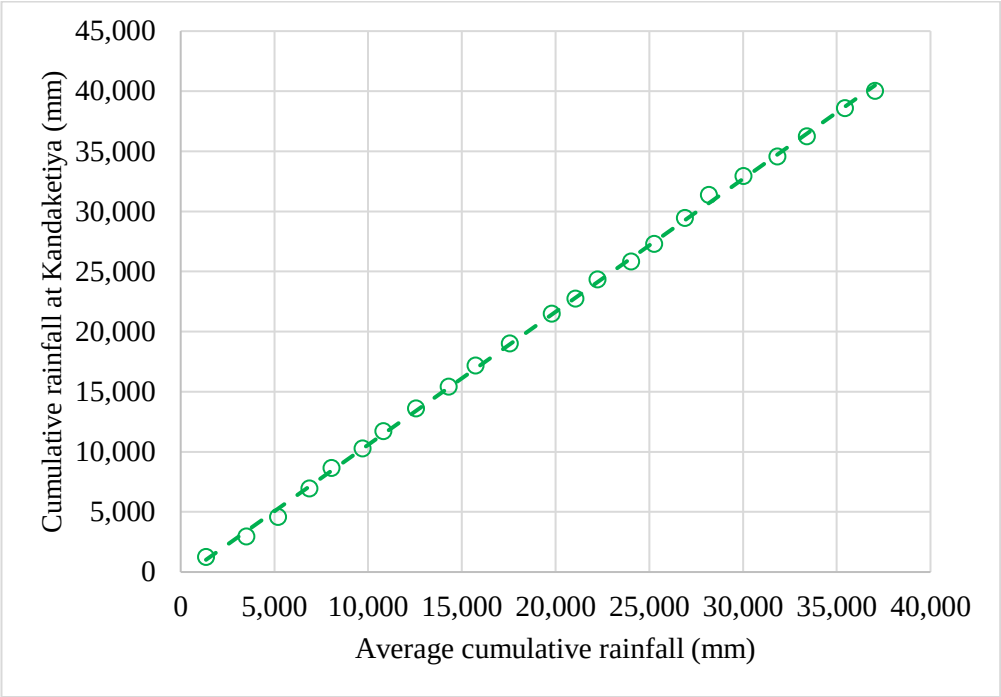

Figure A.1: Double mass curve for Kandaketiya rainfall station (Maduru Oya river basin)

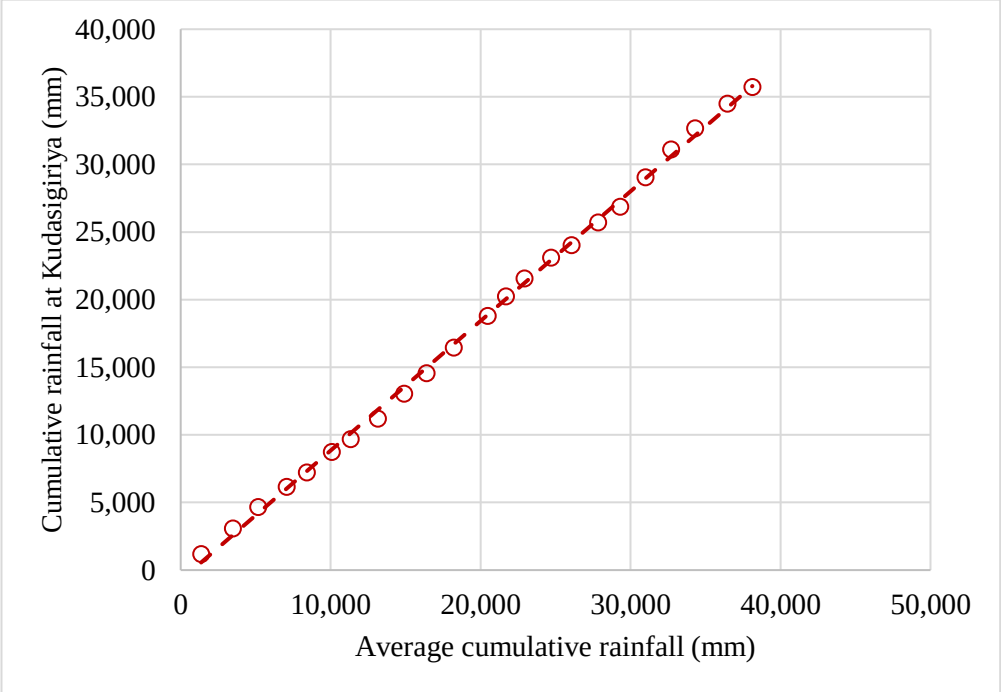

Figure A.2: Double mass curve for Kudasigiriya rainfall station (Maduru Oya river basin)

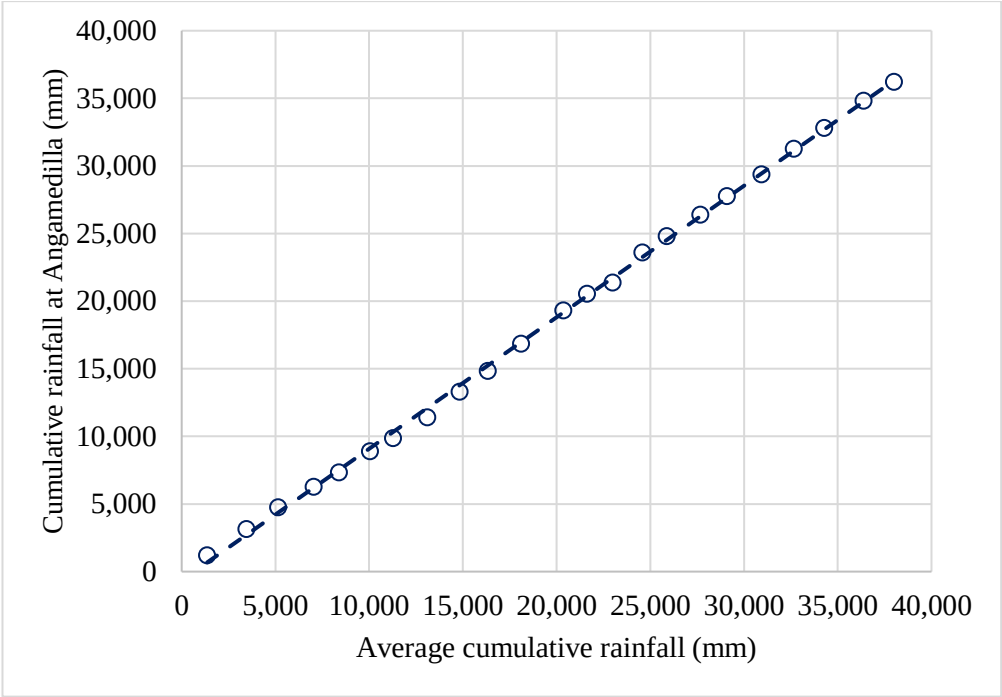

Figure A.3: Double mass curve for Angamedilla rainfall station (Maduru Oya river basin)

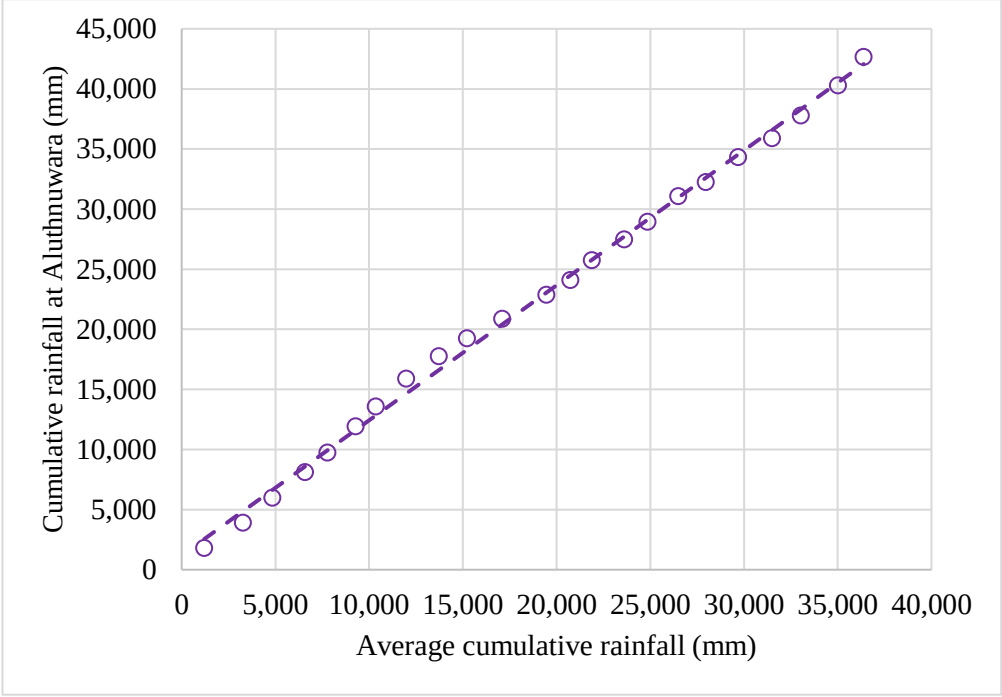

Figure A.4: Double mass curve for Aluthnuwara rainfall station (Maduru Oya river basin)

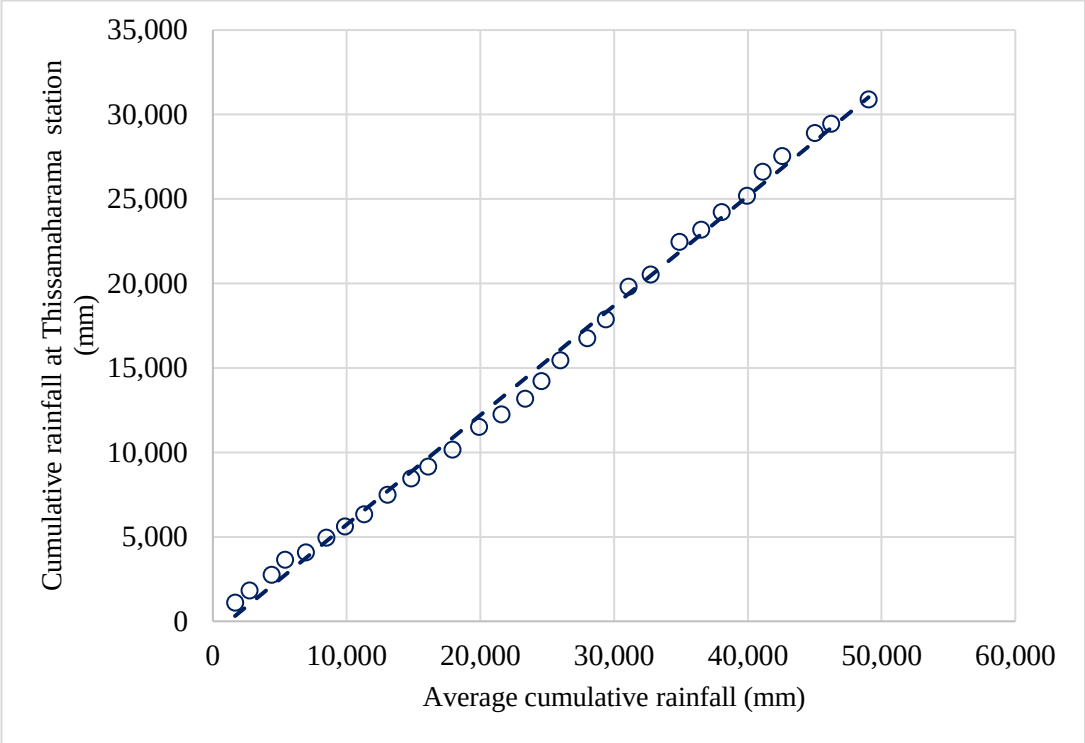

Figure A.5:Double mass curve for Thissamaharama Irrigation rainfall station (Kirindi Oya river basin)

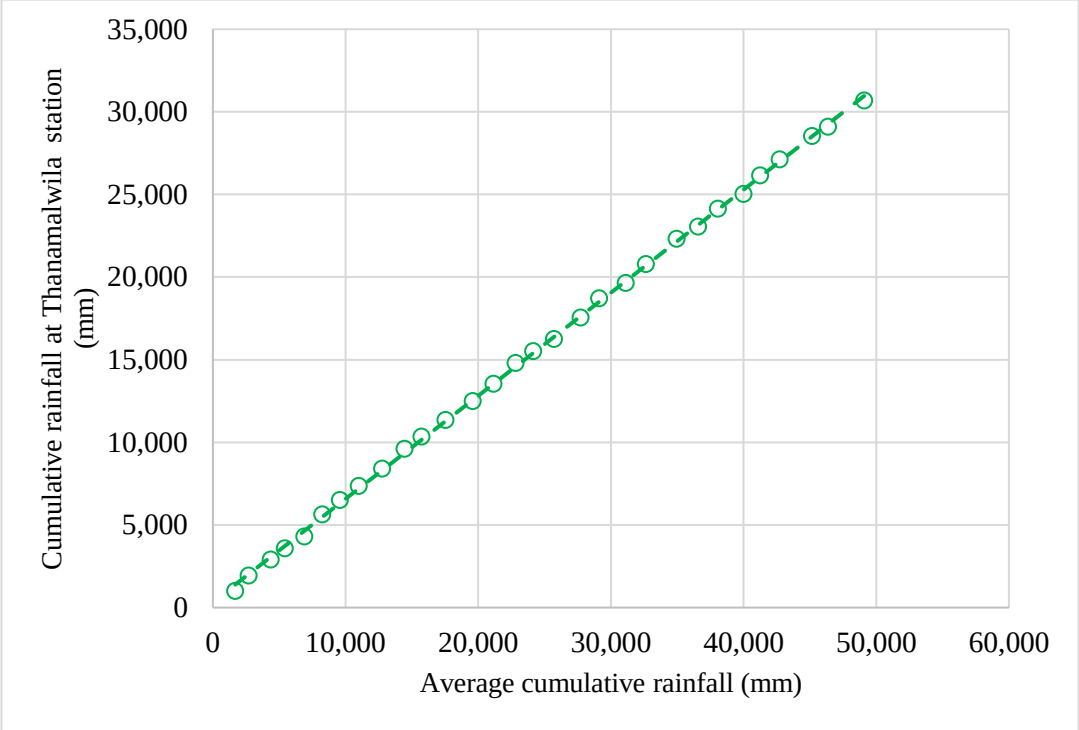

Figure A.6: Double mass curve for Thanamalwila rainfall station (Kirindi Oya river basin)

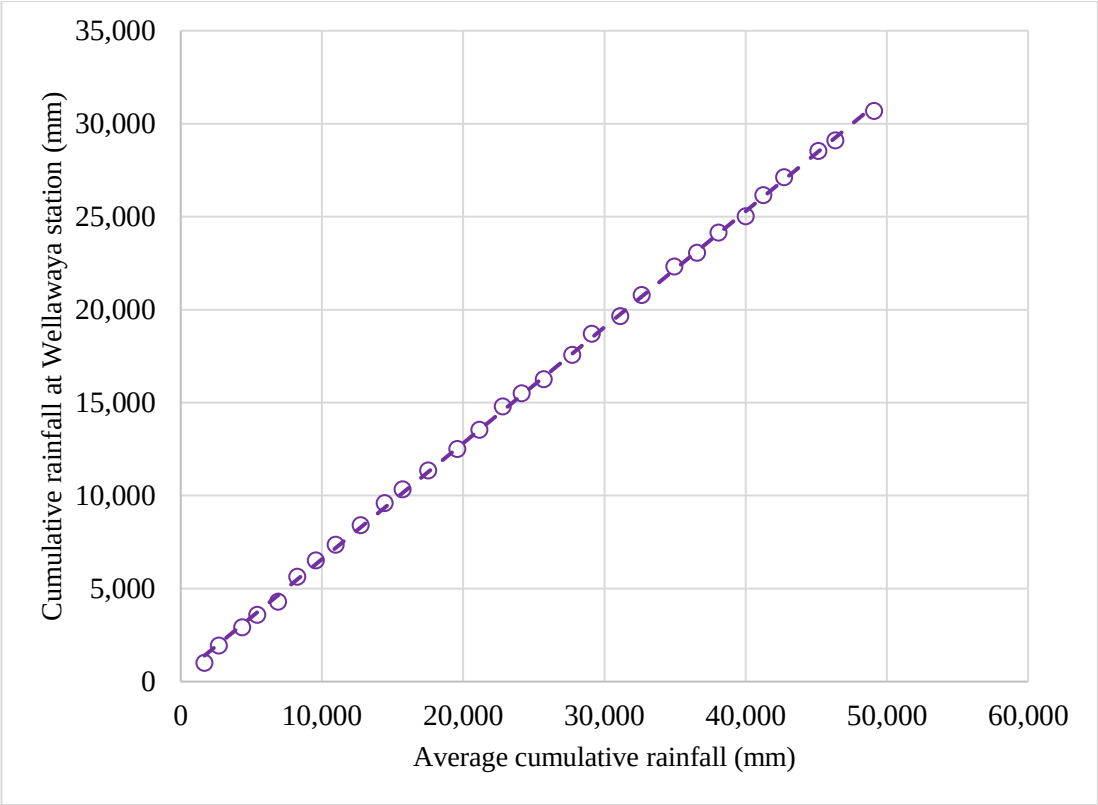

Figure A.7: Double mass curve for Wellawaya rainfall station (Kirindi Oya river basin)

APPENDIX B: ETCCDI INDICES

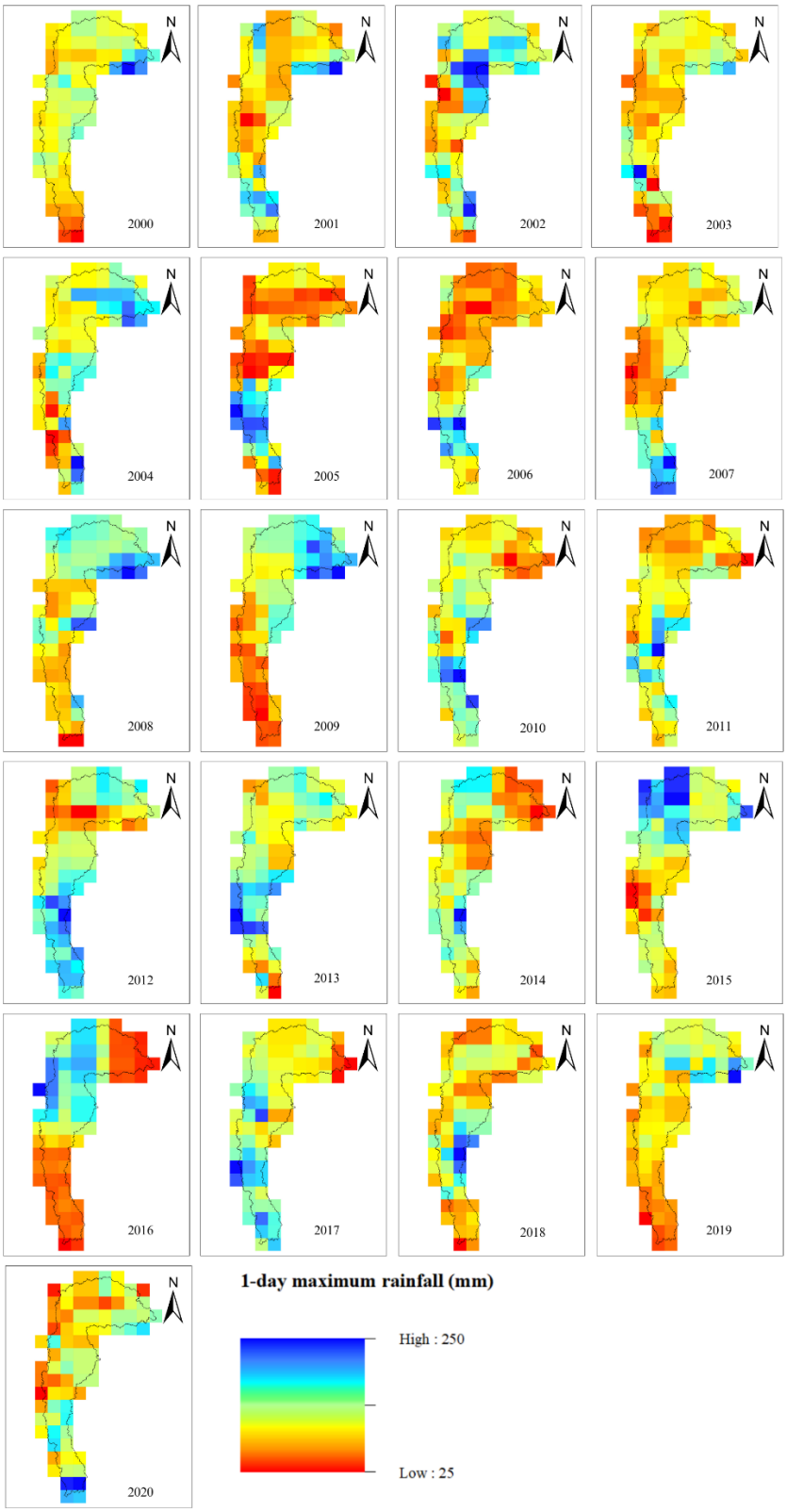

Figure B.1: RX1day variation in the Maduru Oya basin

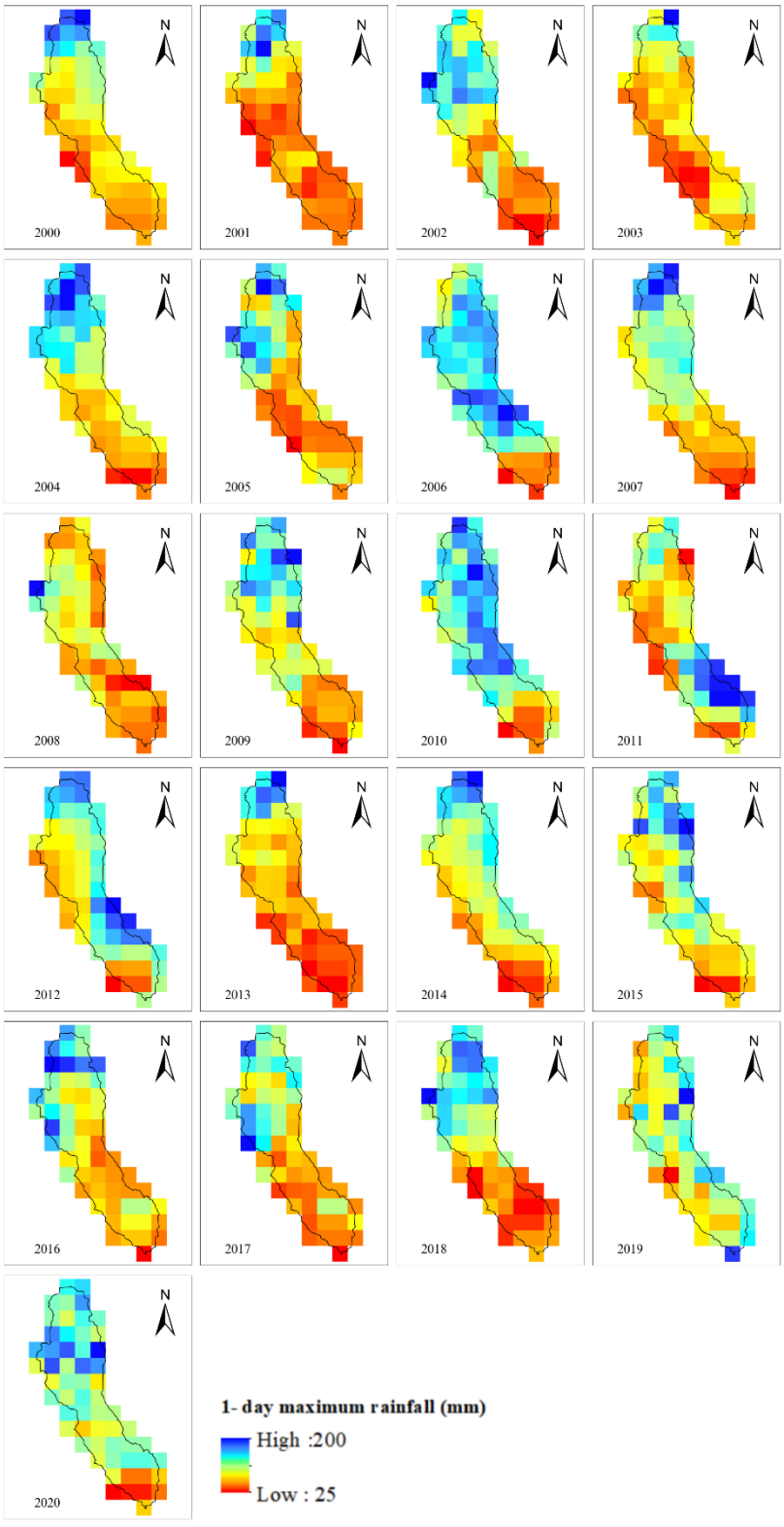

Figure B.2: RX1day variation in the Kirindi Oya basin

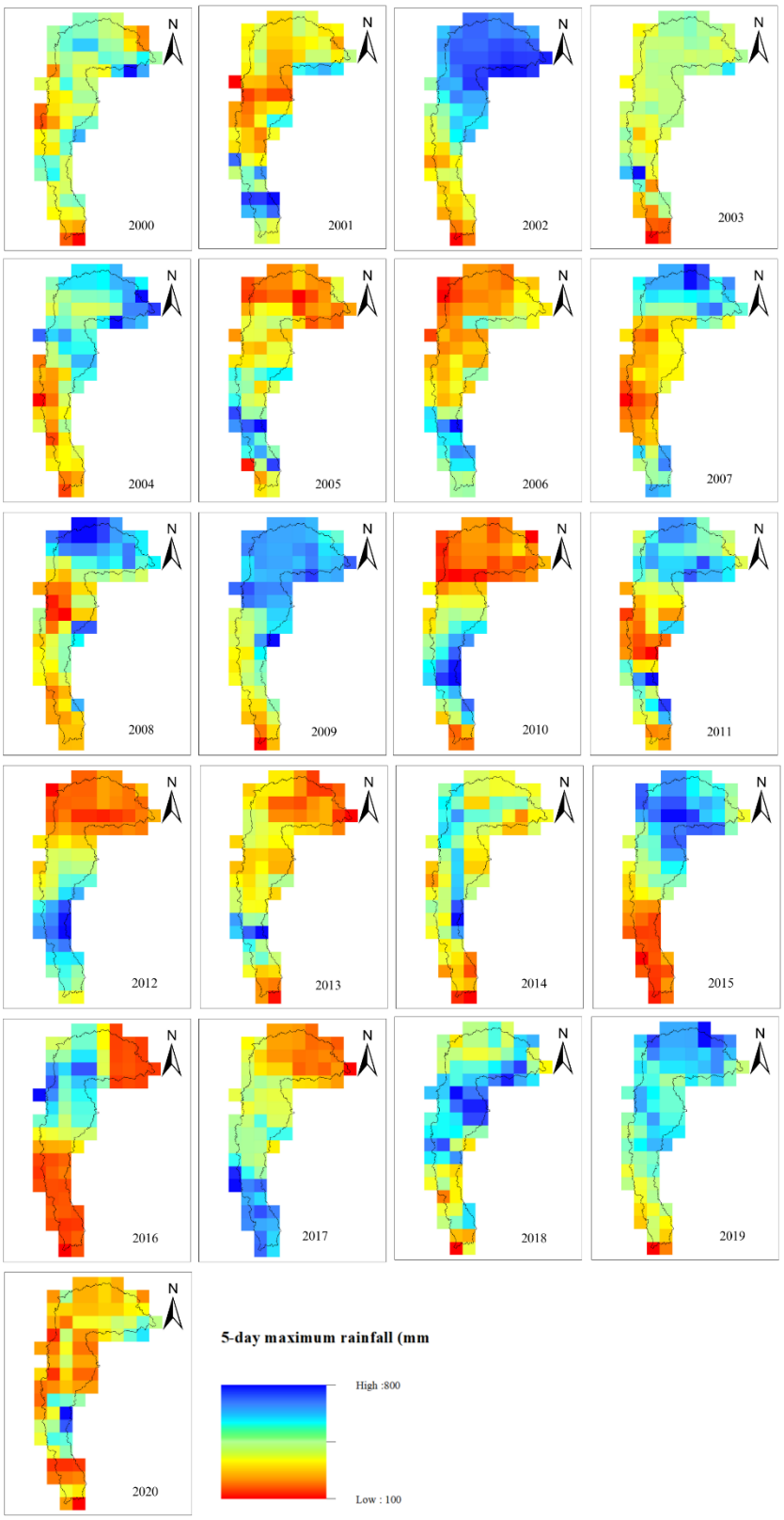

Figure B.3: RX5day variation in the Maduru Oya basin

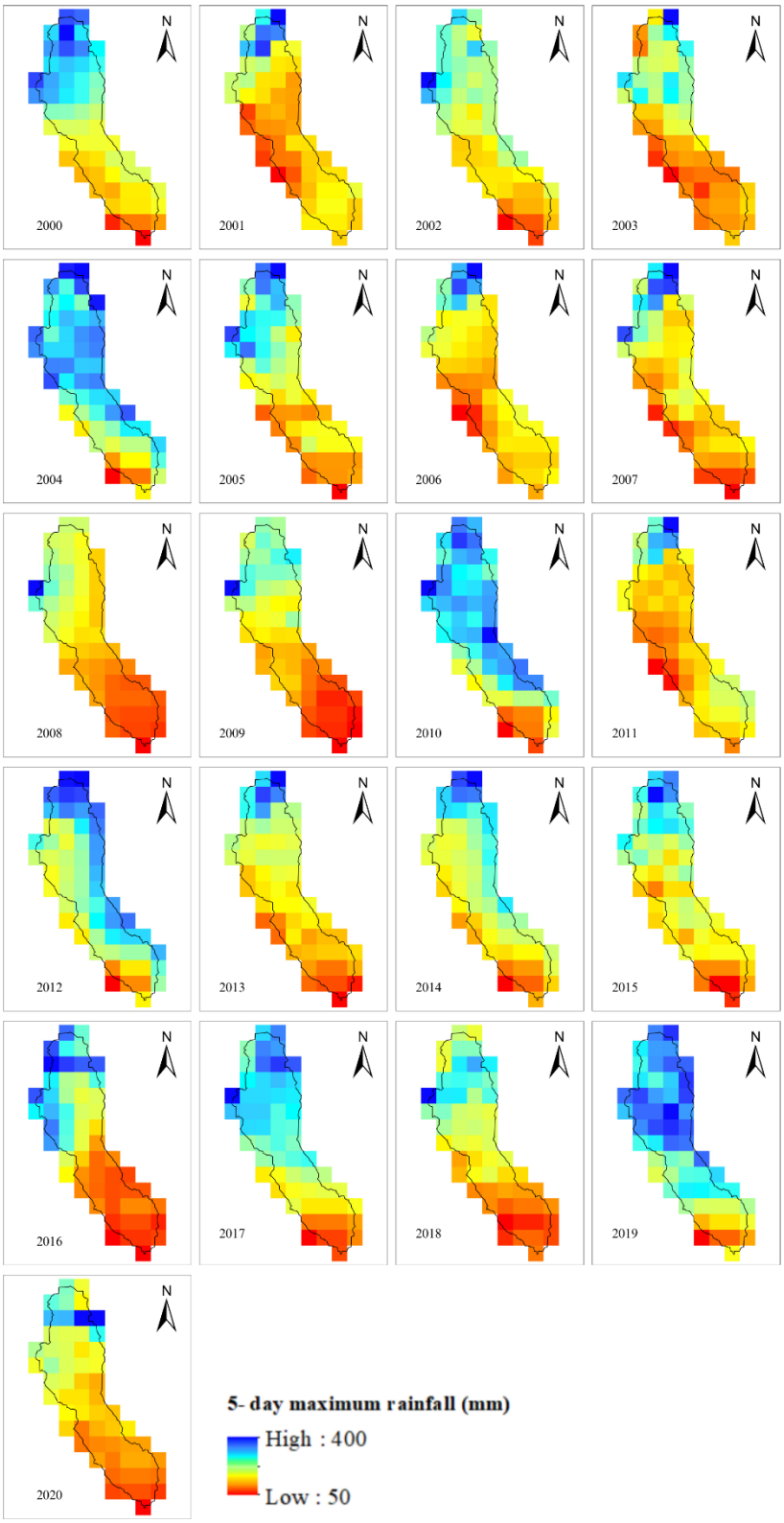

Figure B.4: RX5day variation in the Kirindi Oya basin

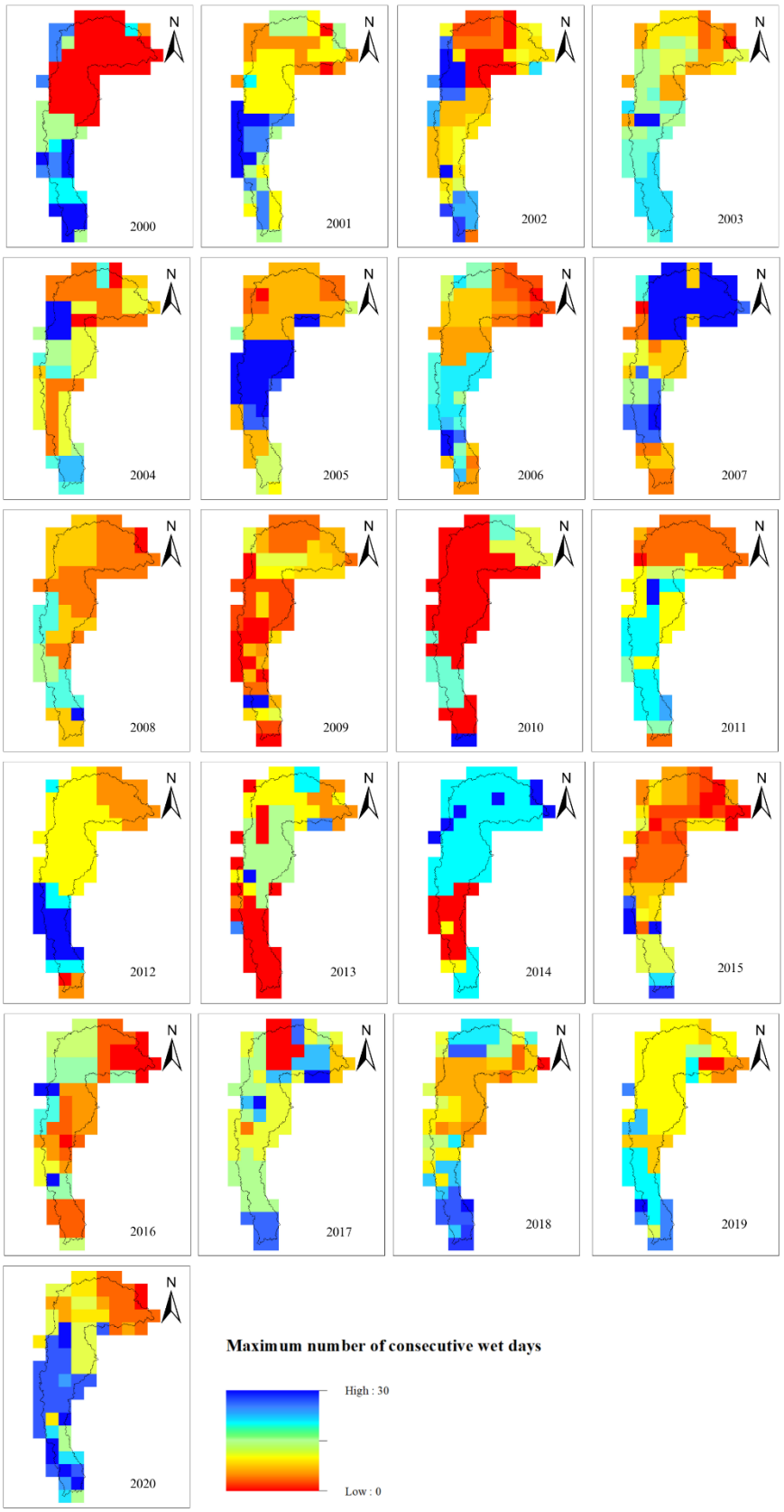

Figure B.5: CWD variation in the Maduru Oya basin

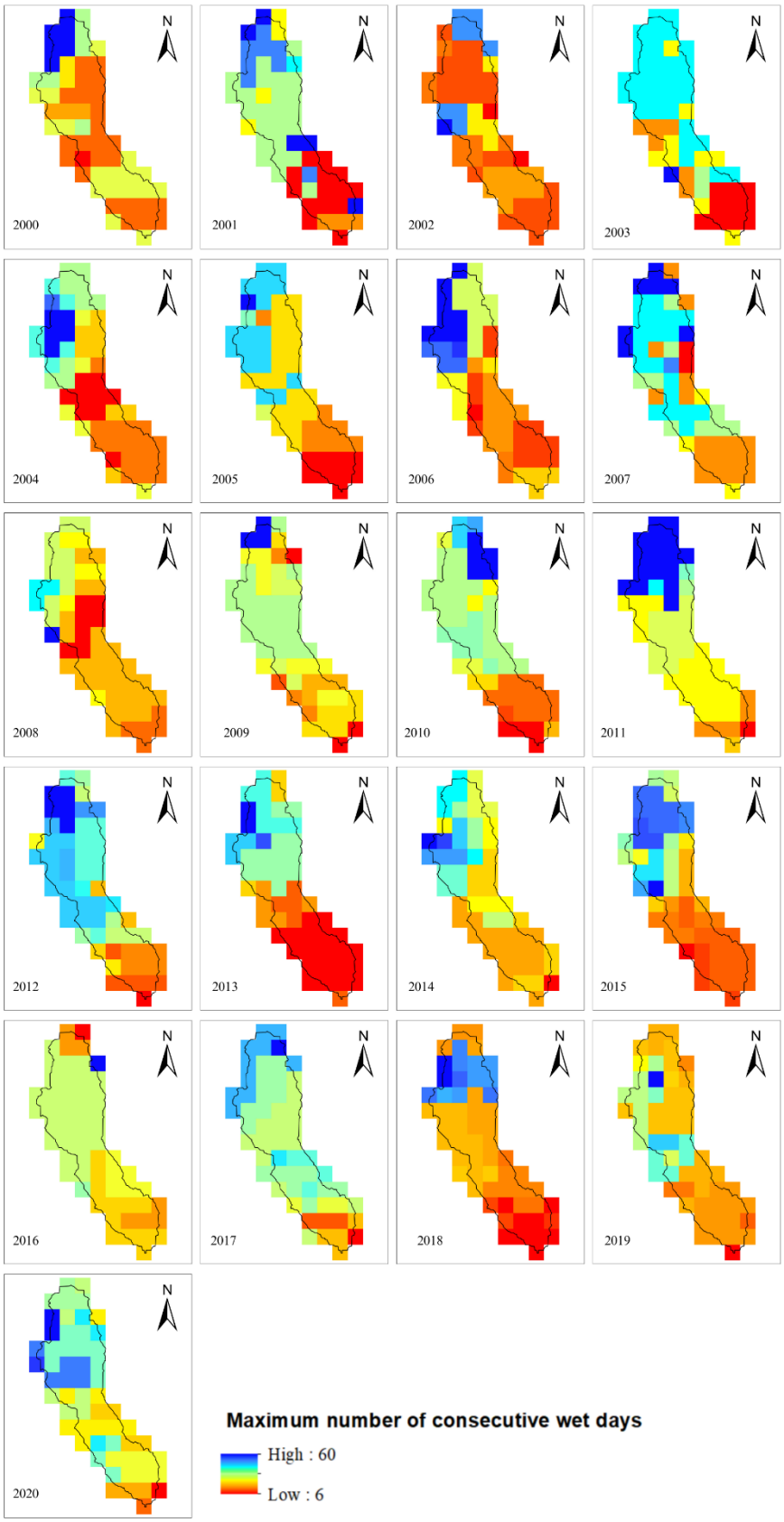

Figure B.6: CWD variation in the Kirindi Oya basin

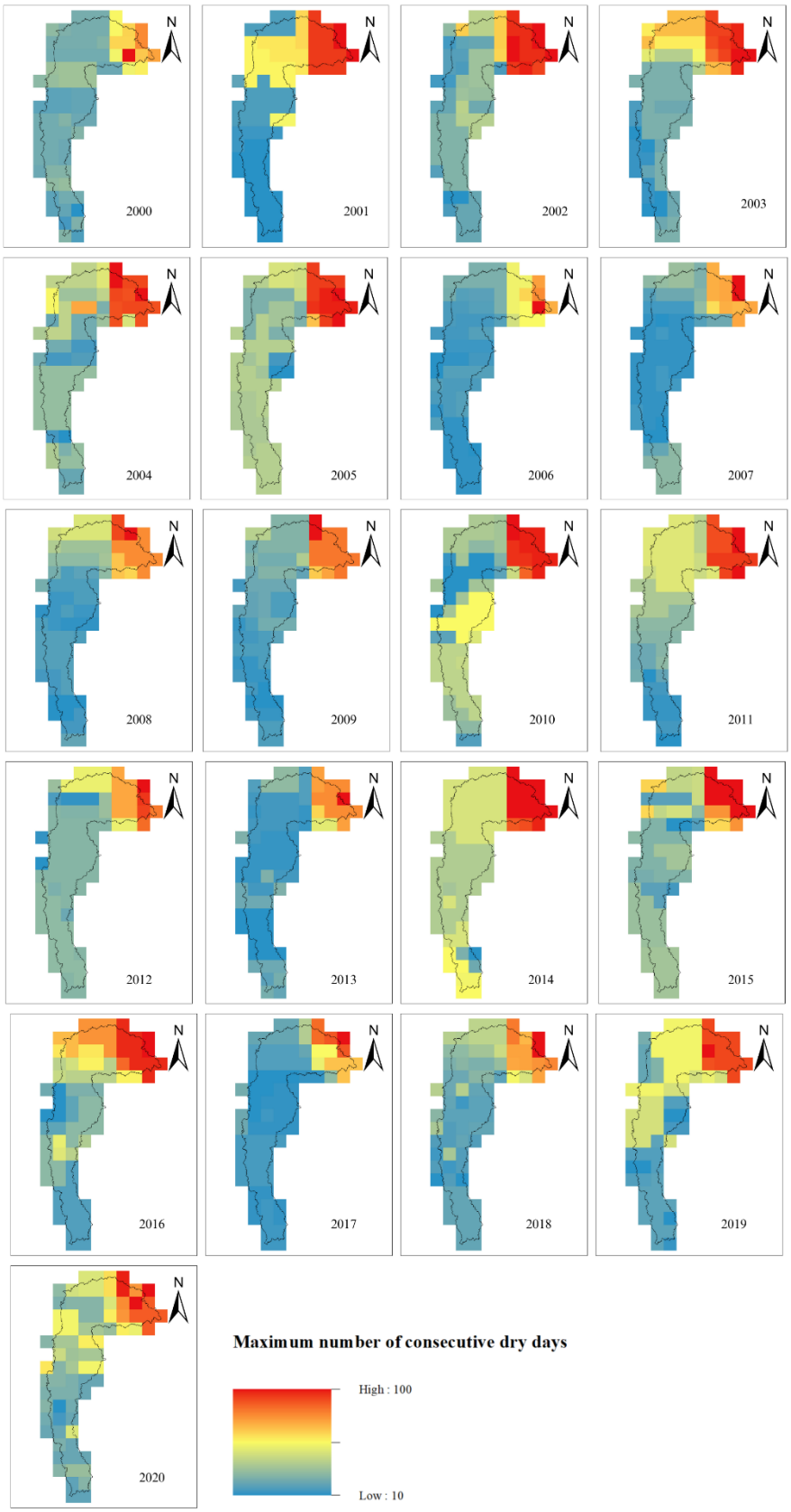

Figure B.7: CDD variation in the Maduru Oya basin

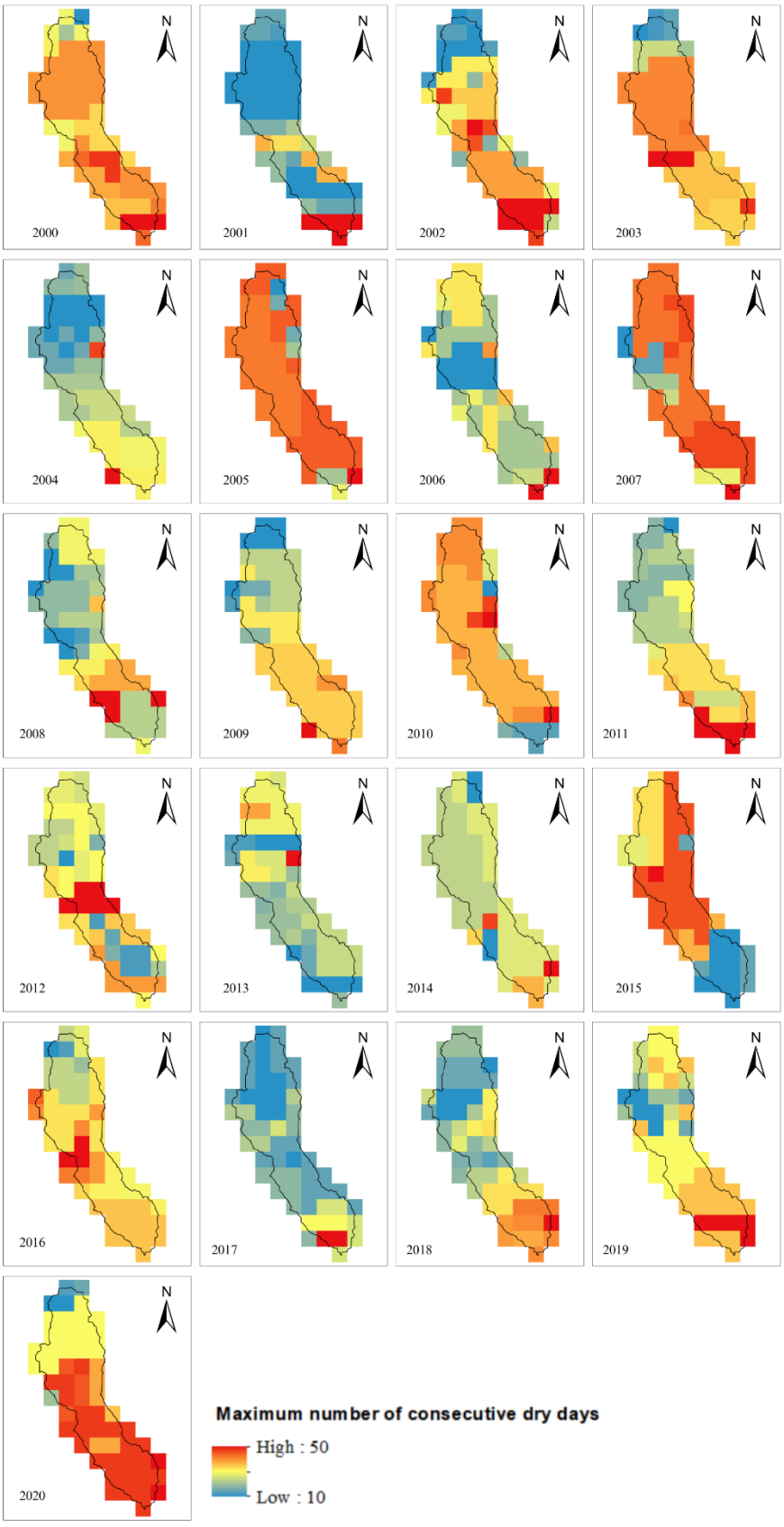

Figure B.8: CDD variation in the Kirindi Oya basin

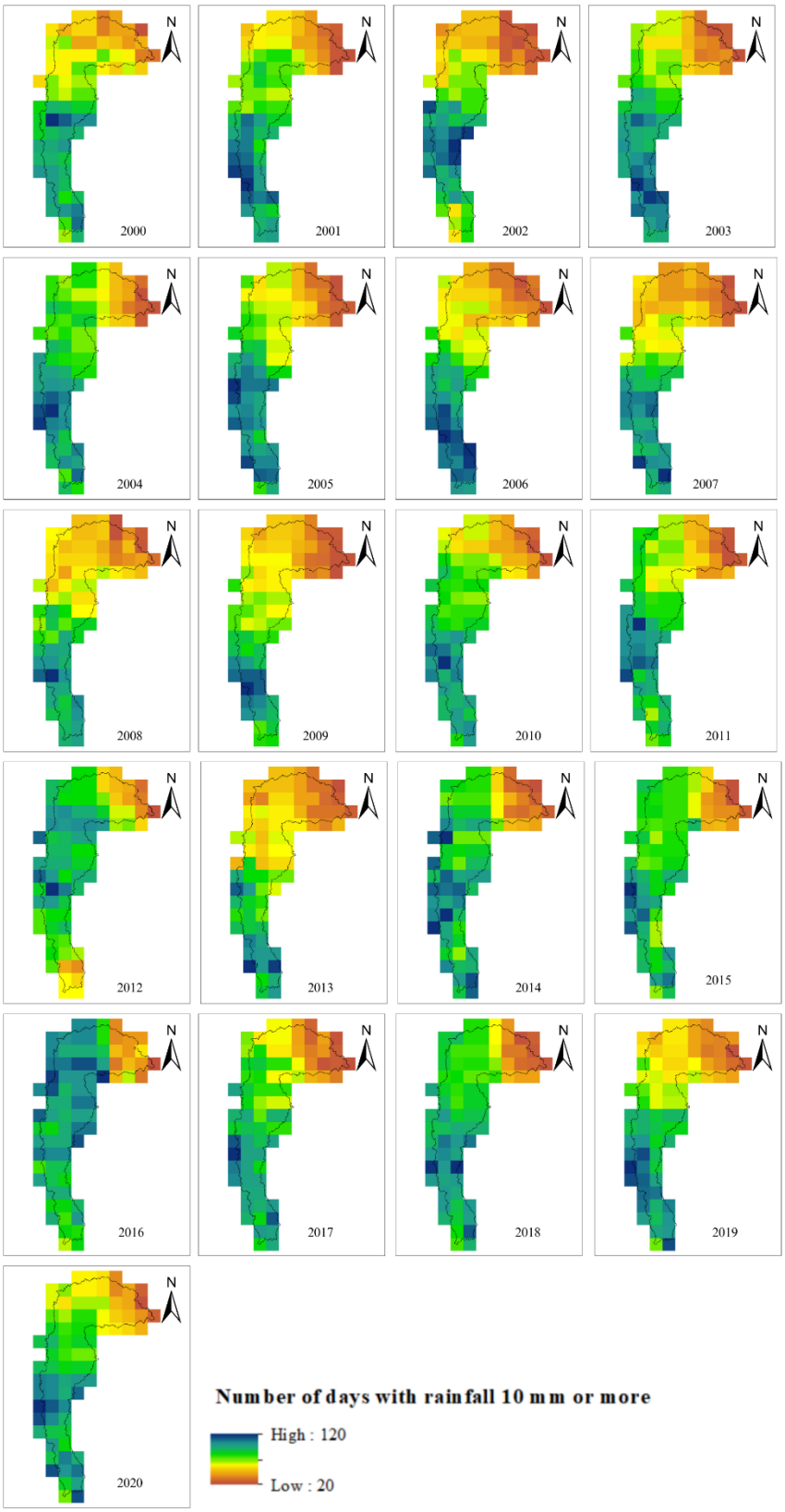

Figure B.9: R10 variation in the Maduru Oya basin

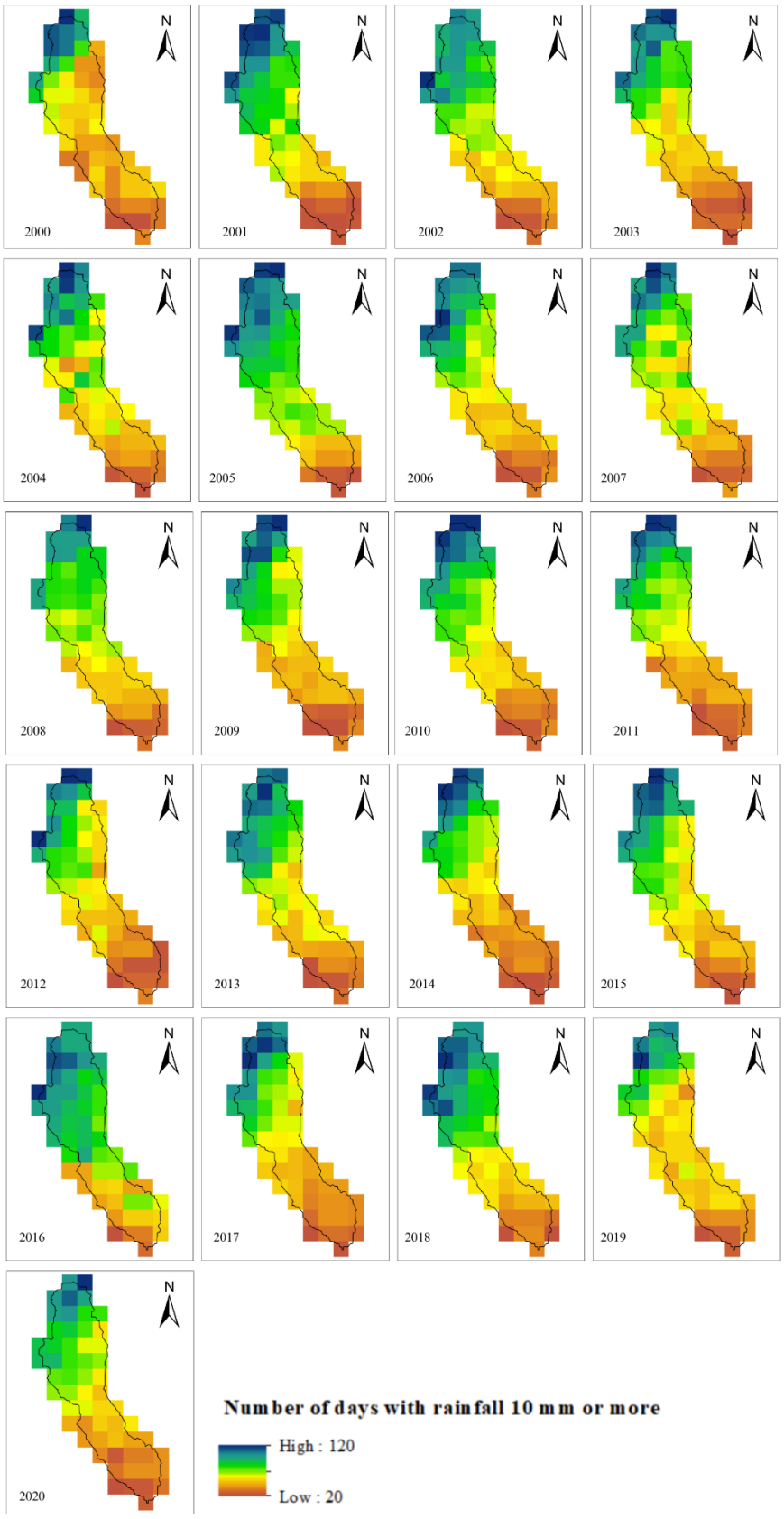

Figure B.10: R10 variation in the Kirindi Oya basin

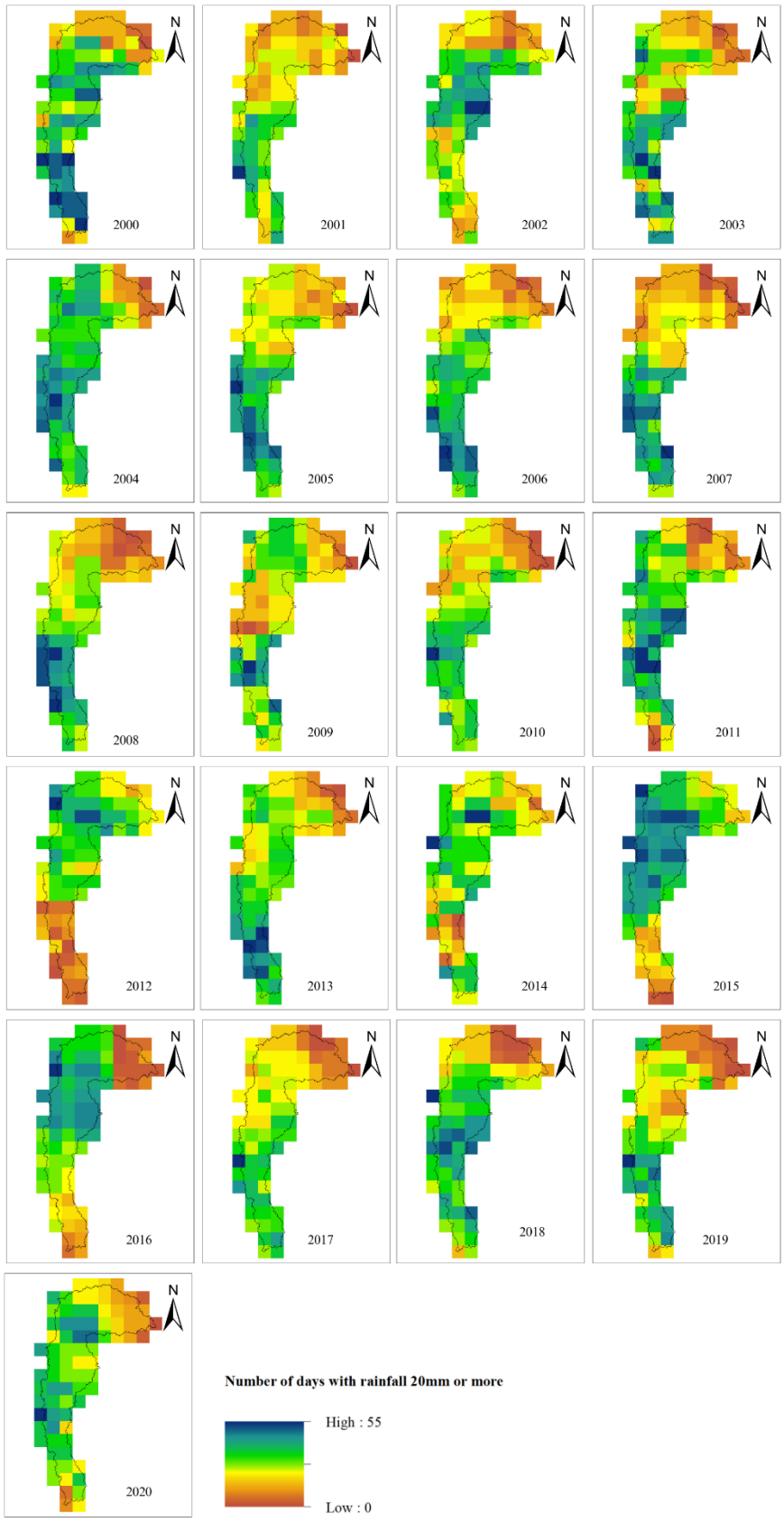

Figure B.11.: R20 variation in the Maduru Oya basin

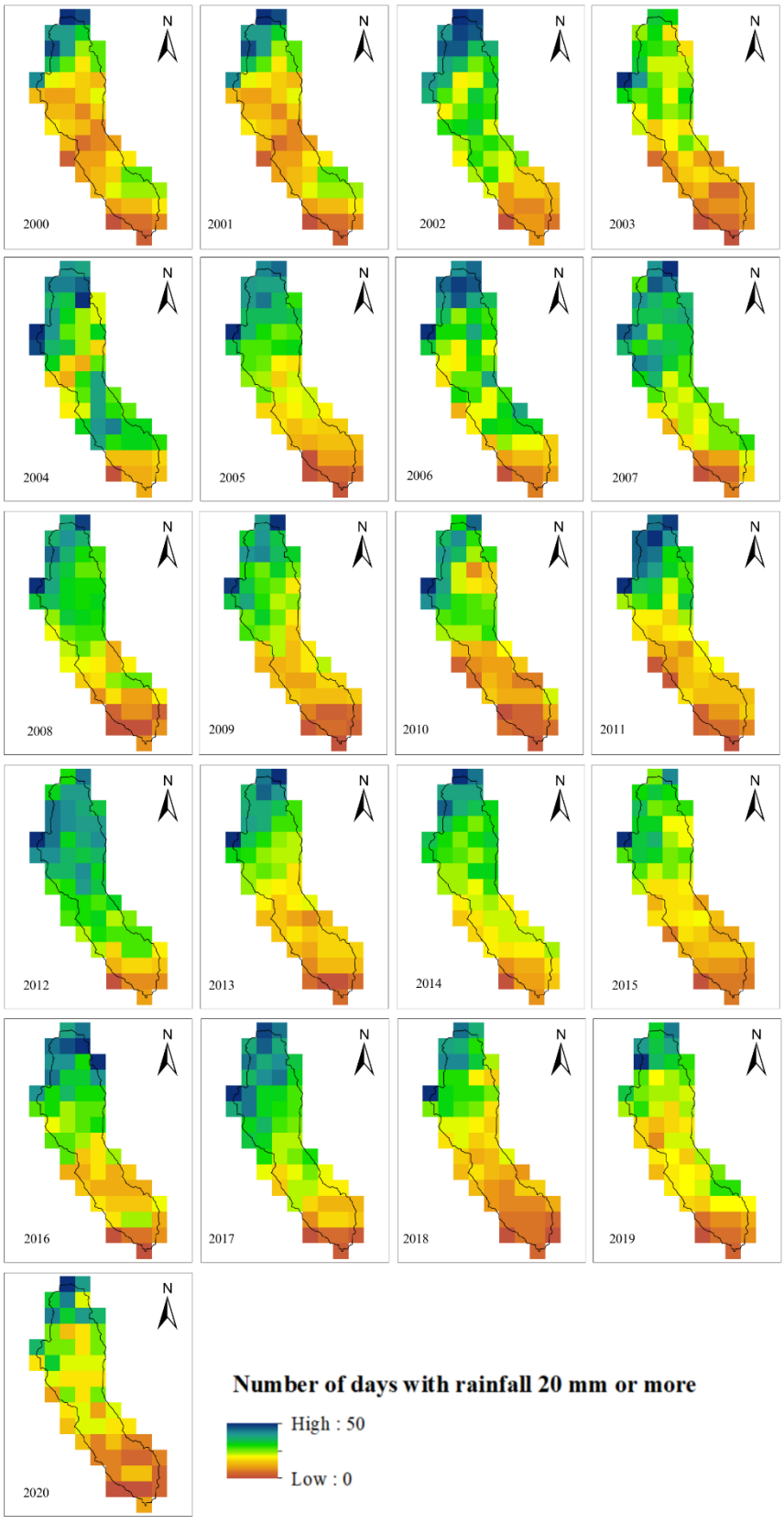

Figure B.12: R20 variation in the Kirindi Oya basin

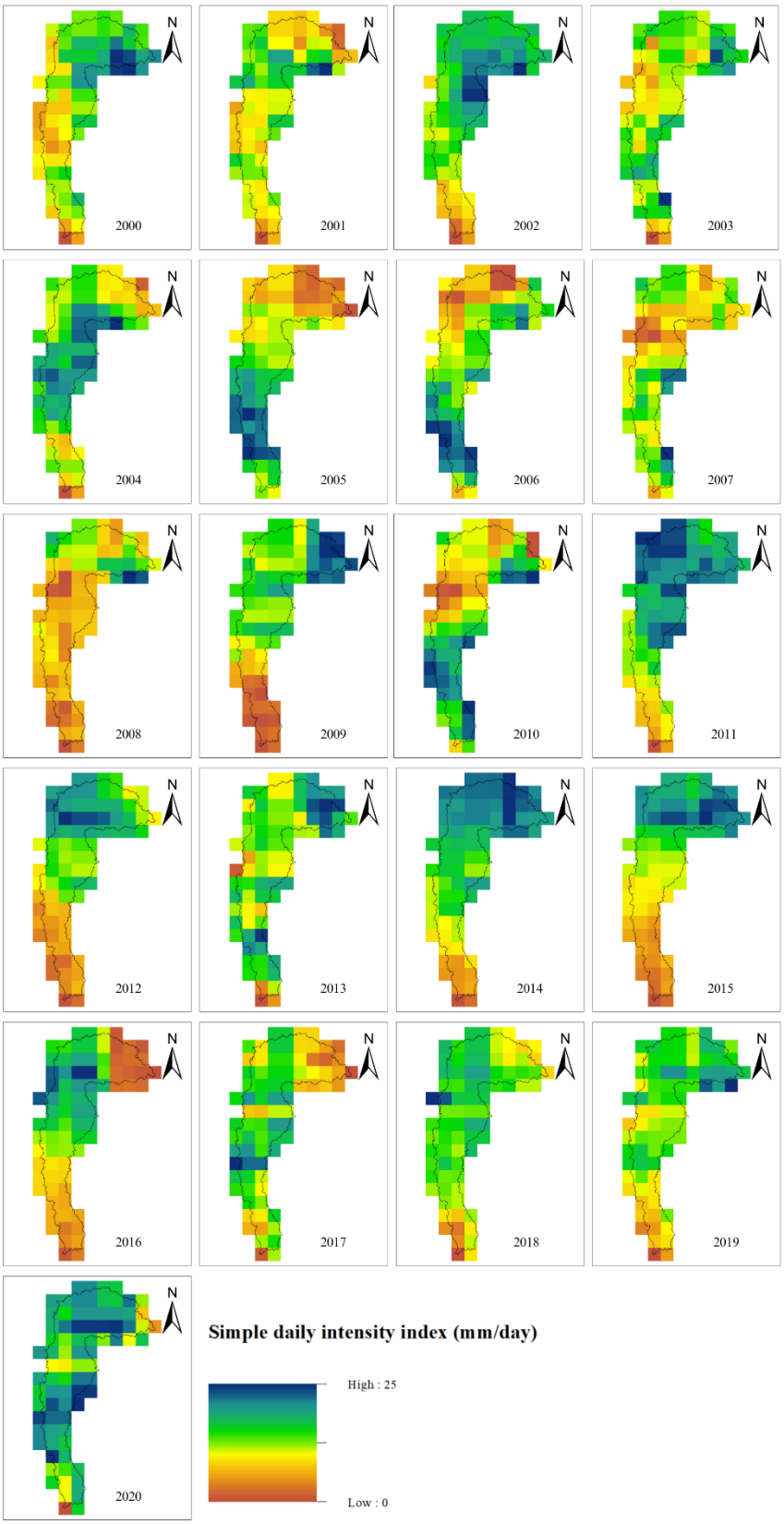

Figure B.13: SDII variation in the Maduru Oya basin

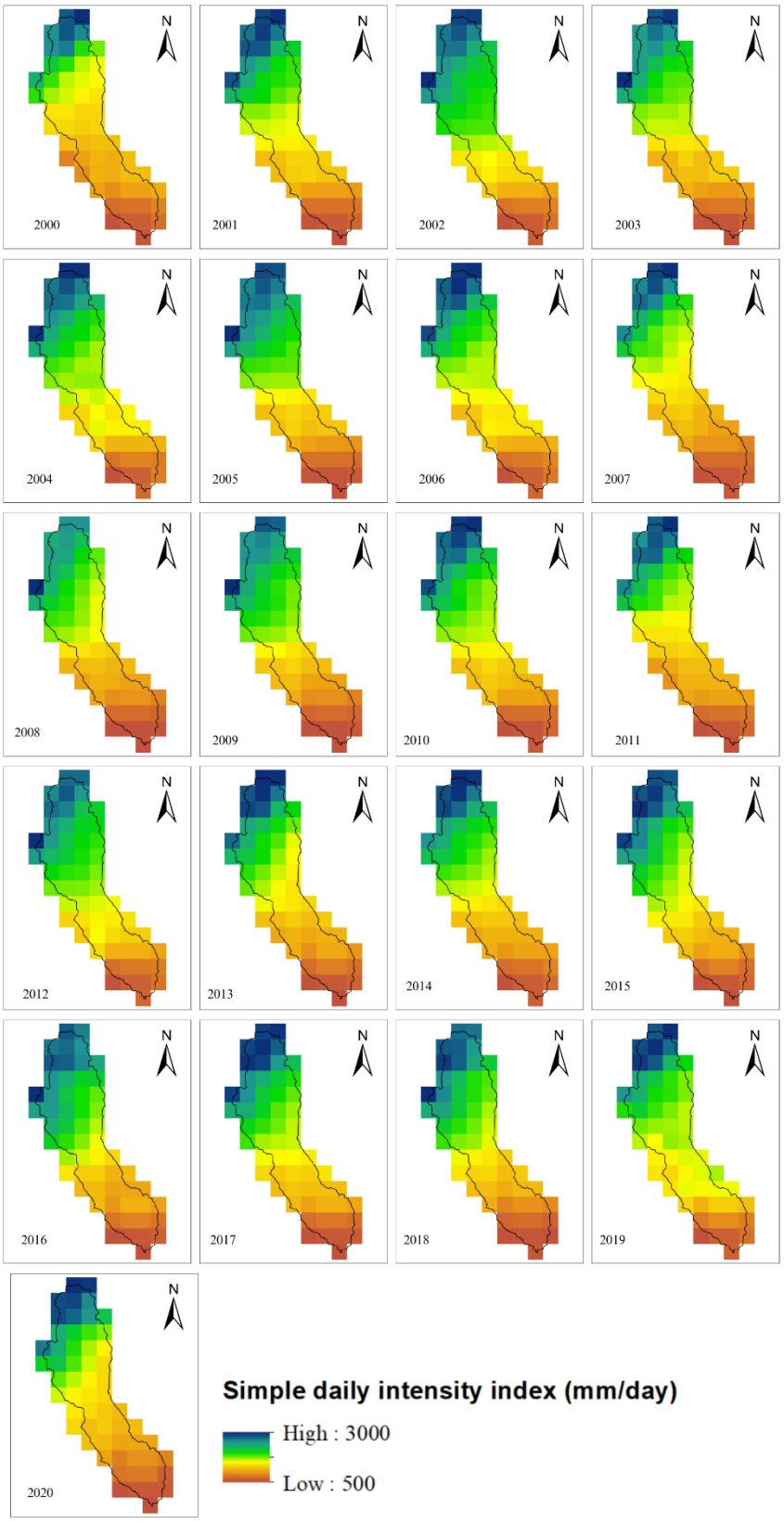

Figure B.14: SDII variation in the Kirindi Oya basin

The findings, interpretations and conclusions expressed in this thesis/dissertation are entirely based on the results of the individual research study and should not be attributed in any manner to or do neither necessarily reflect the views of UNESCO Madanjeet Singh Centre for South Asia Water Management (UMCSAWM), nor of the individual members of the MSc panel, nor of their respective organizations.